Assessing the risk to healthcare workers of hospital-acquired infection from patients infected with aerosol-transmissible pathogens

P Kalliomäki[1], H Koskela[1], M Waris[2], JW Tange[3,4]

[1]Turku University of Applied Sciences, Joukahaisenkatu 3 A, Turku, Finland

[2]University of Turku, Institute of Biomedicine, Kiinamyllynkatu 10, Turku, Finland

[3]Clinical Microbiology, Leicester Royal Infirmary, University Hospitals of Leicester NHS Trust, Leicester, UK

[4]Respiratory Sciences, University of Leicester, Leicester, UK

IOSH, the Chartered body for health and safety professionals, is committed to evidence-based practice in workplace health and safety. We maintain a Research for Public Benefit Fund to support research and inspire innovation as part of our work as a 'thought leader' in health and safety.

All recipients of funding from our Research for Public Benefit Fund are asked to compile a comprehensive research report of their findings, which is subject to peer review.

For more information on how to apply for grants from the Fund, visit iosh.com/research

Acknowledgement: IOSH would like to thank the peer reviewers of this report.

Abstract

Since the outbreak of severe acute respiratory syndrome (SARS) in 2003, healthcare workers (HCWs) caring for patients infected with various emerging/re-emerging viruses (Middle East respiratory syndrome, or MERS; avian and pandemic influenzas; Ebola; and, most recently, SARS-CoV-2, which causes coronavirus disease 2019, or Covid-19) are now acutely aware of the potential risks to themselves, particularly through aerosol transmission. If enhanced protection can be achieved using more informed and evidence-based environmental control methods, such as those to be investigated in this study, then this will potentially benefit all HCWs encountering these patients.

The aim of this study was to investigate and characterise the risk of potential aerosol transmission of infectious agents from patients to their HCWs in typical encounter scenarios in hospital isolation rooms.

Specifically, the objectives were to assess the effect of different air distribution modes, ventilation rates, the exhaust position, the distance between the patient and the HCW, and face masks on HCW exposure to patient-exhaled aerosols, and to evaluate the potential risks to HCWs of patients using medical nebulisers. The study was carried out in a controlled environment in a laboratory-built full-scale isolation-room model using smoke, gas, vaccine virus tracers and computational fluid dynamics (CFD) modelling.

The results showed that isolation-room ventilation should be designed to create sufficient air movement above the patient to dilute and flush away the patient's potentially pathogen-laden exhaled air. In addition, supply air distribution and exhaust location should be designed in such a way as to direct the patient's exhalation air away from the HCW's breathing zone.

The study confirmed that masking the patient is an effective method of containing the patient's exhaled breath. We also confirmed that higher ventilation rates are effective in diluting and removing contaminated air in an isolation room at least up to 12 air changes per hour (ACH), provided that the air distribution is able to mix the air above the patient's bed.

Finally, using a live influenza virus vaccine tracer, we demonstrated that use of nebuliser masks by influenza-infected patients can generate virus aerosols in the vicinity of the patient, which may pose a risk to nearby HCWs.

Executive summary

Project overview and aims

Since the outbreak of severe acute respiratory syndrome (SARS) in 2003, healthcare workers (HCWs) caring for patients infected with various emerging/re-emerging viruses (Middle East respiratory syndrome, or MERS; avian and pandemic influenzas; Ebola; and, most recently, SARS-CoV-2, which causes coronavirus disease 2019, or Covid-19) are now acutely aware of the potential risks to themselves, particularly through aerosol transmission. If enhanced protection can be achieved using more informed and evidence-based environmental control methods, such as those to be investigated in this study, then this will potentially benefit all HCWs encountering these patients.

The aim of this study was to investigate and characterise the risk of potential aerosol transmission of infectious agents from patients to their HCWs in typical encounter scenarios in hospital isolation rooms.

Specifically, the objectives were to assess the effect of different air distribution modes, ventilation rates, the exhaust position, the distance between the patient and the HCW, and face masks on HCW exposure to patient-exhaled aerosols, and to evaluate the potential risks to HCWs of patients using medical nebulisers. In order to achieve the objectives, the study was carried out in a controlled environment in a laboratory-built full-scale isolation-room model using smoke, gas, vaccine virus tracers and CFD modelling.

Methods

This study examined experimentally the effects of two modes of supply air distribution – i) baseline overhead mixing ventilation (MV), and ii) local downward ventilation (LDV) with background mixing ventilation – on the HCW's exposure to the patient's exhaled air. In addition, zonal downward ventilation (ZDV) was studied with computer simulations. The aim with the local and zonal downward ventilations was to mix and dilute possible high contaminant concentrations locally/zonally in the area of the patient's bed (that is, close to the source).

In the MV case, the supply air was distributed to the room along the ceiling from the middle of the room. In the LDV case, one diffuser was placed in the ceiling above the patient's chest and another was placed in the ceiling at the other end of the room. The diffuser above the patient was used to create a downward flow capable of flushing the breathing zone of the patient, and the other diffuser was used to supply the air along the ceiling in all directions to create background mixing ventilation. The total supply flow rate of the test room for both supply air distribution modes was 170 L/s, corresponding to 12 air changes per hour (ACH).

The laboratory experiments were carried out in a full-scale isolation-room model at Turku University of Applied Sciences' indoor environment laboratory. In the experiments, the HCW was simulated with a detailed breathing thermal manikin, and the patient was simulated with a simpler heated dummy. Both the manikin and the dummy had artificial lungs to simulate tidal breathing.

Smoke visualisations were carried out to qualitatively assess the room airflow patterns and the dispersion of the exhalation of the patient. Computational simulations were carried out to further analyse the flow of contaminant and supply air in the room. Air velocities were measured to quantify the airflow velocity near the patient. The effect of air distribution on the thermal comfort of the patient was studied with a thermal manikin.

Tracer gas measurements were carried out for several experimental cases to assess the effect of different parameters on the spreading of the patient's exhaled airborne contaminants and the HCW's exposure to

them. In addition to the gas tracer, an organic live-attenuated vaccine virus tracer was used in this study for enhanced realism.

Results

The following results were obtained with the experiments and simulations:

- The exhaled air of the patient flowed directly towards the HCW's breathing zone with MV when the patient was in a typical reclining position. The exhaled air of the patient should be flushed away from the HCW's breathing zone to protect the HCW from direct exposure as much as possible.
- The highest exposure of the HCW to the exhaled air of the patient occurred when the HCW was leaning over the patient in order to give care (for example, examining the patient or inserting an intravenous drip). In this situation, the inhaled concentration was typically five to six times the average room concentration with MV.
- LDV flow was able to flush the breathing zone of the patient and notably reduced the HCW's exposure. When in the most critical position (leaning over the patient), the HCW's level of exposure with LDV was only about a third of that with MV.
- LDV caused higher velocities over the patient's bed than MV. This air movement can cause a draught that may be uncomfortable for the patient. Therefore, the air distribution must be designed carefully in order to minimise this draught and achieve acceptable thermal comfort. There will always be a need to reach a compromise between HCW protection and patient thermal comfort.
- Generally, patient thermal comfort was slightly lower (that is, the thermal environment was cooler) with LDV mode than with MV, but neither ventilation mode was too far from neutral.
- The potential thermal discomfort for the patient caused by the higher airflow velocities with LDV may be mitigated if it is only turned on during nursing periods, with MV being used the rest of the time.
- According to the CFD simulations, ZDV was even more effective than LDV at protecting the HCW. However, these results require further rigorous experimental validation.
- The exhaust location also plays a role in HCW protection. However, exhausts can capture air only from a short distance away and therefore cannot control the room airflows generally. Nevertheless, placing an exhaust near high-concentration areas can lower the room concentrations notably.
- In this study, the most effective exhaust positions were in the wall behind the patient's bed and in the lighting panel (above and behind the patient), when the supply air was flushing the exhaled air in that direction.
- A higher ventilation rate reduces the HCW's exposure by decreasing the average room concentration and increasing the air mixing and dilution. Our results indicate that increased ventilation rates are effective in lowering the HCW's aerosol exposure near the patient, at least up to 12 ACH, provided that the air distribution is able to mix the air above the patient's bed.
- Masking the patient with an FFP2/N95 mask was found to be an effective method of suppressing the spread of the patient's exhalation jet into the room. However, wearing a mask may be uncomfortable for some patients if maintained for long periods.
- The live cold-attenuated influenza virus vaccine (LAIV) tracer experiments confirmed the findings of the tracer gas measurements: i) the highest exposure occurred when the HCW was leaning over the patient (with MV), and ii) LDV reduced the viral loads compared to MV.

- We demonstrated that using a home nebuliser can spread exhaled virus-laden aerosols, mostly from the nebuliser mask side vents, which can infect carers and others nearby. Substantial viral loads were detected, which could be sufficient to cause infection if such personnel are present for the duration of the nebulisation session.

Conclusions and recommendations

In order to optimise the protection of HCWs from their patients' exhaled breath, which potentially carries airborne pathogens, we recommend that isolation-room designs and planning the care regime should take the following factors into account:

- Set the ventilation rate high enough to dilute and flush away exhaled air from the patient that may be carrying pathogens. Ensure that the air above the patient's bed is sufficiently mixed and diluted to achieve this.
- Design the ventilation layout such that patient exhaled breath is directed away from attending HCWs. The optimal placement of the exhaust vent is in the location of the highest concentration of exhaled air – for example, in the wall just above and behind the patient's head while they are lying or reclining in bed.
- Mask the patient where possible to contain exhaled pathogens – until effective ventilation is established and maintained.
- Nebulisers should be treated as AGPs with the appropriate PPE precautions used when setting up and turning off such a device.

List of figures and tables

List of abbreviations

ACH	Air changes per hour
AGP	Aerosol-generating procedure
AIIR	Airborne infection isolation room
ANSI	American National Standards Institute
ASHRAE	American Society of Heating, Refrigerating and Air-Conditioning Engineers
CBE	Center for the Built Environment – University of California, Berkeley
CDC	Centers for Disease Control and Prevention
CFD	Computational fluid dynamics
CV	Coefficient of variation
dPCR	Digital polymerase chain reaction
EN standard	European standard
FFP mask	Respiratory protection mask certified by the European Union
FFU	Fluorescent focus unit, measure of virus quantification
FT	Fluenz Tetra – influenza vaccine
HBSS	Hank's balanced salt solution
HCW	Healthcare worker
HEPA filter	High-efficiency particulate air filter
HTM	Health technical memoranda
HVAC	Heating, ventilation and air conditioning
IF	Intake fraction
ISO	International Organization for Standardization
LAIV	Live cold-attenuated influenza virus vaccine
LDV	Local downward ventilation
LED	Light-emitting diode
LES	Large-eddy simulation
MERS	Middle East respiratory syndrome

MV	Mixing ventilation
PCR	Polymerase chain reaction
PMV	Predicted mean vote
PPD	Predicted percentage of dissatisfied
PPE	Personal protective equipment
PPVL	Positive pressure ventilated lobby
qRT-PCR	Quantitative reverse-transcription polymerase chain reaction (a specific PCR technique)
RANS	Reynolds-averaged Navier–Stokes
RNA	Ribonucleic acid
SARS	Severe acute respiratory syndrome
SD	Standard deviation
SF_6	Sulphur hexafluoride gas
SST	Shear stress transport model – a specific model for simulating turbulence effects in RANS
TUAS	Turku University of Applied Sciences
URANS	Unsteady RANS
VM	Virus medium
WALE model	Wall-adapting local eddy-viscosity model – a specific model for simulating small-scale turbulence effects in LES
ZDV	Zonal downward ventilation

Contents

1. Introduction

1.1. General introduction

Since the SARS 2003 outbreak, HCWs caring for patients infected with various emerging/re-emerging viruses (Middle East respiratory syndrome, or MERS; avian and pandemic influenzas; Ebola) are now acutely aware of the potential risks to themselves, particularly through aerosol transmission [**1**]. The recent emergence of a novel zoonotic coronavirus, SARS-CoV-2 (causing coronavirus disease 2019, or Covid-19), from Wuhan, Hubei, China, which causes respiratory illness in humans, poses a new threat for both patients and healthcare workers (HCWs) alike [**2, 3**]. So far, about 90,000 HCWs, globally, have been estimated to be infected with SARS-CoV-2 [**4**], with overall infection rates of 10 to 30 per cent among those being tested [**5, 6**].

In recent years, several studies have demonstrated the presence of viable virus in the air around patients infected with influenza, respiratory syncytial virus and MERS, which raises concerns about the risks to HCWs of aerosol-transmitted viruses [**7–9**]. This has emphasised the need for a new way of thinking and assessing these risks, and of highlighting the very real potential threat to HCWs managing such patients. Therefore, if enhanced protection can be achieved using more informed and evidence-based environmental control methods, such as those to be investigated in this study, then this will potentially benefit all HCWs encountering these patients.

Additional non-respiratory bacterial agents (for example, *C. difficile* and multidrug-resistant *S. aureus*), fungal agents (in terms of airborne spores) and viral infectious agents (norovirus, rotavirus) have been reviewed elsewhere [**10–13**]. However, for the purposes of this study, we are mainly focusing on airborne pathogens generated via the respiratory tract that may be disseminated during everyday respiratory activities, such as breathing, talking, coughing, sneezing, laughing and singing [**14–21**].

As part of an attempt to identify and characterise some of these potential risk factors for aerosol transmission, many studies have investigated the potential for various human respiratory activities (breathing, coughing, sneezing) [**22–25**], as well as respiratory support interventions (for example, oxygen masks and nebulisers) [**26**], to disseminate airborne infectious agents that can infect HCWs. Others have examined the protective effect of HCWs wearing masks [**27**], while experimental manikins have been used to assess aerosol exposure risk and the effectiveness of interventions [**28**].

However, less well known is the optimal design of mechanical ventilation systems (including the supply air distribution method and the specific placement of exhaust and supply vents relative to the patient's bed) in single-bedded airborne infection isolation rooms (AIIRs). Ventilation rate and supply air distribution have a notable effect on room airflow patterns, aerosol transmission and HCW exposure in isolation rooms. Many guidelines [**29, 30, 31, 32**] give only general recommendations regarding the design of air distribution in terms of ventilation requirements. This is probably due to the limited knowledge available on this topic.

While many studies have examined different factors that potentially contribute to the risk of aerosol transmission of infectious agents, there is still no clear consensus on what the optimal strategies and parameters should be to provide better protection for people (such as HCWs) against airborne infections and pathogens [**33–35**]. This is a relatively new interdisciplinary field, and many factors are not fully understood [**32**]. Hence, there is a need for more collaborative research to enhance our understanding of how aerosols transmit infection and how to mitigate or prevent this [**36–38**]. Clearly, more investigation is needed of specific factors, such as different types of ventilation, in combination with the use of different types of personal protective equipment (PPE), like face masks, in order to find the optimal approach.

In previous studies, the research team had investigated scenarios with a moving manikin passing through opening/closing doors to simulate and assess how such everyday actions can lead to isolation-room containment failures [**39–42**].

This study takes this work one step further, in order to examine and quantitate the potential risk to HCWs under different ventilation, distance and PPE settings inside an isolation room, using various types of tracers. To assist with this and with other studies in this field, a lifelike breathing thermal manikin was utilized. The use of such humanlike, life-size breathing thermal manikins in these types of studies is well established [**43, 44**]. In an effort to enhance aerosol infection control for other emerging/re-emerging pathogens in the aftermath of SARS, other teams have used these breathing thermal manikins extensively, to further the understanding of aerosol/airborne transmission of infectious agents [**45–49**], particularly in experiments where the use of human volunteers was difficult, either practically or ethically. Hence, our approach of using a breathing thermal manikin as a simulated HCW who was being exposed to aerosolised infectious agents is well recognised and accepted.

Both inorganic (for example, gaseous SF_6) and organic live-attenuated vaccine virus tracers (that is, from FluMist/Fluenz Tetra vaccines) were used in this study. The live-attenuated influenza vaccine virus has been used in exposure experiments before [**50, 51**]. Using such tracers, this study enhances the accuracy of risk assessments for aerosol exposures (which are currently very approximate) for HCWs in AIIRs in hospitals. This data was used to validate the related computational fluid dynamics (CFD) models also developed as part of this study, which are now frequently used in hospital infection control risk assessment and modelling [**52, 53**].

1.2. Air distribution in isolation rooms

Ventilation rate and supply air distribution have a notable effect on room airflow patterns, aerosol spreading and HCW exposure in isolation rooms. However, there are only general guidelines or recommendations on how the air distribution should be designed and what airflow patterns would be beneficial for HCW protection. For example, Centers for Disease Control and Prevention (CDC) guidelines [**30**] and American Society of Heating, Refrigerating and Air-Conditioning Engineers (ASHRAE) standard 170-2018 [**29**] give some recommendations, but more information is needed regarding the design of effective air distribution solutions for HCW protection.

Existing guidelines and standards typically recommend the principle of total volume mixing air distribution with high ventilation rates for isolation rooms [**29, 30, 31, 32**]. This principle is based on dilution of contaminants throughout the whole space. The aim is to reach low concentration levels quickly in the whole room. In addition, negative pressure is recommended in AIIRs to prevent contaminants spreading to adjacent rooms.

The mixing principle, however, is an ideal goal and not always effective in practice. Especially, close to a contaminant source, the air dilution may not be sufficient and high exposures can occur [**54, 55**]. In hospital isolation rooms, HCWs typically work close to the patient when giving care and can be exposed to high concentrations of infectious contaminants.

The general principles for controlling worker exposure to contaminants are well known from literature and textbooks on industrial ventilation [**56**]. Local ventilation solutions, such as exhaust hoods, are often applied to capture the contaminants before they spread to the room air. Local exhaust ventilation in hospital rooms has been studied by Nielsen [**57**], Chau et al. [**58**] and Sadrizadeh and Holmberg [**59**], among others. In principle, an exhaust hood can be placed above the head of the patient to capture exhaled air.

However, exhaust hoods are not easily accepted in hospitals. They can be impractical as far as patient care is concerned and can have a negative effect on patient comfort.

Integrated local air jets and exhausts provide one method of local ventilation. Nielsen et al. [**60**], Melikov et al. [**61**] and Bivolarova et al. [**62**] have studied ventilation solutions integrated into the patient's bed. Such systems could be provided by bed manufacturers as additional options for their products. These kinds of methods are typically not part of the ventilation and air distribution design of the hospital building. In this study, we concentrate on air distribution methods that are part of the standard ventilation system and can be incorporated within the building's ventilation design.

In contaminant control ventilation, the design of the room air distribution is ideally based on a strategic approach to control the contaminant spreading [**56, 63**]. In this approach, the designer first selects the general principle of controlling the room flow pattern and contaminant transport. The designer must consider the flow phenomena existing in the room. These flows typically consist of the convective flows created by heat sources. In a hospital room, typical heat sources creating convective flows are persons (the patient and HCWs), equipment, lighting, the window surface (warm or cold) and solar radiation to the room surfaces. The designed air distribution can either try to utilise these flows or prevent them.

The direction of the exhalation jet affects the contaminant spreading. The direction is different depending on the posture of the person. Exhalation from a patient lying supine is pointed upwards, whereas a reclining patient produces a more horizontal jet and a sitting patient can even create a downward jet. Also, exhalation through the mouth produces a different jet compared to exhalation through the nose. The exhaled air is lighter than typical room air, and it creates an upward convective flow.

Basic room air distribution strategies can be divided into four categories: piston flow, stratification, zoning and mixing (**Figure 1.1**) [**56**]. Piston flow controls the whole room flow pattern by creating a unidirectional flow. Contaminants are transported towards the exhaust, and mixing is prevented. This strategy requires high flow rates and is possible only in special applications, such as operating theatres. The stratification strategy utilises the convective flows from heat sources and uses low-velocity-displacement air supply. Contaminants and heat are allowed to stratify to the upper part of the room, and the exhausts are placed there. Due to low-velocity air distribution, this strategy provides no means to control the actual room flow pattern or promote the dilution of contaminants. The zoning strategy aims to create mixing in certain parts of the room and allows stratification and convective flows to be created in other parts of the space, while the mixing strategy aims to mix the whole room air volume, dilute contaminants and avoid thermal stratification.

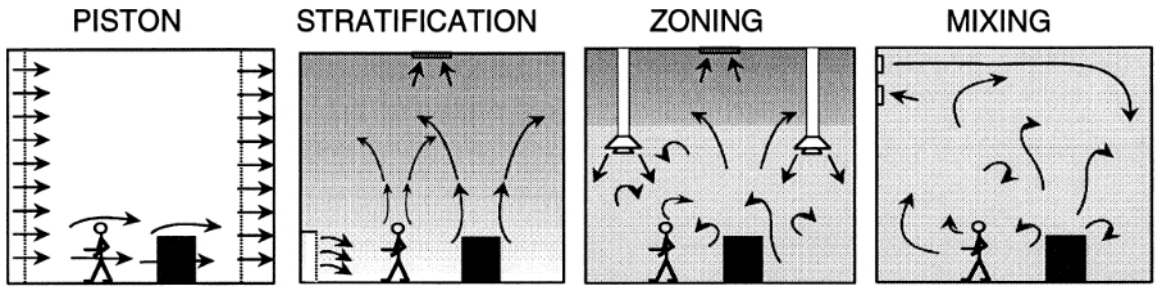

Figure 1.1. Strategic principles for room air distribution [**56**].

The stratification approach has been successfully applied, especially to large enclosures with warm contaminant sources. The convective flows (plumes) transport the contaminants to upper unoccupied parts of the space, and clean cool air from displacement units keeps the lower occupied part relatively clean.

Qian et al. [**45**] studied the performance of displacement air distribution in hospital patient rooms. They found that the convective flows from patients are not capable of transporting the exhaled contaminants to the upper part of the room. Due to lock-up phenomena, the exhaled contaminants can stay in the occupied zone in a stable, thermally stratified indoor environment, and hence high concentrations can occur in the breathing zone [**64**]. Qian et al. [**45**] concluded that displacement ventilation cannot be recommended, generally speaking, for patient rooms. On the other hand, Berlanga et al. [**65**] found that displacement ventilation can perform well in isolation rooms, in certain cases.

In a recent review paper, Yang et al. [**66**] provided an overview of different air distribution methods and their properties. They considered various types of air distribution methods, from local and personalised solutions to whole-room air distribution and ended up with 11 different classes of methods. The whole-room air distribution methods include mixing, displacement, diffuse ceiling ventilation, underfloor ventilation, wall/column attached ventilation, impinging jet ventilation and stratum ventilation. Protected occupied zone ventilation is a zoning system where the room is divided into zones with air curtains. Local air distribution methods include personalised ventilation, local exhaust ventilation and laminar airflow. Laminar airflow can also be used as a local piston-type air distribution that provides clean air locally. The examples of air distribution methods presented in Figure 1.2 are not a complete sample but give a picture of the variety of possible methods.

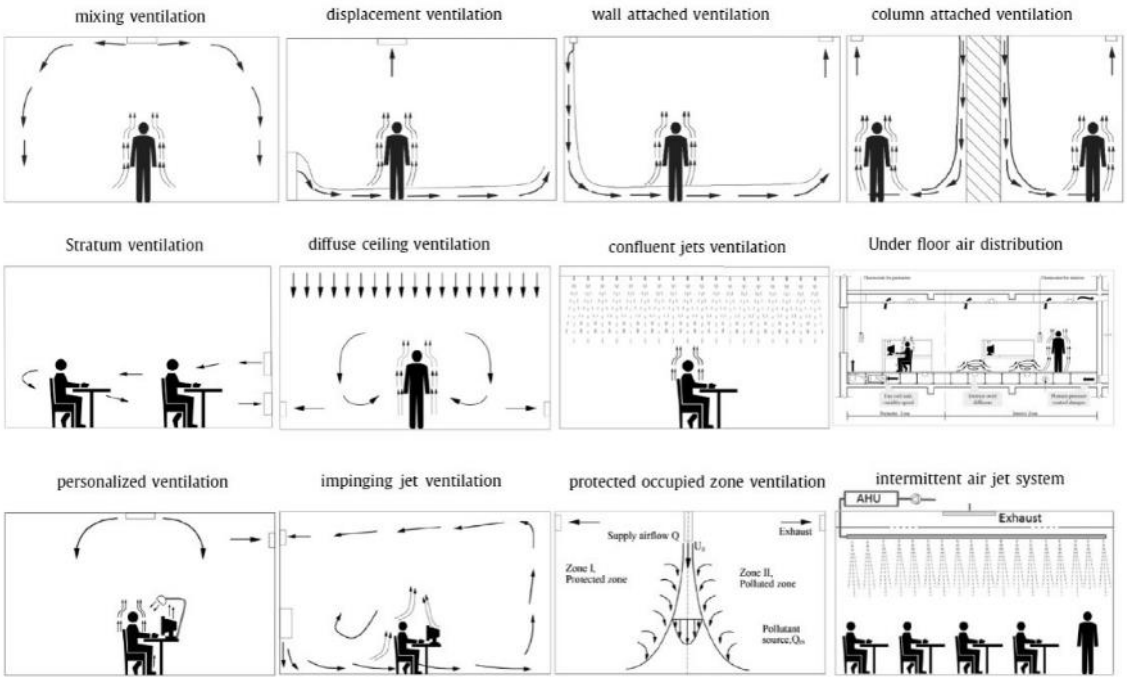

Figure 1.2. Examples of room air distribution methods [**66**].

The use of laminar supply air flow has been studied in isolation rooms by Qian et al. [**67**]. They found that supplying air downwards above the feet of the patient performed relatively well in removing potential air contaminants from that area. The flow pattern flushed the exhaled air towards the upper end of the bed away from the HCW's breathing zone. However, in their study the patient was lying flat on their back and exhaling through the mouth. The situation changes when the patient is in a reclined position and exhaling through the nose. Qian et al. [**68**] also examined other downward ventilation solutions in hospital environments. They found that supplying fresh air to the breathing zone can reduce exposure but that

further investigations need to be carried out to find the optimal solution. It should also be noted that they focused on the airborne cross-contamination between patients but not between patients and HCWs.

Also other types of ventilation modes for isolation rooms have been suggested and studied in the past. For instance, CDC guidelines [**30**] mention several air distribution methods, including horizontal stratum supply and vertical supply from the ceiling with laminar units. The guidelines recommend a supply velocity of around 0.5 m/s, with the exhaust being located on the far side of the room.

Huang and Tsao [**69**] studied the performance of stratum-type ventilation in isolation rooms. They found that the performance was not always optimal. Room obstacles and convective airflows can disturb the supply flow pattern, and the method can require high flow rates to perform properly. Cheong and Phua [**70**] studied downward supply from the ceiling and found that exhaust locations at floor level gave better results than exhausts in the ceiling.

ASHRAE standard 170-2018, 'Ventilation of health care facilities' [**29**], gives some recommendations regarding the air distribution in isolation rooms. It mentions the general principle that air movement should be from low- to high-concentration (clean to less-clean) areas but does not give more detailed instructions for the air distribution. Exhaust openings are recommended to be placed directly above the patient's bed or in the ceiling over the bed. In protective environment rooms or combined isolation/protection rooms, the standard recommends that supply diffusers are placed above the patient's bed.

ASHRAE's *HVAC Design Manual for Hospitals and Clinics* [**71**] does not provide detailed instructions for air distribution in isolation rooms. Laminar or radial diffusers are recommended for critical areas, but no recommendations are given for the airflow pattern.

In a British guide (HTM 03-01: Specialised Ventilation for Healthcare Premises: Part A – Design and Validation [**31**]), laminar ceiling units are recommended for air distribution with ventilation rates lower than 15 ACH. With higher ventilation rates, square or circular ceiling-mounted diffusers should be used. In another British guide [**72**], an alternative ventilation mode – a positive pressure ventilated lobby (PPVL) – is suggested for isolation rooms. In a PPVL, air is supplied to the anteroom, directed to the isolation room through a transfer air grille and exhausted from the en suite. However, not having a supply air diffuser in the isolation room reduces the flexibility of supply air distribution design and the control of the airflow patterns inside the room.

Generally, it seems that the research into air distribution in hospital isolation rooms is still at an early stage, and no clear consensus has yet been reached on the performance of different air distribution principles and methods. The available publications present results on specific systems in specific conditions, and it is difficult to draw general conclusions from them. Hence it appears that more research is needed to find a more systematic approach to air distribution design.

1.3. Aim of the study

The aim of this study was to investigate and characterise the risk of potential aerosol transmission of infectious agents from patients to their HCWs in typical encounter scenarios in hospital isolation rooms.

More specifically, the objective was to assess the effect of different air distribution modes, ventilation rates, the exhaust position, the distance between the patient and the HCW, and face masks on HCW exposure to patient-exhaled aerosols. The study was carried out in a controlled environment in a laboratory-built full-scale isolation-room model using smoke, gas, vaccine virus tracers and CFD modelling.

This report is divided into several sections, which cover different approaches to the investigation of HCW exposure to patient-exhaled airborne pathogens:

i) full-scale experiments with smoke and tracer gases

ii) CFD modelling

iii) live vaccine virus tracer experiments.

The final sections of the report provide a summary of the study's findings, and conclusions and recommendations.

2. Full-scale laboratory experiments using smoke and tracer gases

The research was carried out in the ventilation laboratory at Turku University of Applied Sciences (TUAS), Turku, Finland. The laboratory already had an isolation-room mock-up that the team had used to study containment failures of isolation rooms generated by door openings and passage of HCWs through them [**42, 73**]. Tracer gas measurements, smoke visualisations, air velocity and thermal comfort measurements are covered in this section to understand the interactions of different room airflows and their effects on HCW exposure to the exhaled air of the patient.

2.1. Methods

2.1.1. Isolation-room model

The laboratory experiments were carried out in a full-scale isolation-room model at TUAS' indoor environment laboratory. The model was made of cleanroom elements that isolated it from the larger laboratory hall. The isolation-room model was 4.7 m wide, 4.0 m long and 2.6 m high. In the experiments, both the HCW and the patient were simulated with breathing thermal manikins.

The HCW was simulated with a detailed breathing thermal manikin (Pernille manikin, PT Teknik, Denmark), and the patient was simulated with a simpler heated dummy. Both the manikin and the dummy had artificial lungs (that is, pumps connected to the mouth and nose with tubes) to simulate tidal breathing. The HCW manikin was set to inhale through the nose and exhale through the mouth. The patient dummy was set to inhale through the mouth and exhale through the nose. For both manikins, the volume of the breathing was set to conform to 10 L/min and the respiratory frequency to 14 breaths/min. These values correspond to typical adult breathing parameters [**22**].

The exhaled air was heated to 34 °C (but was not humidified), which is close to a typical temperature of exhaled air [**74**]. During the baseline experiments, the patient was lying supine on the bed with the backrest tilted 20° up from the horizontal plane. See **Figure 2.1** for an illustration of the isolation-room model and the manikins.

In this study, the effect of two modes of supply air distribution on the HCW's exposure to the patient's exhaled air was examined more closely: i) baseline overhead mixing ventilation (MV), and ii) local downward ventilation (LDV) with background mixing ventilation. In the MV case, the supply air was distributed along the ceiling through two multi-nozzle diffuser units (Halton DHN-595-3, Halton Oy, Finland) located side by side in the ceiling in the middle of the room. The total supply flow rate of the test room was *c.*170 L/s, which corresponds to 12 air changes per hour (ACH).

In the LDV case, the same nozzle diffusers were used, but one diffuser unit was placed in the ceiling above the patient's chest, and the other was put in the ceiling on the other side of the room. In the unit located above the patient, the nozzles were directed to create a downward flow capable of flushing the breathing zone of the patient. The flow rate through the diffuser above the patient unit was set to 40 L/s. The nozzles in the other diffuser unit (located on the other side of the room) were directed to supply the air along the ceiling in all directions (that is, to create background mixing ventilation). In this diffuser unit, the flow rate was set to 130 L/s. The total supply air flow rate corresponded to 12 ACH. The supply air temperature was kept at 19 °C throughout the experiments. The supply air diffusers and nozzle directions are shown in **Figure 2.2**.

In the baseline experimental set-up, the air was extracted through three different locations in the room: two ceiling exhausts and one floor-level exhaust. The locations of the supply air diffusers and exhaust grilles

are shown in **Figure 2.3**. The larger main exhausts (in the ceiling) had a total flow rate of 150 L/s, and the floor-level exhaust (simulating an ensuite exhaust) had a flow rate of 40 L/s. In total, the exhaust flow rate was 190 L/s. As the exhaust was higher than the supply flow rate, the isolation-room model had negative pressure of c.15 Pa compared to the adjacent spaces. This prevented tracers from escaping to the surrounding spaces. All exhausts had high-efficiency particulate air (HEPA) filters, and hence all the exhausted air was filtered immediately after evacuation from the isolation-room model.

A total heat load of 750 W was applied to the room (including the patient, the HCW, lighting, equipment and simulated solar load), raising the room air temperature to 22.5 °C. Solar load was simulated with four 1,020- x 550-mm radiant heating panels (Infraheat ALK 600 SL, Polarheat Oy, Finland) placed on the floor in the corners of the isolation room (see **Figure 2.3** for more details). The temperature of the room air was measured in the middle of the room at 100 cm above the floor, from the main exhausts and from the supply air diffusers. The temperatures were measured with thermistors (Craftemp, Sweden, 0.2 °C accuracy).

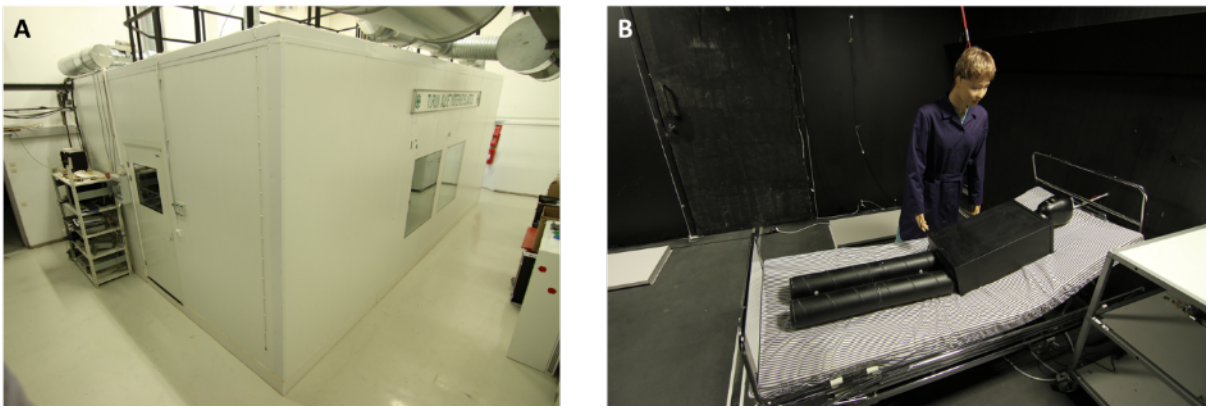

Figure 2.1. Isolation-room model seen from the outside (**A**) and the inside (**B**).

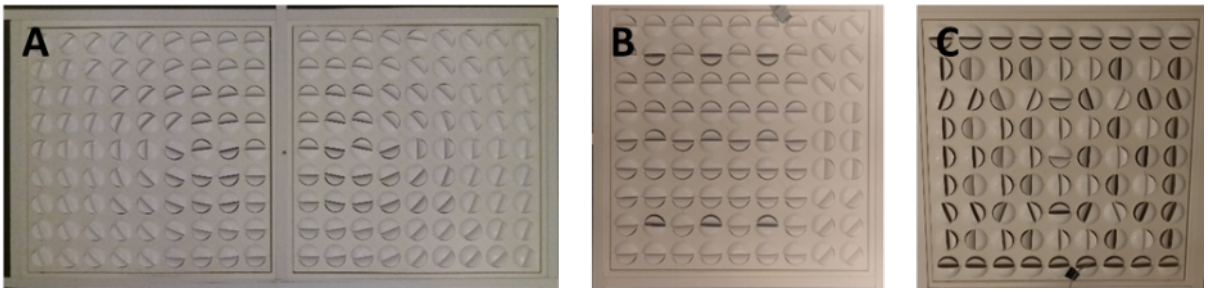

Figure 2.2. Supply diffusers and nozzle directions for overhead mixing ventilation (**A**) and local downward ventilation (**B** and **C**). **B** shows the diffuser that was positioned on the other side of the room, away from the patient's bed, and **C** shows the diffuser above the patient.

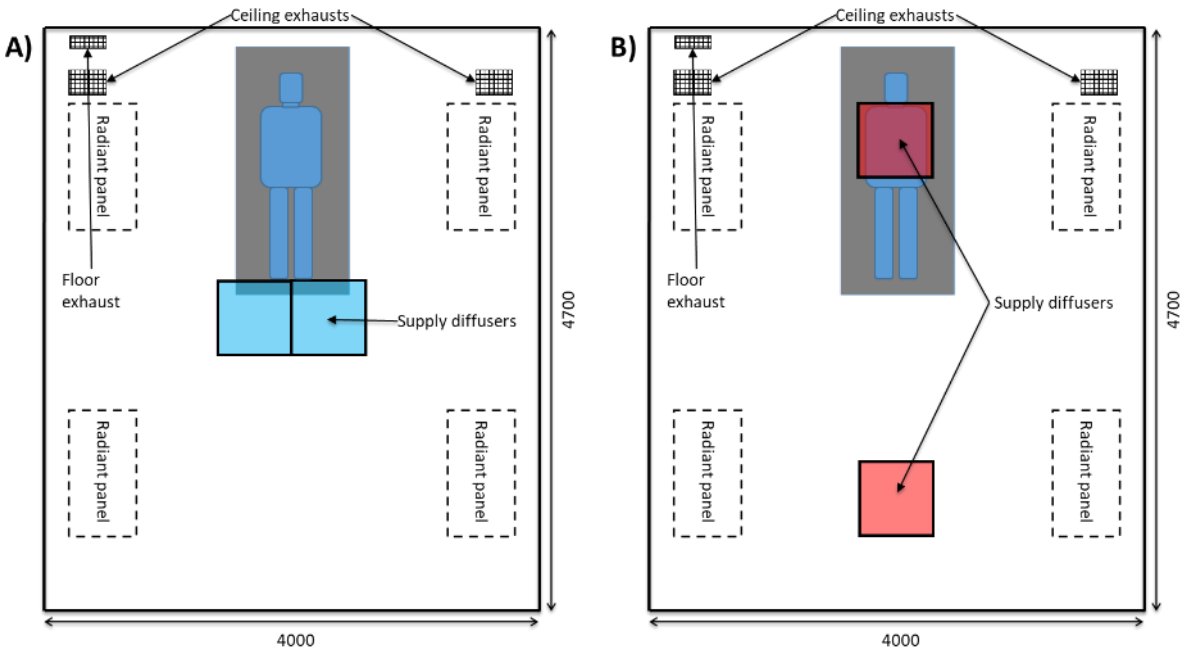

Figure 2.3. Set-ups for overhead mixing ventilation (**A**) and local downward ventilation (**B**). Room dimensions in mm.

2.1.2. Smoke visualisations

Smoke visualisations were carried out to assess qualitatively the room air flow patterns and the dispersion of the patient's exhalation.

The smoke used in the visualisations was generated with a smoke machine (JEM Techno Fog, JEM Pro-Fog Fluid, Martin, Denmark). According to the manufacturer's information (www.martin.com/en/site_elements/martin-hints_and_tips-particle-size-fluid-density-and-refractive-index-values, Martin, 2018, accessed 12 February 2020), the average particle size is 1.0–1.5 µm and thus capable of following the air flows realistically. The smoke was dosed to the exhalation of the patient manikin prior to being exhaled into the room. The supply air flow pattern was visualised by dosing smoke into the supply air duct.

In the test room, a light sheet was generated by an array of LED lights to make the smoke flow more clearly visible against the background (there was a black background to enhance the visibility of the smoke). Smoke movements were recorded with a digital camera (Sony α7 III, Sony Corporation, Japan). Still images extracted from the captured videos are shown in this report. The camera and the lights were positioned as far as possible from the manikins and the supply diffusers in order not to interfere with the room and the exhalation flows.

2.1.3. Air velocity measurements

Air velocities were measured to quantify the airflow velocity near the patient. Dantec hot-sphere anemometers (Dantec Dynamics A/S, Denmark) were used to measure the velocity distribution on a horizontal plane over the patient's bed at 1.1 m above the floor. The sensors were able to measure the magnitude of the air velocity but not the direction of the flow. Twenty sensors were attached, at 10-cm intervals, to a bar that ran across the patient's bed (see **Figure 2.4 A**). The bar was moved 10 cm at a time

(from the head of the bed towards the foot of the bed), after which the velocities were measured with each sensor at the same time. Hence a measurement plane with a 10-cm x 10-cm measurement grid was established over the bed (**Figure 2.4 B**).

The room air flows were allowed to stabilise for five minutes after the bar had been moved to a new measurement location in order to stabilise the transient effects caused by moving the sensor bar. Three-minute averages of the velocities were measured in each location.

The measurements were carried out for the overhead MV and the LDV with background mixing ventilation cases. The measurements were carried out for a baseline ventilation rate of 12 ACH with two ceiling exhaust grilles and one floor-level grille (see **Figure 2.4 B**). There was no HCW manikin inside the isolation room (it would have been in the way of the sensor bar), and the patient manikin was not breathing during the measurements.

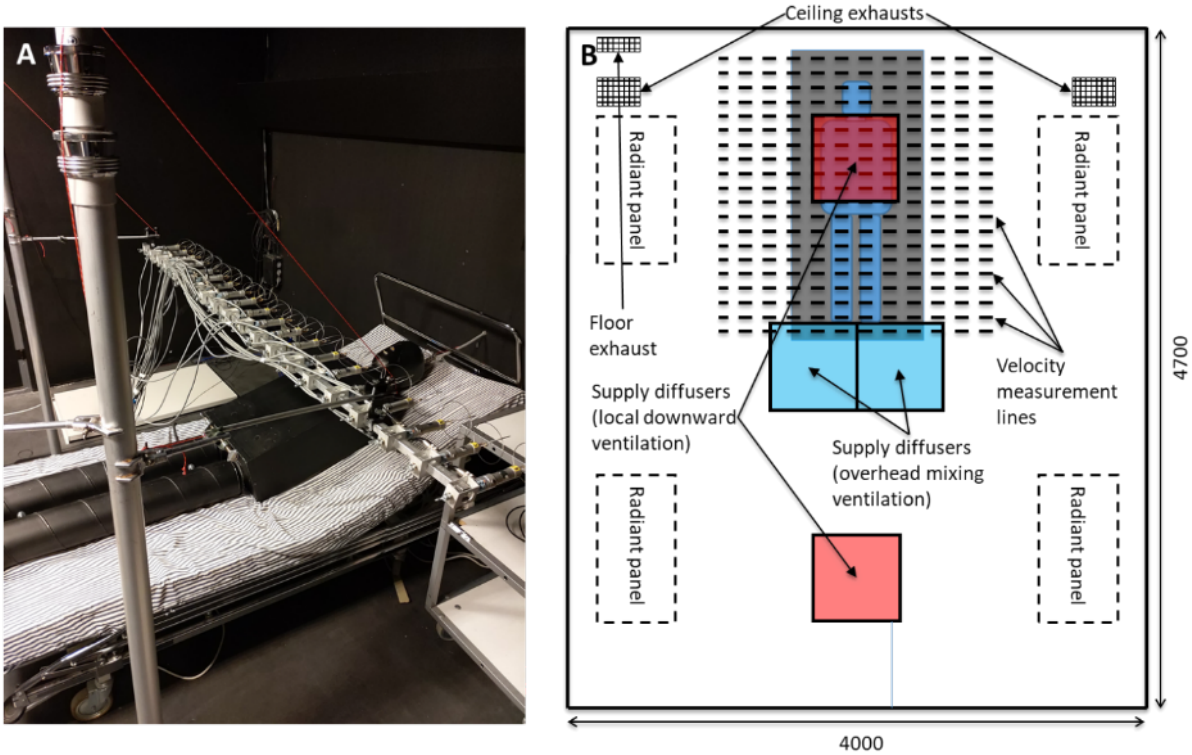

Figure 2.4. The air velocity measurement set-up.

2.1.4. Thermal comfort

The effect of air distribution on the thermal comfort of the patient was studied with a thermal manikin (Pernille, PT Teknik, Denmark). The manikin can simulate human-body heat exchange with the environment realistically and hence can be used to assess thermal comfort.

In the experiments, the thermal manikin was lying supine with a duvet cover on (see **Figure 2.5**). In the test cases, the manikin was dressed in a typical patient outfit consisting of underwear (underpants and bra), socks, long trousers and a long-sleeved shirt. The total clo value for the manikin lying on the bed (including the clothes, the duvet cover and the mattress) was measured as 1.5 clo. For thermal comfort assessment, the metabolic rate of the manikin was set to 0.9 met, which is close to adults at rest [**75**]. During the

measurements, the manikin was used in ‘comfort mode’, which means that the manikin was heated by simulating the thermal resistance of human skin.

In the experiments, whole-body thermal comfort was measured in steady-state conditions for both MV and LDV cases. The thermal comfort was assessed with equivalent temperature (T_{eq}) as well as with predicted mean vote (PMV) and predicted percentage of dissatisfied (PPD) indices. T_{eq} is a measure of the environmental conditions (air temperature, radiant heat, air movement) and does not take into account subjective factors like perception, sensation, clothing and metabolic rate (a detailed description of T_{eq} can be found in SAE [**76**] and Nilsson et al. [**77**]). On the other hand, PMV and PPD focus on perceived thermal comfort. PMV predicts the average thermal comfort vote of a large group of people on a seven-point thermal sensation scale (see **Table 2.1** for the scale). PPD predicts the average percentage of thermally dissatisfied persons among a large group of people. PPD is calculated from the PMV value. A more detailed description of the indices can be found in the ASHRAE/ANSI 55-2004 [**78**] and ISO 7730 [**79**] standards.

Figure 2.5. Thermal manikin lying in the bed with a duvet cover on during the thermal comfort measurements.

Table 2.1. The seven-point thermal sensation scale.

+3	Hot
+2	Warm
+1	Slightly warm
0	Neutral
-1	Slightly cool
-2	Cool
-3	Cold

2.1.5. Tracer gas measurements

Tracer gas measurements were carried out to quantitatively assess the exposure of the HCW to the exhaled air of the patient.

In the experiments, sulphur hexafluoride (SF_6) was dosed to the exhalation of the patient to simulate the spreading of airborne infections. Tracer gases are a generally accepted alternative that are widely used to simulate airborne contaminants and droplet nuclei (possibly carrying airborne infections) in exposure studies [**80-82**]. The exhalation of the patient consisted of a mixture of fresh air and SF_6. The mixture was formed by diluting 0.15 L/min of raw SF_6 with 10 L/min of fresh air. This mixture was discharged to the isolation-room model through the nostrils of the patient manikin. The breathing cycle of the two manikins was described earlier (see section **2.1.1. Isolation-room model**).

As SF_6 is much heavier than air (at ambient temperature and pressure conditions), the mass density of the exhaled mixture became 1.28 kg/m^3 and hence notably higher than the density of normally exhaled air, which is 1.15 kg/m^3 (at 34 °C, 100 per cent relative humidity). Thus, the exhaled air of the patient (a mixture of SF_6 and fresh air) was heated to 50 °C to compensate for the density difference. The heating reduced the density of the mixture to 1.15 kg/m^3, and hence the heated mixture realistically simulated the normal density of exhaled air at a temperature of 34 °C.

The tracer gas concentration was measured from the room exhausts and from the inhalation of the HCW manikin during each experiment. The sampling was carried out with a multi-gas analyser (Gasera One Pulse, Gasera Oy, Finland). The background concentration (in the surrounding laboratory and in the test room) was measured before each experiment. After the background concentration measurements had been carried out, the tracer supply was turned on and the isolation room concentration was monitored until a steady-state condition was reached. Once the steady state had been reached, the exhaust concentrations were monitored for 30 minutes. Then the inhaled concentration of the HCW manikin was monitored for an hour. After the HCW inhalation monitoring was over, the exhaust concentrations were again monitored for 30 minutes. The sampling interval of the gas analyser was about 45 s. The concentration monitoring times were considered long enough to produce low uncertainty for the concentration averages used for the HCW exposure assessment [**82**].

The HCW's exposure to the patient-exhaled tracer gas was assessed with two different indices: i) the susceptible exposure index and ii) the intake fraction. Both indices are well known and have been used in past exposure assessment studies [**28, 67**, **83-86**]. The susceptible exposure index (ε) describes the ratio between the local (inhaled) concentration and the concentration in the exhaust and is defined as:

$$\varepsilon = \frac{C_i(t) - C_s(t)}{C_e(t) - C_s(t)}, \quad (1)$$

where C_i is the tracer gas concentration in the HCW inhalation, C_s the concentration in the supply air and C_e the concentration in the exhaust. If the SF_6 concentration is taken to be 0 in the supply air (the concentration in outdoor air is very low and hence it can be considered to be negligible) and by using averaged values in steady-state conditions, the susceptible exposure index becomes:

$$\varepsilon = \frac{C_i}{C_e}. \quad (2)$$

The intake fraction (IF) describes the ratio between the contaminant mass inhaled by the HCW and the contaminant mass released into the environment. The IF is defined as:

$$IF = \frac{m_i}{m_{exh}} = \frac{\int \dot{m}_i \, dt}{\int \dot{m}_{exh} \, dt} = \frac{\int Q_i(t) \cdot C_i(t) \, dt}{\int Q_{exh}(t) \cdot C_{exh}(t) \, dt}, \quad (3)$$

where m_i is the total contaminant mass inhaled by the HCW (during time t), m_{exh} is the total contaminant mass released (exhaled) to the room through the patient manikin nose (during time t), Q_i is the inhalation flow rate of the HCW manikin and Q_{exh} is the exhalation flow rate of the patient manikin. In the cases examined in this study, all the tracer released to the test room was removed through the exhausts, as the test room was isolated and in negative pressure compared to the surrounding spaces. Hence, the tracer gas mass released to the environment was defined based on the exhaust measurements.

In steady-state conditions, IF can be calculated as:

$$IF = \frac{Q_i \cdot C_i}{Q_{exh} \cdot C_{exh}}, \quad (4)$$

where Q_i is the average inhalation flow rate, C_i is the average concentration of SF_6 in the HCW inhalation, Q_{exh} is the average exhaust flow rate and C_{exh} is the average concentration of SF_6 in the exhaust.

2.1.6. Tracer gas measurement test cases

The tracer gas measurements were carried out for several experimental cases to assess the effect of different parameters on the spreading of the patient-exhaled airborne contaminants and the HCW's exposure to them.

The effect of distance from the source (patient)

The HCW's exposure to the exhaled air of the patient was examined in relation to four different HCW positions inside the isolation-room model: i) leaning over the patient (caregiving scenario), ii) standing next to the bed (for example, chatting with the patient), iii) standing at the foot of the bed (for instance, checking the patient's chart) and iv) standing far away from the patient (for example, getting equipment). See **Figure 2.6** for more details. The measurements were carried out for MV and for LDV with a 12-ACH ventilation rate, with exhausts in the corners of the ceiling and the backrest of the patient's bed raised 20°.

The effect of patient posture on HCW exposure

The previously described case (***the effect of distance from the source (patient)***) was tested with the patient lying supine with the backrest tilted 20° up from the horizontal plane. As patients may have their backrest tilted to different angles during the hospital stay and during HCW examinations, it was considered that different patient postures should be studied. Three different backrest positions were tested: i) flat, ii) tilted 20° up and iii) tilted 40° up. See **Figure 2.7** for illustrations of the different backrest angles. The effect of the different backrest angles was studied in relation to only one HCW position, that is, when the HCW was leaning over the patient. It was considered that the highest exposure would happen in this position, and hence this position was regarded as the most important case to examine. The measurements were carried out for MV and for LDV with a 12-ACH ventilation rate, with exhausts in the corners of the ceiling.

The effect of exhaust location on HCW exposure

Although exhausts have a very local contaminant-capturing effect, the location of the exhaust might still affect the HCW's exposure to the patient's exhaled air, especially if placed close to the patient. The effect of four different exhaust grille locations was investigated: i) in the corners of the room in the ceiling, ii) above the patient's head in the ceiling, iii) in the lighting panel above the bed on the wall, and iv) at floor level behind the bed. See **Figure 2.8** for illustrations of the different exhaust grille locations. For all exhaust location cases investigated, the HCW was leaning over the patient and the backrest of the patient's bed was tilted 20° up from the horizontal plane. The measurements were carried out for MV and LDV cases with a 12-ACH ventilation rate.

The effect of ventilation rate on HCW exposure

The effect of 4-, 6- and 12-ACH ventilation rates on HCW exposure was examined so that the results could be generalised to other space types besides isolation rooms. With LDV, the flow rate of the diffuser above the patient was kept constant – that is, at 40 L/s – and the flow rate of the background mixing ventilation diffuser (on the other side of the room) was adjusted so that the overall ventilation rate in the room corresponded to 4, 6 and 12 ACH. The number of nozzles was adjusted to keep the flow rate through each nozzle similar in each case and so that the throw pattern would resemble the 12-ACH case. The experiments were carried out for MV and LDV cases with the HCW manikin leaning over the patient (caregiving scenario) and with the backrest of the patient's bed tilted 20° up.

The effect of face masks on HCW exposure

PPE constitutes an important part of HCW protection against transmission of diseases when working in AIIRs. It was therefore considered important to investigate the effect of face masks on HCW exposure to airborne contaminants. FFP2 masks (corresponding roughly to N95) were chosen to be used in the study. Four different cases were studied: i) no masks on the HCW or the patient, ii) a mask on the HCW, iii) a mask on the patient and iv) masks on the HCW and the patient. In the experiments, the masks were placed on the manikins' faces as they would have been put on normally. However, the masks were not fit-tested, as the main objective was to suppress the exhalation jet. In all test cases, the HCW was leaning over the patient, with the backrest of the patient's bed tilted 20° up from the horizontal plane. Measurements were carried out for MV and LDV cases with a 12-ACH ventilation rate and with exhausts in the corners of the ceiling.

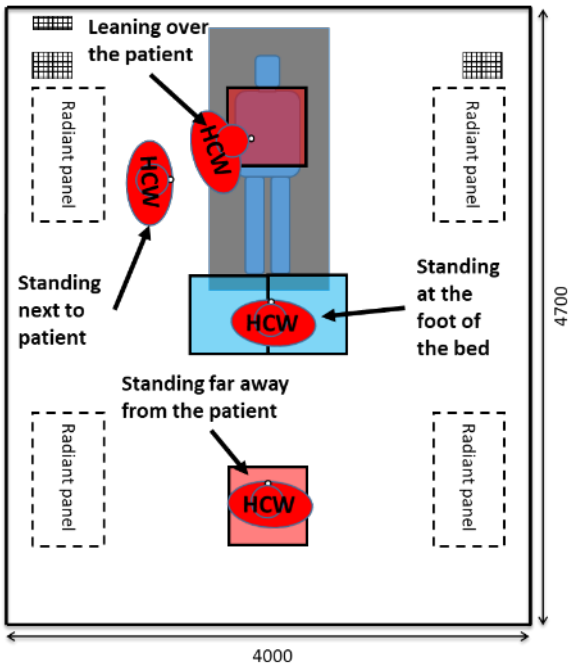

Figure 2.6. HCW locations inside the isolation-room model.

Figure 2.7. Patient postures with different bed backrest angles.

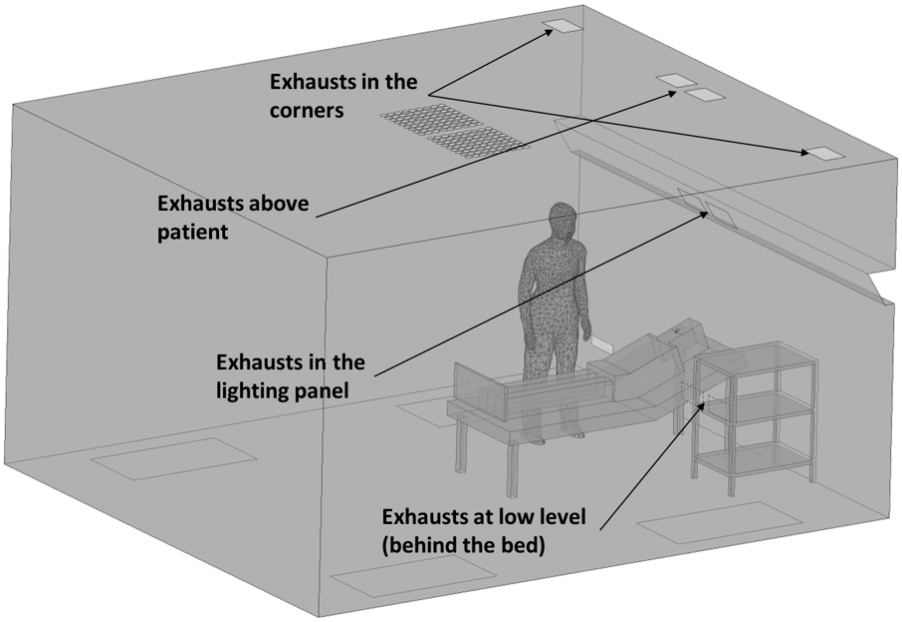

Figure 2.8. The different exhaust locations that were used to examine the effect of the exhaust grille location on HCW exposure.

2.2. Results

2.2.1. Smoke visualisations

The smoke visualisations of the supply air flow patterns and the spreading of the exhalation of the patient are shown in **Figures 2.9–2.11**.

The supply air flow patterns for MV and LDV are shown in **Figure 2.9**. With MV, the supply air flows along the ceiling over the whole room. The central part of the room (including the patient's bed area) is not effectively mixed by the supply airflow. LDV, on the other hand, flushes the breathing zones of the HCW and the patient effectively. The background mixing ventilation of LDV also supplies fresh air to the perimeter of the room. Hence, LDV appears to mix the air more effectively throughout the space than MV, especially in the critical areas close to the patient.

The dispersion of the exhaled air of the patient when the backrest of the bed was at different angles is shown in **Figure 2.10**. With LDV, the exhalation flow of the patient did not appear to enter the HCW's breathing zone at any of the angles. The local downward flow seemed to flush the breathing zone of the patient effectively and direct the exhalation away from the HCW's breathing zone. However, with MV, the exhalation seemed to enter the HCW's breathing zone and hence expose the HCW to high concentrations of the exhalation. This result was seen with all tested patient postures.

The effect of masking the patient on the spread of the exhalation for MV and LDV cases is shown in **Figure 2.11**. For both ventilation cases, similar effects were seen: the mask suppressed the formation of a free exhalation jet, and hence the exhaled air stayed close to the patient's head, where it was quickly mixed with room air. Thus, the mask prevented the exhalation from entering the breathing zone of the HCW. Masking the patient appeared to be an effective way to reduce the direct exposure of the HCW to the exhaled air of the patient regardless of the ventilation mode.

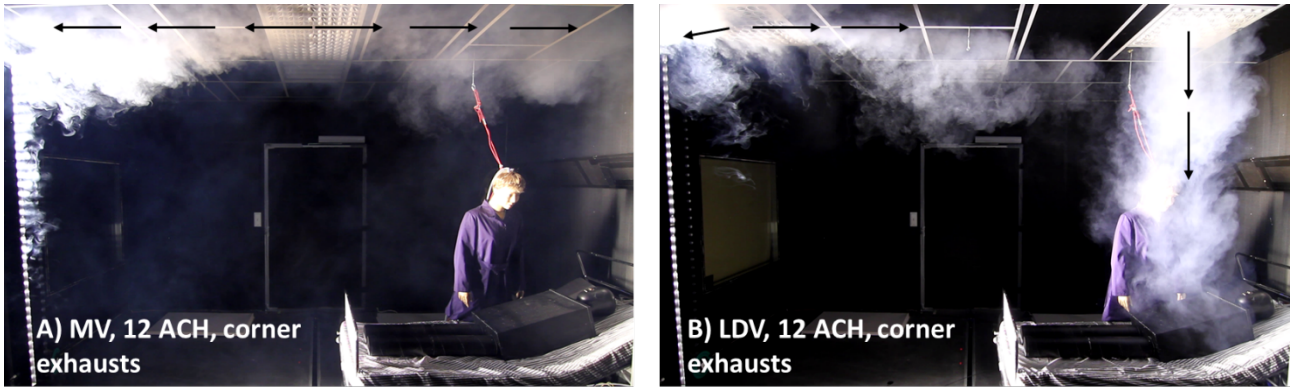

Figure 2.9. Smoke visualisations of the supply air flow patterns. Arrows show the supply air directions with overhead mixing ventilation (MV) (A) and with local downward ventilation (LDV) with background mixing ventilation (B). Exhausts were in the ceiling corners and the HCW was leaning over the patient in both cases.

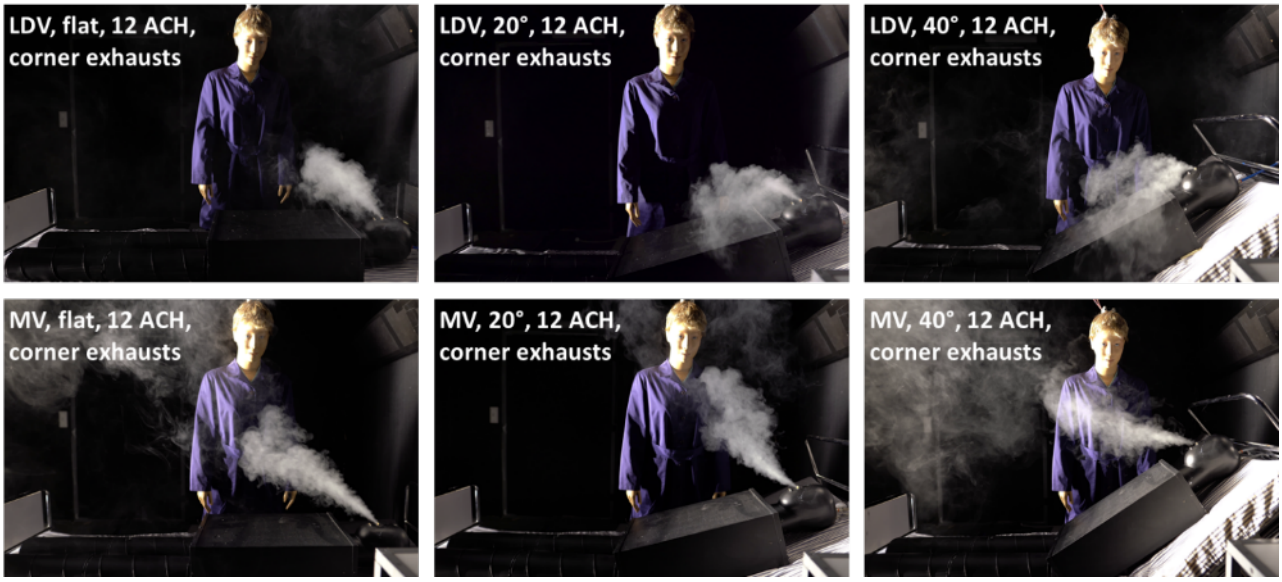

Figure 2.10. Smoke visualisations of the dispersion of the exhalation of the patient for mixing ventilation (MV) and local downward ventilation (LDV) cases when the backrest of the patient's bed was at different angles (flat, 20° and 40°). Exhausts were in the ceiling corners and the HCW was leaning over the patient in all cases.

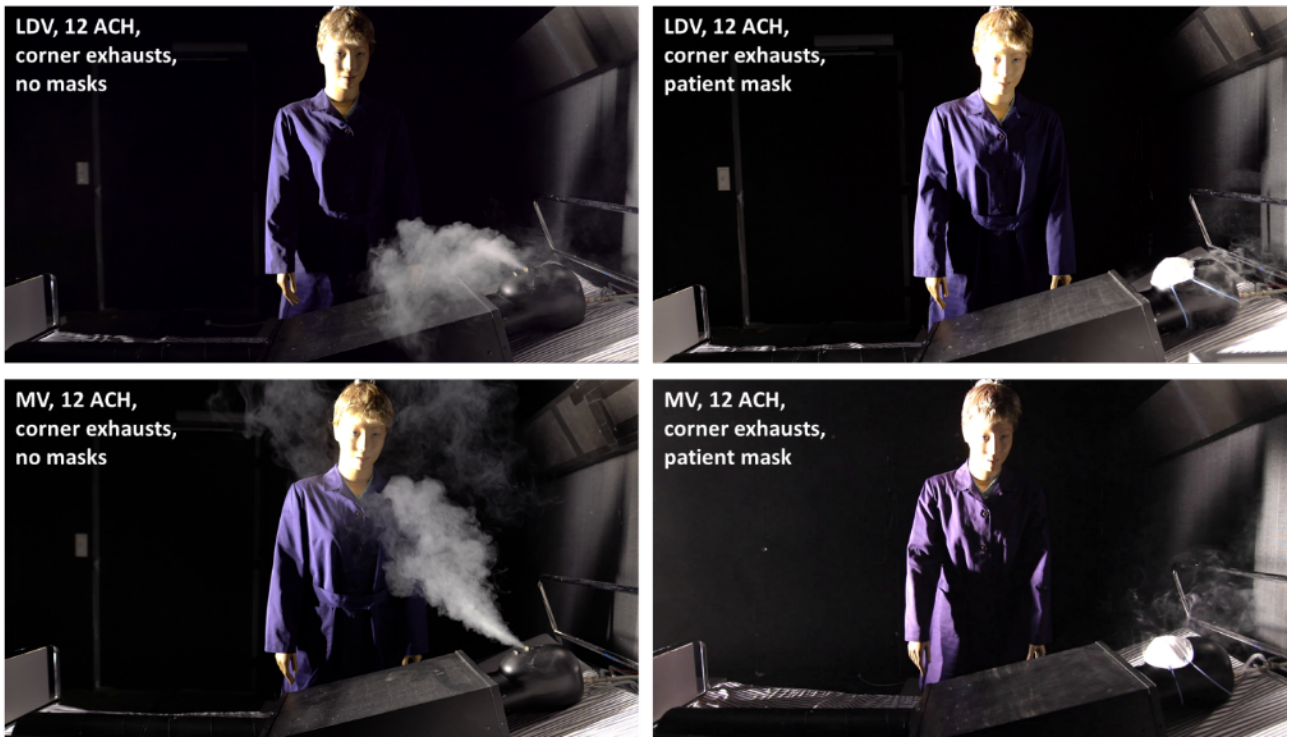

Figure 2.11. Smoke visualisations of the effect of masking the patient on exhalation dispersion for mixing ventilation (MV) and local downward ventilation (LDV) cases. The backrest of the patient's bed was tilted 20° up, the HCW was leaning over the patient and the exhausts were in the ceiling corners in all cases.

2.2.2. Air velocity measurements

Air velocity measurement results for different modes of supply air distribution are shown in **Figures 2.12** and **2.13**. As the figures show, MV (**Figure 2.12**) created only low velocities on the measurement plane (velocities always below 0.2 m/s) and hence did not flush and direct the patient's exhalation effectively away from the HCW's breathing zone around the patient's bed area. On the other hand, LDV (**Figure 2.13**) seemed to create notable air velocities over the patient's chest area. At other areas around the bed, the velocities were much lower. LDV appeared to create air movement in the critical area (from the point of view of reducing HCW exposure) and hence is expected to reduce the HCW's exposure to the exhaled air of the patient when near the patient compared to the MV case. However, the velocities generated by the LDV case might cause thermal discomfort for the patient. A more detailed description of thermal comfort is given in the Thermal comfort section 2.2.3.

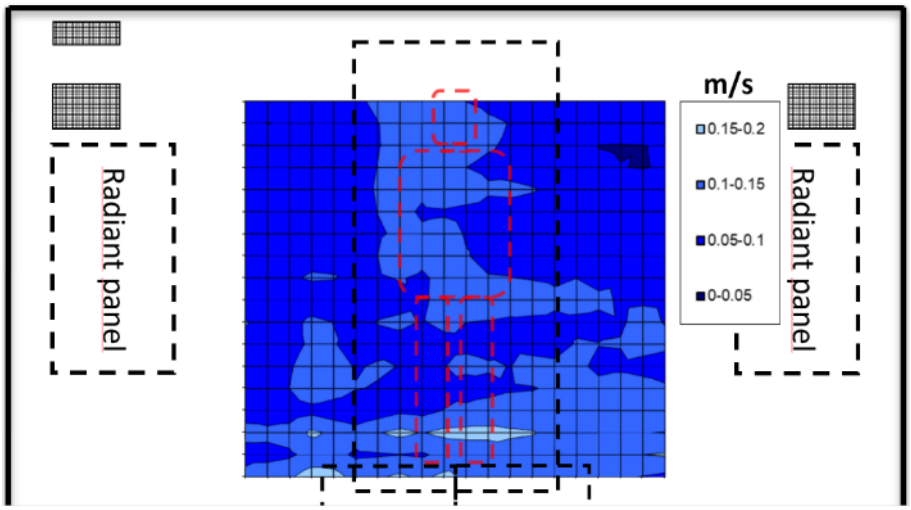

Figure 2.12. Air velocity measurement results for overhead mixing ventilation (12 ACH, corner exhausts).

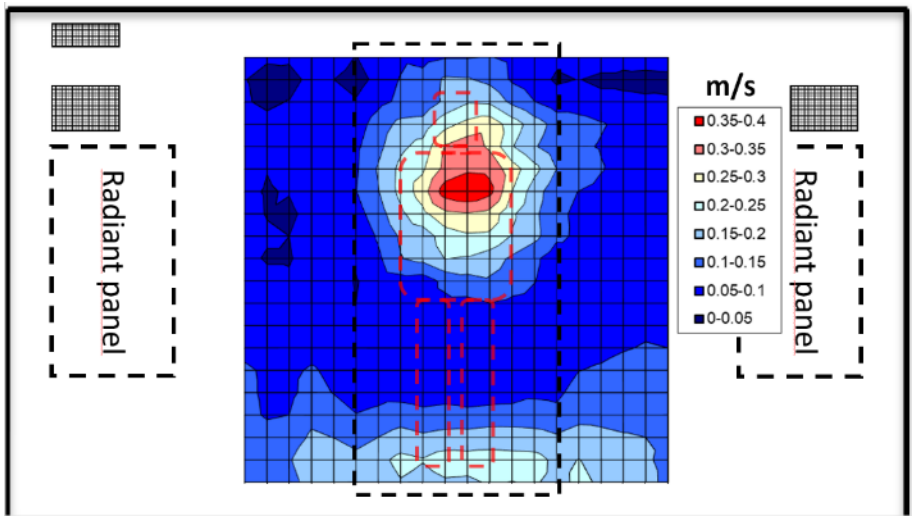

Figure 2.13. Air velocity measurement results for local downward ventilation with background mixing ventilation (12 ACH, corner exhausts).

2.2.3. Thermal comfort

The whole body equivalent temperatures measured with the thermal manikin are shown in **Table 2.2**. As the table shows, T_{eq} was the same as the average room temperature (estimated by the exhaust air temperature) in the MV case. With LDV, the T_{eq} was 1.7 °C lower than the average room temperature. The reduction was caused by the supply air flushing the patient's bed area.

Calculated values of PMV and PPD indices based on the measured T_{eq} values and 50 % relative humidity are shown in **Table 2.3**. PMV was close to neutral and PPD was low for the MV case. This was expected, as the environment in the isolation-room model was quite stable (no high air velocities or temperature gradients), at least at the occupied zone.

With LDV, the thermal environment was slightly cooler than with MV but still close to neutral. The PMV and PPD values fell within the category B limits in the EN ISO 15251 standard [**87**] and hence were acceptable. To fully comply with EN ISO 15251, other constraints must also be satisfied. Unfortunately, measurement of all of those parameters was beyond the scope of this study. Nevertheless, the investigation of thermal

comfort shown here implies that LDV could be considered acceptable and hence a practical solution from the point of view of the patient's thermal comfort.

Additionally, as higher room temperatures are allowed (up to 24–26 °C, depending on the standard [**29, 31, 32**]) than the temperature used in this study (22.5 °C), thermal comfort values can be adjusted. Calculations with different parameter values can be done utilising PMV and PPD equations [**79**] or by using online calculators, such as the CBE Thermal Comfort Tool (2019) (**https://comfort.cbe.berkeley.edu/EN**).

Table 2.2. Measured average room temperature (T) and equivalent temperature (T_{eq}) values. MV – mixing ventilation. LDV – local downward ventilation

Case	T (°C)	T_{eq} (°C)	T–T_{eq} (°C)
MV	22.6	22.6	0.0
LDV	22.5	20.8	1.7

Table 2.3. PMV and PPD values for the whole body with measured T_{eq} values.

	Parameters				Results	
Case	clo	met	T_{eq} (°C)	RH (%)	**PMV**	**PPD (%)**
MV	1.5	0.9	22.6	50	**0.1**	**5**
LDV	1.5	0.9	20.8	50	**-0.4**	**8**

2.2.4. Tracer gas measurements

Measured susceptible exposure index (ε) and IF values are shown in **Figures 2.14–2.18** for different test cases.

HCW exposure to the patient's exhaled air in various locations inside the isolation-room model with different tested supply air distribution modes is shown in **Figure 2.14**. Generally, with MV and LDV, the highest exposure was found close to the source (patient), as expected. As the distance between the HCW and the patient grew, the HCW exposure notably reduced. Similar results have been found in recent studies [**84, 85**].

In addition, the standard error of the results increased the closer to the source the HCW was (with MV and LDV). This was probably due to the cyclic exhalation and lack of mixing close to the patient. The results also showed that MV induced higher standard errors compared to LDV when the HCW was close to the contaminant source (that is, leaning over the patient). However, as the HCW's position was moved further away from the patient, the differences between the ventilation modes notably reduced.

HCW exposures with different patient bed backrest angles are shown in **Figure 2.15.** The results show that MV produced higher exposures with all backrest postures compared to LDV. It seemed that there were some differences between different backrest postures, but not much. The highest exposure was found with the backrest tilted 20° up from the horizontal plane. The standard error did not appear to change much between different backrest angles.

HCW exposure with different exhaust grille locations is shown in **Figure 2.16**. The lowest exposure for both ventilation modes (MV and LDV) was found when the exhaust grilles were in the lighting panel on wall

behind the patient's bed. Exhaust grilles in the lighting panel seemed to perform well especially with LDV. The low-level exhausts appeared to work poorly, especially with LDV.

The results show that LDV produces lower HCW exposure with all exhaust locations compared to MV. However, it is difficult to ascertain the effect of the exhaust location on its own, since it appeared that the location of the exhaust also slightly affected the supply air flow pattern, and hence the exposure might also have been affected by the changed supply flow patterns. Typically, the effect of the exhaust (capture effect) is quickly reduced when moving away from the vicinity of the exhaust location. Although there seems to be no clear consensus in the literature on the best exhaust location, there is growing evidence that low-level exhausts are not an optimal arrangement [**67, 69, 86**]. The results shown here also support the impression that low-level exhausts do not work as well as higher-level exhausts in the studied cases. However, there is also evidence that low-level exhausts can perform well too [**70, 88, 89**]. The supply air distribution method, together with the exhaust location, room configuration and boundary conditions, creates a system which needs to be evaluated as a whole. Clearly, this topic needs more examination before any final conclusions can be drawn.

The tracer gas measurement results for HCW exposure when the MV and LDV modes were set at different ventilation rates are shown in **Figure 2.17**. In this case, the exposure was evaluated with the IF index, which describes the ratio of the contaminant mass (tracer gas) inhaled by the HCW to the mass released to the environment. The exposure seemed to reduce notably when the ventilation rate was increased from 4 ACH to 12 ACH. Such a drastic reduction was not expected, especially with LDV, since the local downward flow, which flushed the patient's breathing zone, was kept constant (40 L/s). However, the overall mixing and dilution increases with an increasing ventilation rate, which can explain the trend seen in the results.

The effect of a FFP2 respiratory mask on HCW exposure in the MV and LDV cases is shown in **Figure 2.18**. The results show that masking the patient was an effective way to reduce the HCW's exposure to the exhaled air of the patient. While the FFP2 mask itself was not able to filter the gaseous tracer and could not therefore notably reduce the exposure when the HCW manikin was wearing the mask, it could still be beneficial against different-sized airborne particles [**90**]. The gaseous tracer used in this study modelled a worst-case scenario, where the mask is unable to filter inhaled particles present in the room. This could be due to side leakages, which can lead to poor filtering performance. It would have been more realistic to use a particle tracer, but that would have required consideration of a proper particle source and measuring method. That was not possible within this study but should be considered in future studies.

Nevertheless, when the patient wore the mask, it did obstruct the dispersion of the exhalation jet (and hence also the gaseous tracer) and prevented it from physically entering the breathing zone of the HCW.

There is now good evidence for the protective effect of masks [91], and the smoke visualisations and tracer gas measurements shown here further confirmthat masks can reduce the spread of the patient's exhalation jet into the HCW's breathing zone and, in turn, the HCW's exposure. However, compliance among staff and patients with usage of face masks can be an issue, as many factors (humidity, heat, breathing resistance, and so on) can cause discomfort [**92**] in long-term use. Additionally, some medical interventions (nasal tubes, for example) can hinder patients' usage of face masks. Nevertheless, it might still be acceptable for patients to wear a mask in certain scenarios (for example, during caregiving scenarios), although more research is needed before final conclusions can be drawn.

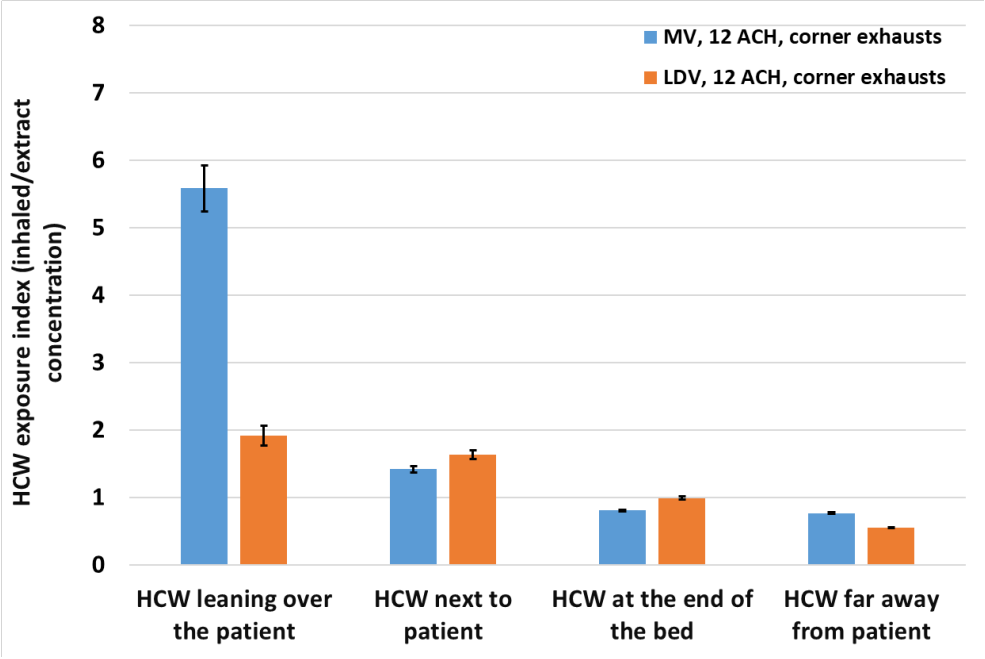

Figure 2.14. Tracer gas measurement results for HCW exposure in different locations inside the isolation room with different supply air distribution modes. The black whiskers represent the standard error.

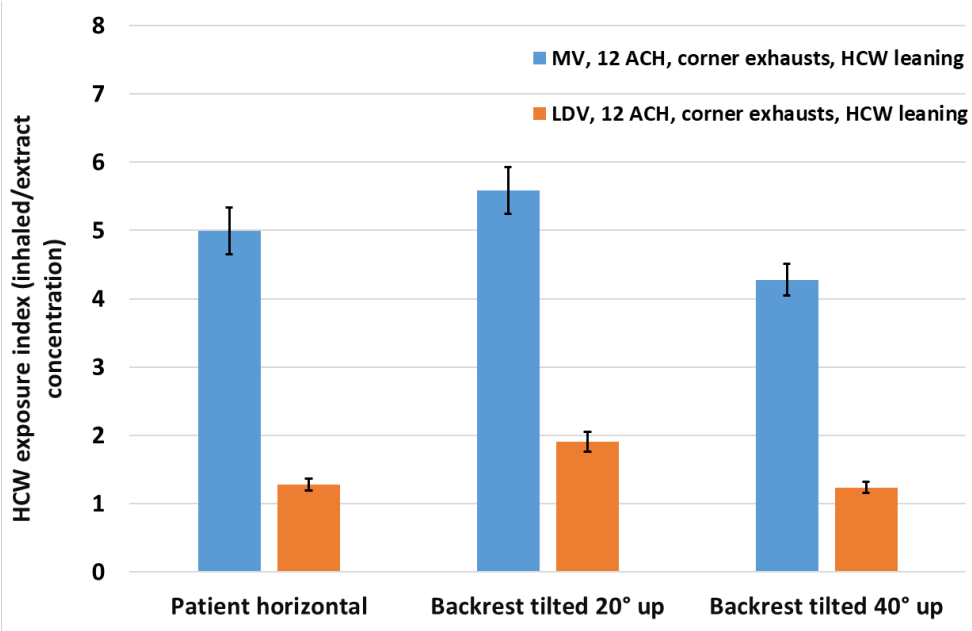

Figure 2.15. HCW exposure with different patient bed backrest angles. The black whiskers represent the standard error.

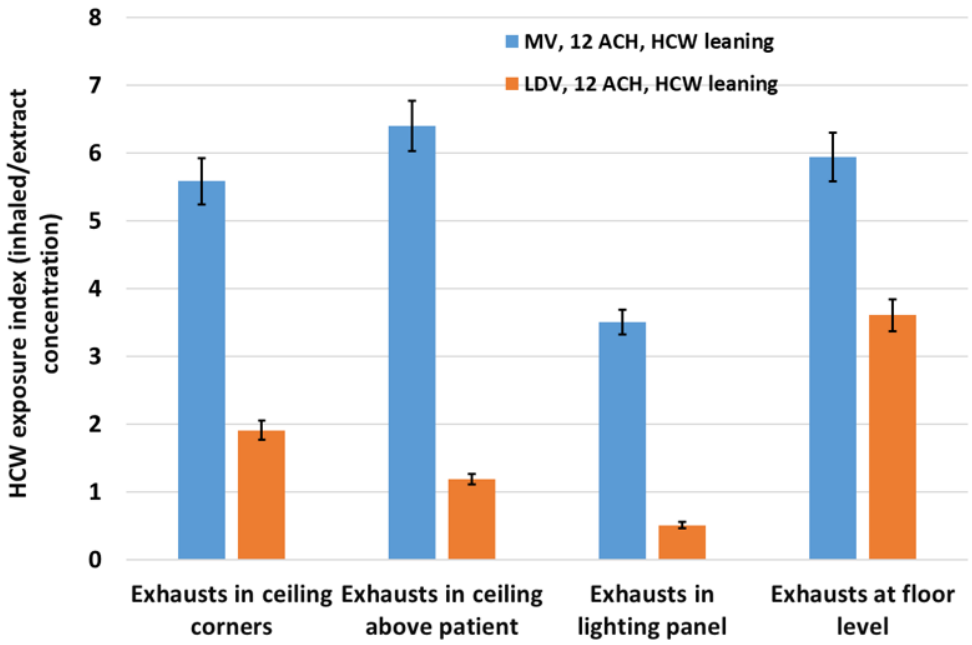

Figure 2.16. HCW exposure with different exhaust locations. The black whiskers represent the standard error.

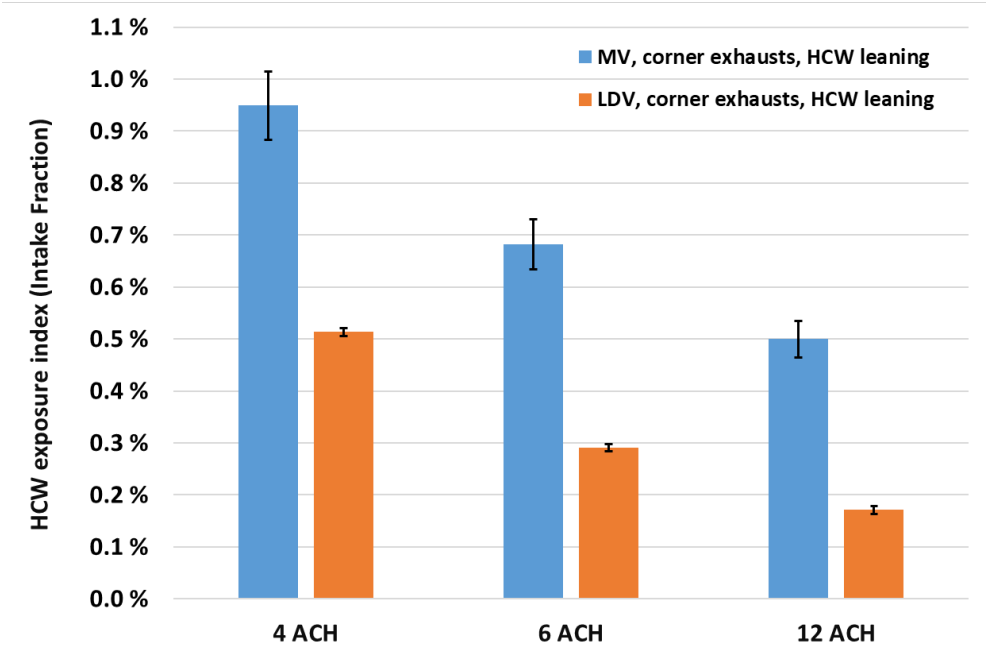

Figure 2.17. Tracer gas measurement results for the effect of ventilation rate on HCW exposure. The black whiskers represent the standard error.

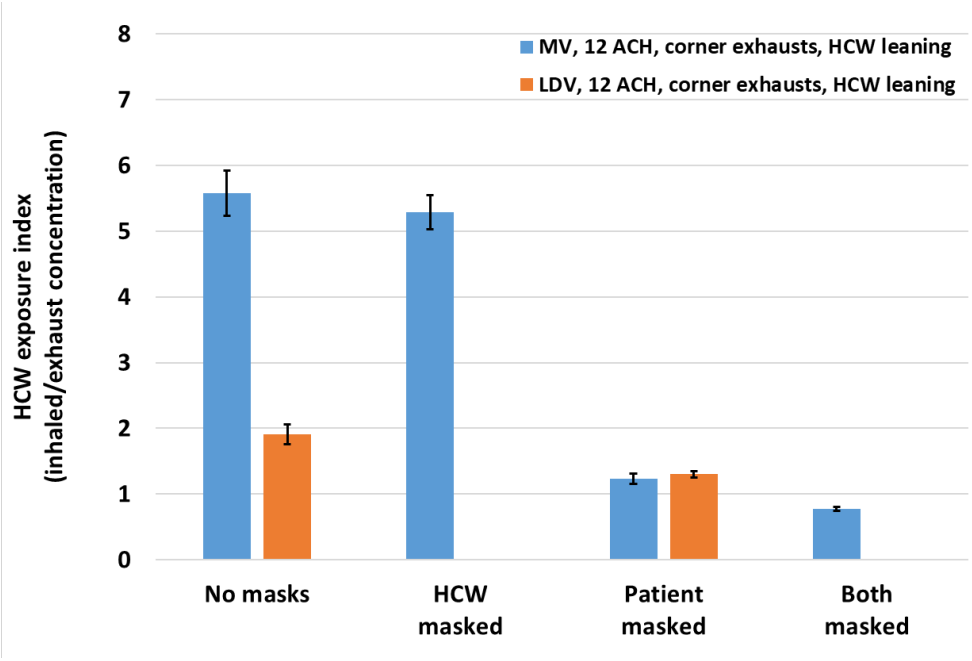

Figure 2.18. Tracer gas measurement results for the effect of respiratory masks (FFP2) on HCW exposure. The black whiskers represent the standard error. Local downward ventilation (LDV) was tested for the 'No masks' and 'Patient masked' cases only.

2.3. Summary of the findings from full-scale experiments

- Smoke visualisations showed that with MV, the exhalation of the patient can enter the HCW's breathing zone. LDV was able to flush the breathing zone of the patient effectively and direct the exhalation away from the breathing zone of the HCW.
- Thermal comfort, defined with PMV and PPD indices, was found to be slightly lower (that is, the thermal environment was cooler) with LDV than with MV, but close to neutral with both modes.
- Air velocities with MV were found to be low above the patient bed, resulting in less effective mixing around the patient's bed area. Higher velocities were measured with LDV, as part of the supply air flow was specifically directed into the patient's bed area, enabling efficient flushing of the patient's breathing zone.
- Higher air velocities with the LDV mode could be felt as draught. If this causes thermal comfort issues, the LDV mode could be turned on only during nursing periods, with MV used routinely at all other times, while the patient is alone in the isolation room.
- The highest exposures to patient-exhaled airborne pathogens occurred while the HCW was leaning over the patient – that is, during caregiving activities. The exposure was found to reduce drastically when the HCW was positioned at greater distances away from the patient.
- Patient posture (backrest elevation) had only a slight impact on the degree of HCW exposure during caregiving activities. For example, this was a much less significant factor than the ambient air distribution mode.
- The ventilation rate notably affected the degree of HCW exposure to patient-exhaled airborne pathogens. Increasing ventilation rates from 4 to 12 ACH enhanced the dilution of airborne contaminants and reduced the degree of HCW exposure.

- The closer to the patient any downstream exhausts are, the more efficient they are at capturing the patient's exhaled contaminants. Low-level (that is, floor-level) exhausts appeared not to be effective.
- Masking the patient suppressed the spread of the patient's exhaled contaminants into the HCW's breathing zone, substantially reducing the exposure of the HCW.

3. Computational fluid dynamics simulations

This section gives a description of the applied computational models and how the airflows and the spreading of the exhaled air of the patient were simulated with computational fluid dynamics (CFD). CFD is a general simulation technique that divides the 3D model of space into small volumes and then calculates the flow in the space numerically following the flow equations. The quality of the simulation depends on the applied simulation methods and the validity of the given boundary conditions. Typically, the time-averaged Reynolds-averaged Navier–Stokes (RANS) simulation method is applied because of the moderate computational power requirements. RANS simulation gives an averaged flow pattern and describes the turbulent flow fluctuations with turbulence models. If the flow pattern is unstable, which is usually the case in room airflows, the unsteady RANS (URANS) method can be applied, which can simulate the unsteady large-scale flow fluctuations. When the real turbulent flow structure is important for the simulated case, the LES (large-eddy simulation) method can be used. It simulates the time-dependent flow and does not use turbulence models. Only the eddies that are smaller than the simulation grid size are described by models. LES typically requires a dense computational grid and a small time step, and therefore requires high computational power.

CFD simulation has been widely applied to hospital ventilation, especially for modelling of operating and isolation rooms [**55, 69, 86, 93–96**]. When drawing conclusions from the CFD simulation results, their validity needs to be checked. This usually means that the simulation is compared against experimental data from a similar case. This ensures that the selected models and the given boundary conditions are valid for the case. Simulations are most useful for gaining a better understanding of the flow phenomena and the effects of different factors on the resulting flow structure.

3.1. Simulation methods

3.1.1. Room geometry and mesh

The computational geometry was a copy of the full-scale isolation-room model used in the experiments (**Figure 3.1**). It consisted of the model room, the HCW manikin, the patient manikin, a bed, a bedside table, and a lighting panel running across the wall above the bed. Mesh consisted of tetrahedral cells. Mesh refinement was used near the critical boundaries, like the HCW's nose and mouth, the patient's nose and mouth, and supply diffusers. Additionally, two refinement volumes were defined above the patient's bed close to the HCW's breathing zone in order to accurately model the exhalation flow patterns. See **Figure 3.2** for an illustration of the mesh and the refinement regions.

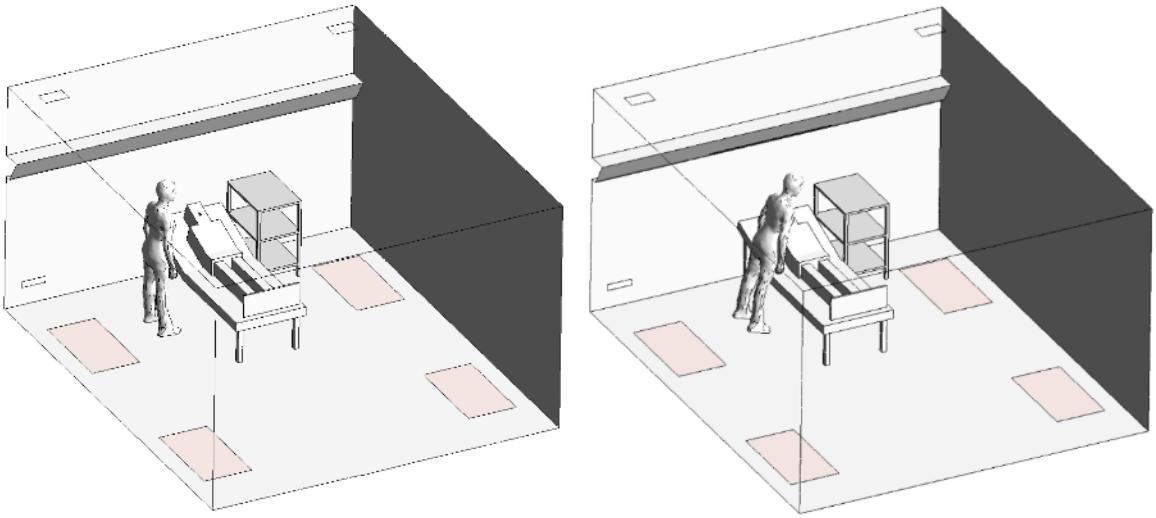

Figure 3.1. The geometry of the isolation-room model with the HCW and patient manikins. The HCW is standing beside the patient's bed in the image on the left and leaning over the patient in the image on the right.

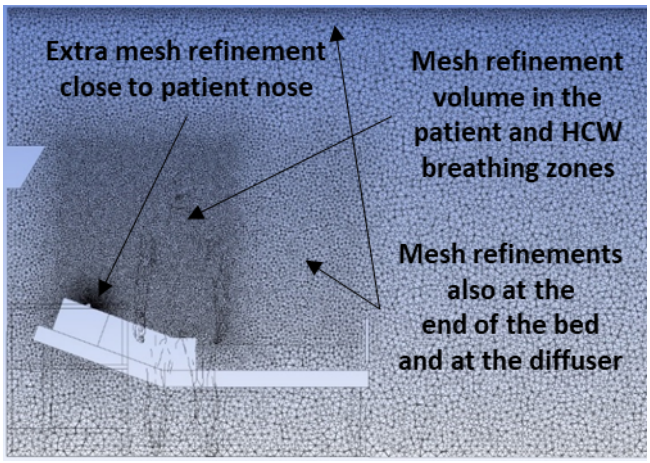

Figure 3.2. Illustration of the mesh (2.3 million nodes) used in the simulations.

Before the actual simulations, five different mesh sizes of between 0.2 million and 5.3 million nodes were tested to examine the effect of different mesh densities on the dispersion of the patient's exhalation and the subsequent HCW exposure to it. Based on these simulations, a grid of 2.3 million nodes was selected as the final grid. With coarser grids, the local effects near the HCW were not captured properly. However, a finer grid with 5.3 million nodes did not provide better results near the HCW.

In the simulations, the HCW was positioned standing next to the patient's bed (chatting with the patient) or leaning over the patient (giving care). The HCW's exposure was also examined in two additional locations for comparison: with the HCW at the end of the bed (checking the patient's chart), and with the HCW far away from the patient (getting equipment). However, in these locations the HCW manikin was replaced with monitoring points.

3.1.2. Geometry of the HCW and the patient

The geometry of the HCW manikin was created by scanning the real manikin using a camera and 3D scanning software (**Figure 3.3**). The patient manikin was a simple box model based on the dimensions of the real manikin. The shapes and dimensions of the nostrils and mouth openings used in CFD-model geometry for defining the breathing boundary conditions were similar to the real dimensions of these orifices for both manikins.

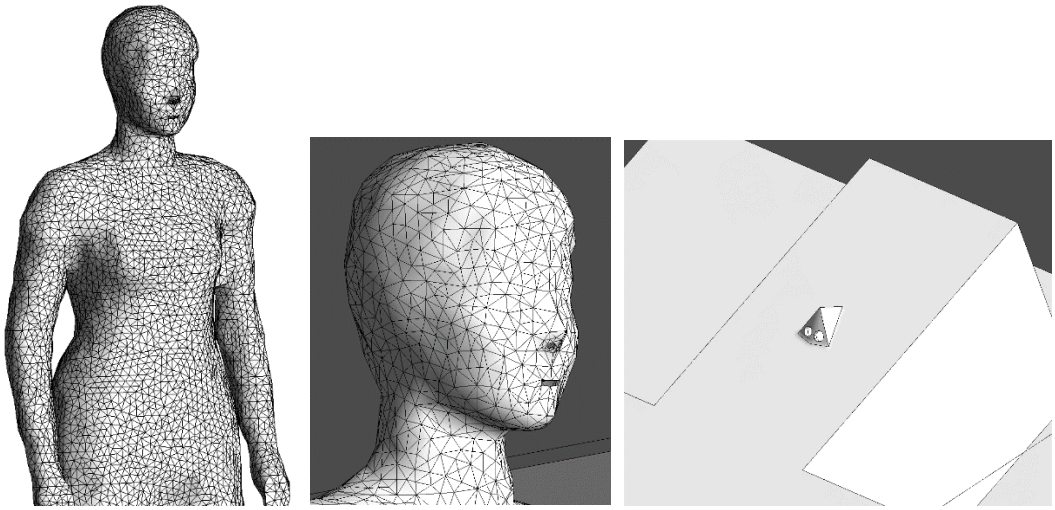

Figure 3.3. HCW manikin geometry and grid of the mouth (left), nose and nostrils (left and middle – close-up), with the more simplified geometry of the patient manikin (right).

3.1.3. Boundary and initial conditions

The boundary conditions were set to simulate the conditions of the full-scale experiments. The time step of the simulations was set to 0.1 s. Before the actual simulations, an initial simulation was carried out to stabilise the airflow patterns and concentration. It was allowed to run for 36,000 time steps (one hour) before the conditions reached a fully developed state, and was then used as initial conditions.

The air was extracted from the room through three rectangular exhaust openings. Two of the exhausts were larger in area and considered to be the main exhausts. The third exhaust was smaller and was located at a low level near the floor, simulating a toilet exhaust. The opening areas of the exhausts were the same as those used in the full-scale experiments.

The HCW manikin was set to exhale through the mouth and inhale through the nose. The patient manikin exhaled and inhaled through the nose. Otherwise, both manikins had the same breathing boundary conditions. The exhalation temperature was set to 34 °C. The respiratory frequency was set to 14 times/min. The breathing cycle consisted of a 1.9-s exhalation, a 0.2-s pause, a 1.9-s inhalation and a 0.2-s pause, with a volume of 10 L/min. These values are close to typical adult breathing parameters [**22**].

The exhalation air of the patient was marked in the simulations with a tracer gas concentration of 15,000 ppm. With a ventilation airflow rate of 170 L/s and a respiratory flow rate of 10 L/min, this provided a steady-state concentration of 15 ppm in the exhaust air.

A heat load of 600 W was applied to the model. This consisted of the patient (90 W), the HCW (90 W), lighting (120 W), and equipment and solar load (300 W), which was simulated with four heating panels, one in each corner of the room. The heat loads were given as a constant heat sources to the surfaces. It was

assumed that 50 per cent of the heat load was convective, which was set directly as heat output to heat-source surfaces, and 50 per cent was considered as radiation to other surfaces. This was done in order to simplify the simulations by avoiding thermal radiation modelling.

3.1.4. Numerical methods

All the simulations were carried out with Ansys CFX software (CFX, Ansys, Inc., PA, USA). The URANS modelling method was used to simulate the transient breathing and room airflows with a time step of 0.1 s. The simulations were carried out with a transient incompressible solver using the SIMPLE algorithm. The SST (Shear stress transport) model was applied for turbulence. The SST model has been found to be suitable for various scenarios, including modelling of room airflows [**97**]. The buoyance-driven effects were simulated with Boussinesq approximation. A second-order high-resolution spatial discretisation was used for all governing equations. A second-order implicit discretisation was used with respect to time. A passive scalar was set to model the dispersion of the patient-exhaled tracer gas. The exposure was quantified by a susceptible exposure index, as in the full-scale experiments (see **equation (2)**).

Additionally, the LES method was applied to specific cases to include turbulent flow structures in the simulations and to investigate their effect on the development and dispersion of the exhalation flows and subsequent HCW exposure to them. The wall-adapting local eddy-viscosity (WALE) sub-grid scale model was applied to model the smaller-than-grid-size eddies. The WALE model also works well close to boundary layers and hence is suitable for room airflow simulations [**98**]. A time step of 0.02 s and a central differencing scheme were used in the simulations.

3.2. Simulation cases

The different supply and exhaust set-ups of the test cases are described in **Table 3.1** (see section 3.3 for further details of supply air diffuser modelling). The basic exhaust set-up in all cases was two exhaust grilles in the corners of the ceiling with a 75-L/s flow rate and a floor-level exhaust with a 20-L/s flow rate. Additional exhaust locations were tested with mixing and zonal downward ventilation. The total airflow rate of the room was 170 L/s in all cases. This was the same as the supply flow rate in the full-scale experiments. In the experiments, however, the exhaust flow rate was slightly higher (190 L/s) because of the desired pressure difference to the surrounding spaces.

Table 3.1. Test cases with CFD simulation. MV – mixing ventilation; LDV – local downward ventilation; ZDV – zonal downward ventilation

	Supply air	**Exhaust**
1	MV	Ceiling/corners
2		Ceiling/above patient
3		Wall/lighting panel
4		Wall/floor level
5	LDV	Ceiling/corners
6	ZDV	Ceiling/corners
7		Wall/lighting panel
8		Wall/head level

3.3. Supply air diffuser modelling

3.3.1. Mixing ventilation

Mixing ventilation (MV) was modelled based on the full-scale laboratory experiments. The air was supplied to the room by two multi-nozzle diffusers located in the ceiling in the middle of the room (**Figures 3.4** and **3.5**). Both diffuser units consisted of 81 individual adjustable nozzles. In the simulations, circular openings were used to simulate the nozzles at the surface of the supply air diffuser for simplicity. The vertical velocity component from the nozzle openings was obtained by dividing the flow rate by the total area of the nozzle openings. The horizontal velocity components in the openings were chosen to give the correct flow direction based on the nozzle direction as well as the correct momentum flow rate of the jet. This set-up has been found to realistically simulate the supply flow through nozzle diffusers [**99**].

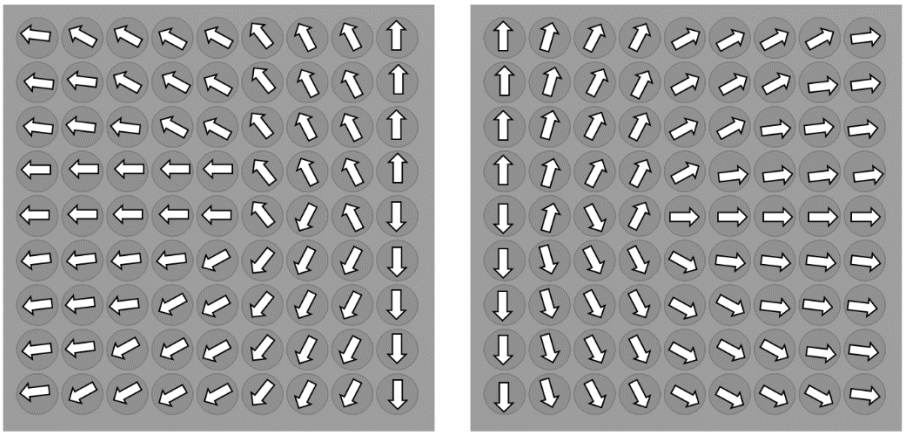

Figure 3.4. Nozzle set-up of the diffuser for mixing ventilation.

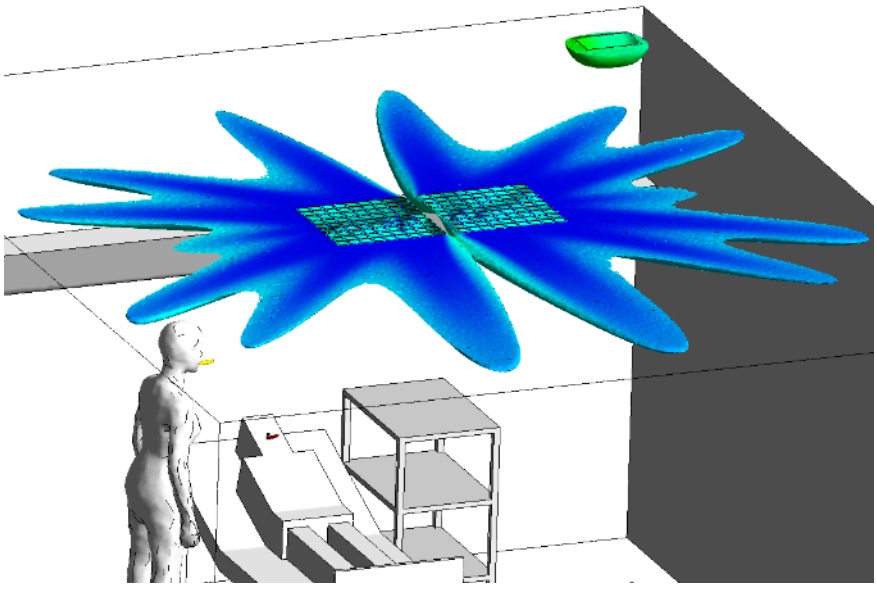

Figure 3.5. The supply air flow pattern with mixing ventilation presented as a velocity isosurface.

3.3.2. Local downward ventilation

Local downward ventilation (LDV) with background mixing ventilation was also simulated based on the full-scale experiments. In the simulations, one diffuser was placed above the patient's bed, which supplied air locally downwards, and another was placed on the other side of the room, which supplied air along the ceiling, thus creating background mixing ventilation (**Figure 3.6**). The downward flow was achieved by turning the nozzles of a multi-nozzle diffuser against each other (**Figure 3.7**). The collisions of the jets resulted in a downward total flow. The modelling principle was thus the same as with MV, with circular openings being used to simulate the nozzles at the surface of the supply air diffuser.

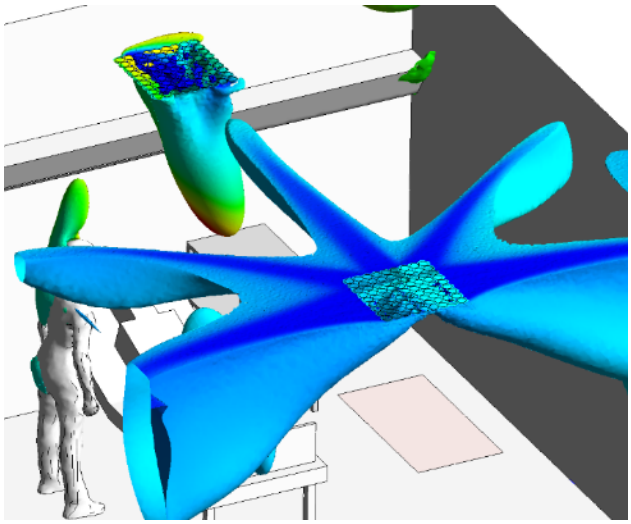

Figure 3.6. The supply air flow pattern with local downward ventilation presented as a velocity isosurface.

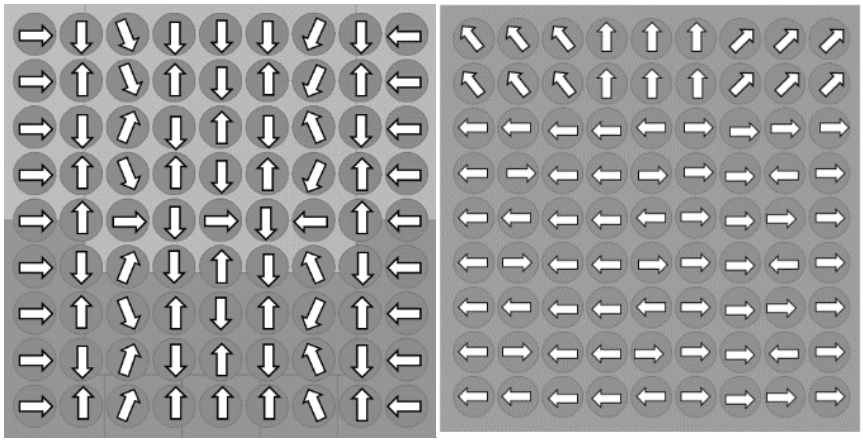

Figure 3.7. The nozzle set-ups of the diffusers for downward flow (left) and background mixing (right) seen from above. The locations of the diffusers in the room are shown in Figure 3.6.

3.3.3. Zonal downward ventilation

Zonal downward ventilation (ZDV) was tested with CFD simulation only. It was based on a nozzle duct placed above the patient's bed. The selected nozzle-duct model has a 300-degree nozzle area on the lower part and on the sides of the duct, whereas the top has no nozzles. This allows induction air to flow from

above and mix with the supply jets from the nozzles. The nozzle duct was 3.0 m long with a diameter of 0.25 m. The end of the duct was 0.2 m from the wall and the upper surface 0.2 m from the ceiling.

The CFD model is based on a model for a similar type of nozzle duct described by Koskela et al. [**100**]. The model uses momentum sources that present the flow of the room air induced by the nozzle jets. The induction airflow was assumed to be 2.5 times the supply flow rate. Momentum sources were placed at angles of ±30 degrees from the top of the duct (see Figure 3.8 A). The momentum sources were 0.1 m high and 5 degrees wide. The strength of the momentum sources was calculated from the induction air flow rate and the cross-sectional area of the flow (0.1 m x 2.0 m). Supply air was introduced as a mass source in the same volume as the momentum source. The principle of the model is shown in **Figure 3.8**.

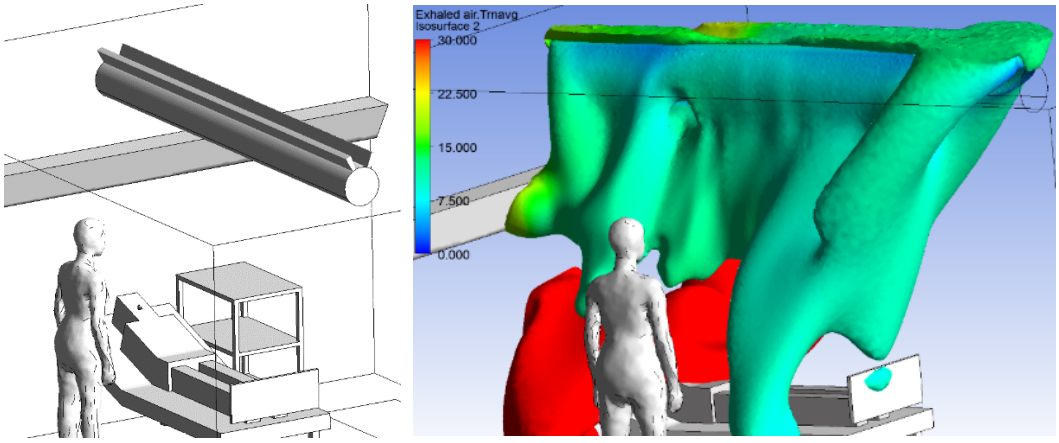

A **B**

Figure 3.8. Model of the nozzle duct diffuser with momentum sources of induction airflow at the edges of the nozzle sector (**A**), and a typical flow pattern (**B**) presented as a velocity isosurface.

3.4. CFD results

3.4.1. Mixing ventilation

Exposure

The modelled HCW exposure results with MV are shown in **Figure 3.9**. The CFD results with the URANS method depict similar trend as the measured exposures, i.e. the exposure increases the closer to the patient the HCW gets..

Flow pattern

The flow pattern is shown in **Figure 3.10**. The supply air spreads along the ceiling, and turns down the wall where the lighting panel affects the flow pattern. The downward flow along the wall is separated from the wall surface by the panel, and a circulating zone is formed above the panel. Without the panel, the supply flow would have continued further downwards along the wall. Lighting panels are common structures in hospital patient rooms, and the panel was therefore included in the room model.

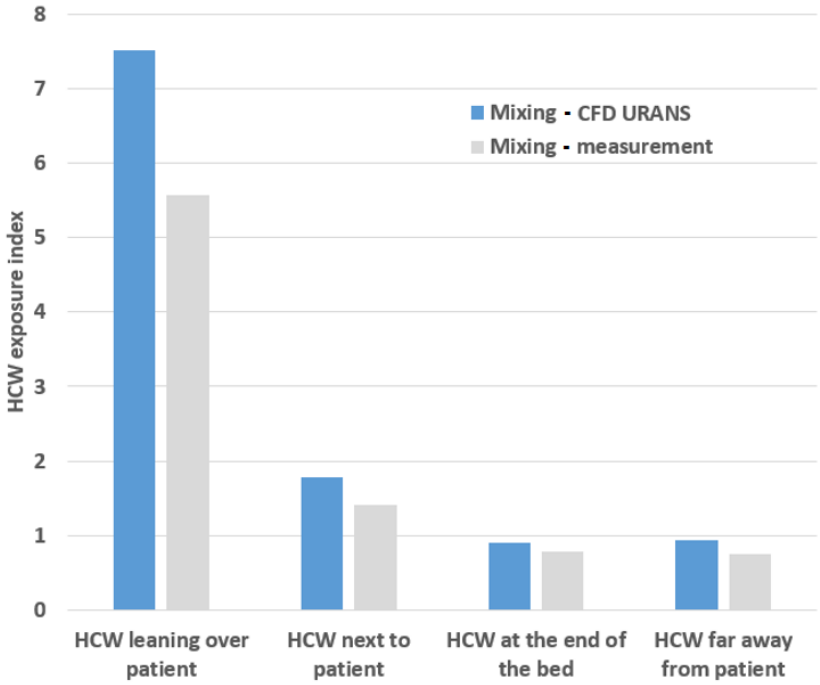

Figure 3.9. Computational fluid dynamics (CFD) simulation results for HCW exposure with mixing ventilation (12 ACH, corner exhausts, HCW leaning) compared to measurements.

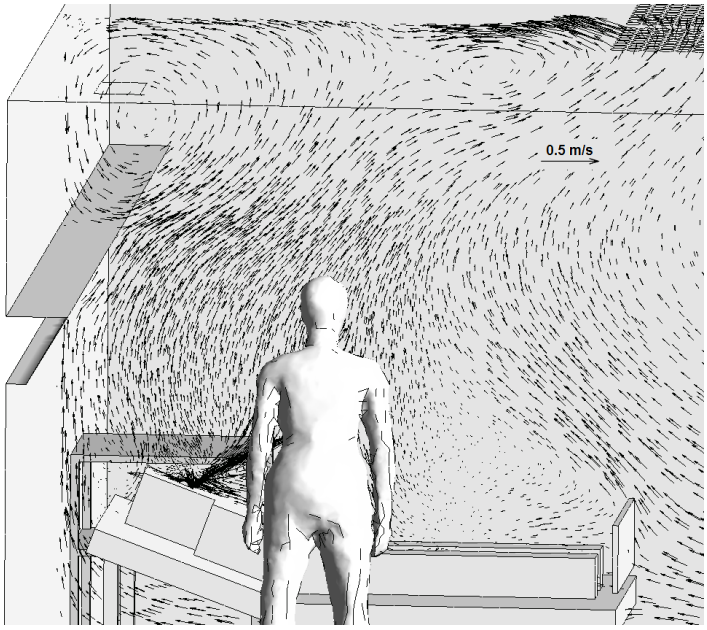

Figure 3.10. Flow pattern close to the HCW and the patient's bed (12 ACH, ceiling corner exhausts, HCW leaning, URANS).

The spreading of exhaled air can be seen in **Figures 3.11** and **3.12**. High concentrations exist above the patient and close to the HCW's breathing zone. The supply air spreads along the ceiling in all directions. The velocities above the bed are low, as can be seen in **Figure 3.13**. Therefore, the supply air is not able to dilute or flush the exhaled air from the HCW's breathing zone.

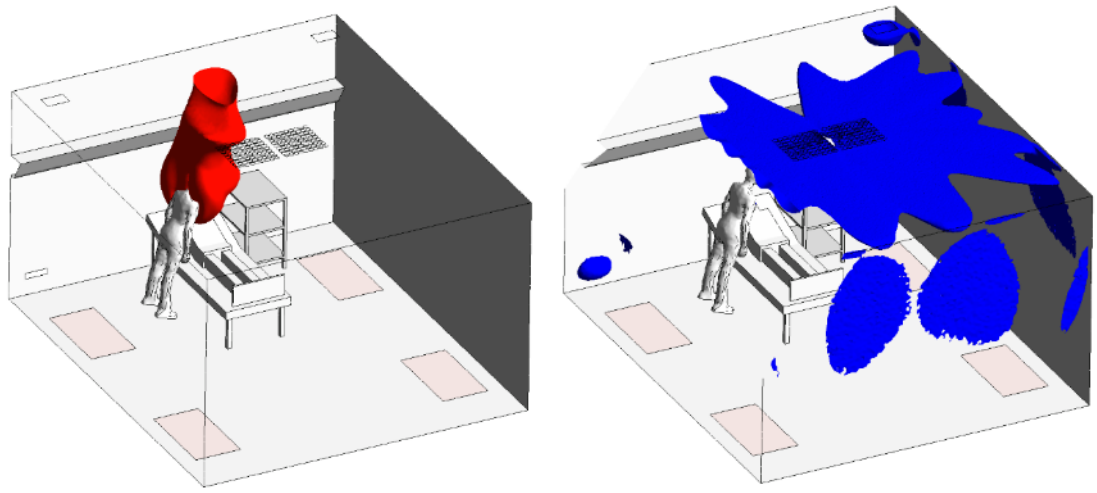

A **B**

Figure 3.11. Spreading of supply air and exhaled air with mixing ventilation (12 ACH, corner exhausts, HCW leaning, URANS), with a concentration isosurface of 30 ppm (**A**) and a velocity isosurface of 0.3 m/s (**B**).

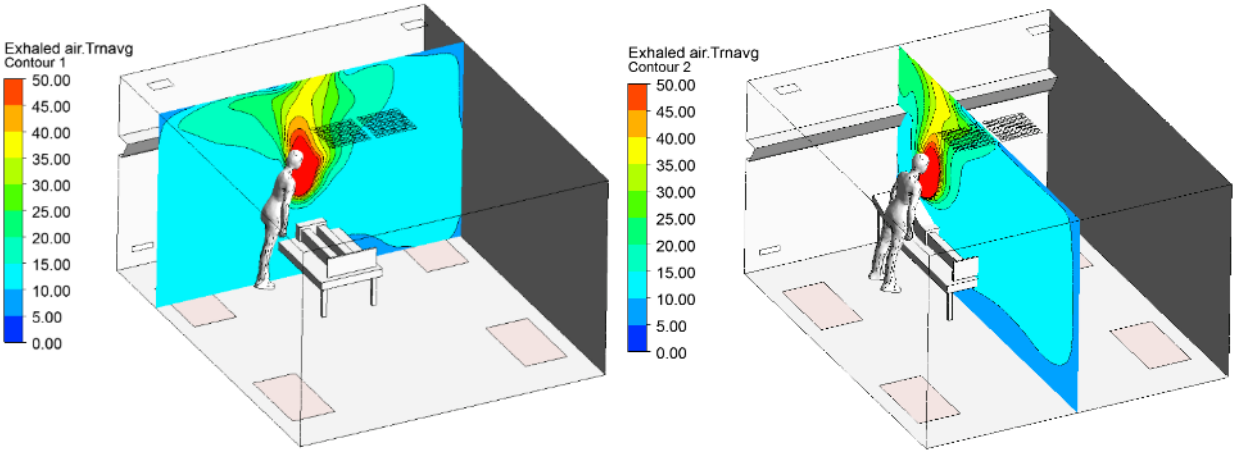

Figure 3.12. Contours of concentration with mixing ventilation (12 ACH, corner exhausts, HCW leaning, URANS).

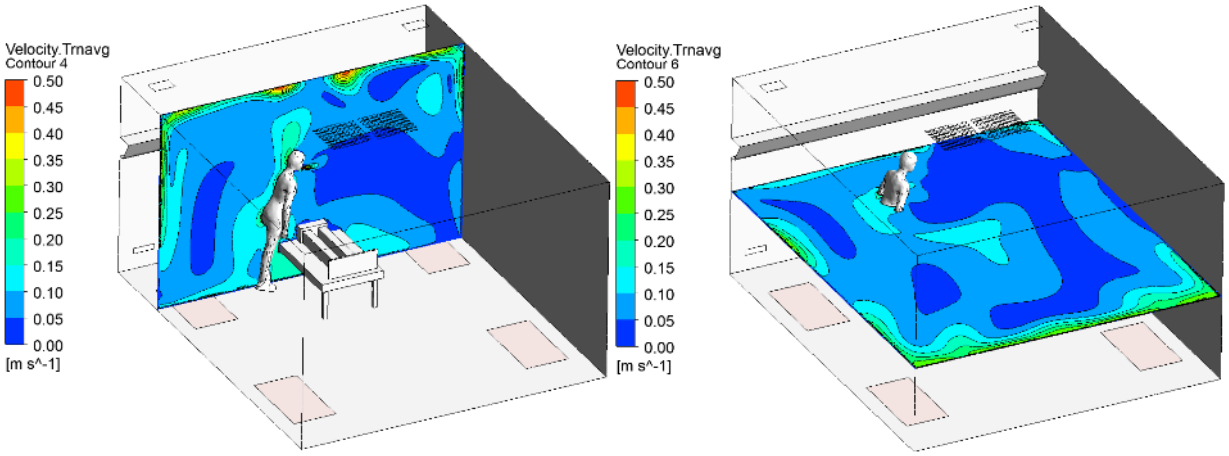

Figure 3.13. Velocity contours in a vertical plane and above the patient's head (1.1 m level) with mixing ventilation (12 ACH, ceiling corner exhausts, HCW leaning, URANS).

Effect of exhaust location

Based on the CFD results, the exhaust location has a notable effect on the HCW's exposure (**Figure 3.14**). In general, the most effective exhaust location was in the lighting panel over the bed. The reason for this can be seen in **Figure 3.15**. The exhaled air is partly captured by the lighting-panel exhaust before spreading to the room. In reality, this effect is probably not as strong as in simulations, due to disturbances and temporal variations in the flow pattern. Previous studies have found evidence supporting low [**70, 88, 89**] and ceiling-level exhausts [**67, 69, 86**] for different air distribution types. However, our findings suggest that none of those are optimal and that the exhaust should be closer to the patient's head. Nevertheless, in all cases the HCW's breathing zone is close to the high-concentration area, and even a small change in the HCW's location can change the exposure substantially, especially when the HCW is leaning over the patient.

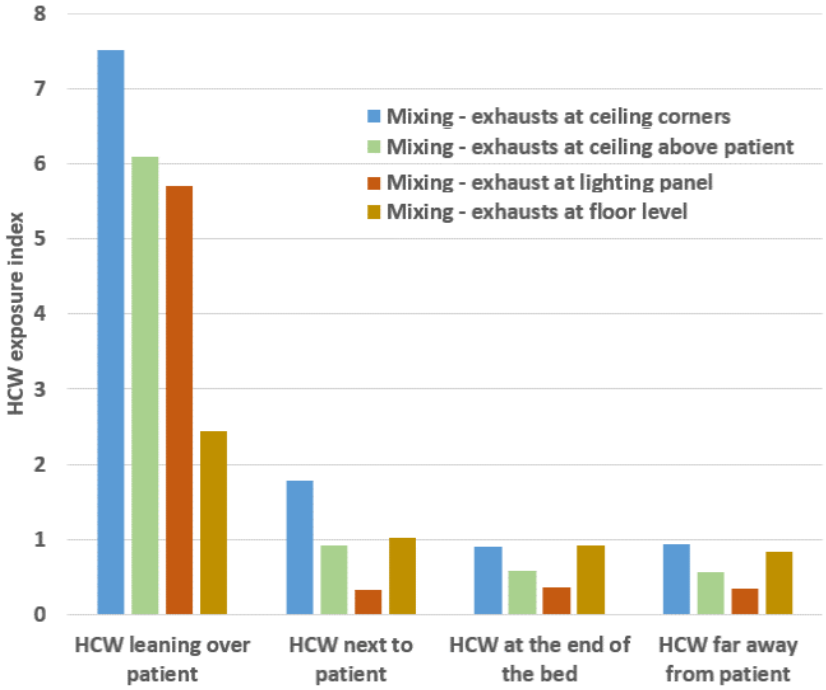

Figure 3.14. The CFD results for the effect of the exhaust location with mixing ventilation (12 ACH, URANS).

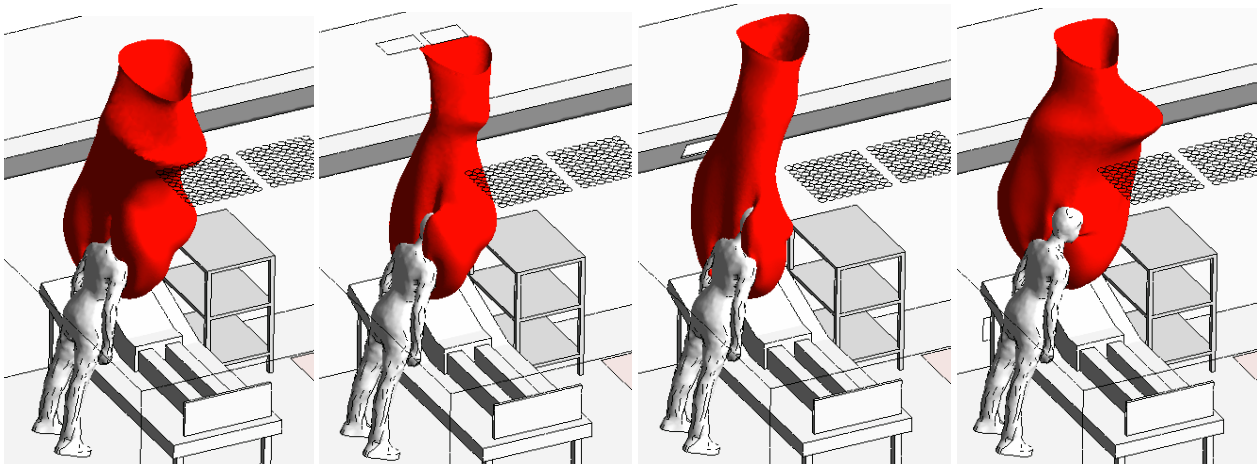

A **B** **C** **D**

Figure 3.15. Spreading of patient-exhaled air (mixing ventilation, 12 ACH, HCW leaning, URANS) with different exhaust locations: in ceiling corners (**A**), in the ceiling above the patient (**B**), in the lighting panel (**C**) and at floor level (**D**). The red isosurface represents a constant concentration level of 30 ppm.

3.4.2. Local downward ventilation

Exposure

The modelled HCW exposure results for LDV are shown in **Figure 3.16**. The CFD results with the URANS method differ notably from the measurements, especially when the HCW is leaning over the patient. Therefore, this case was also modelled with LES to find explanations for this difference. The LES results were closer to the measurements, but there was still a notable difference.

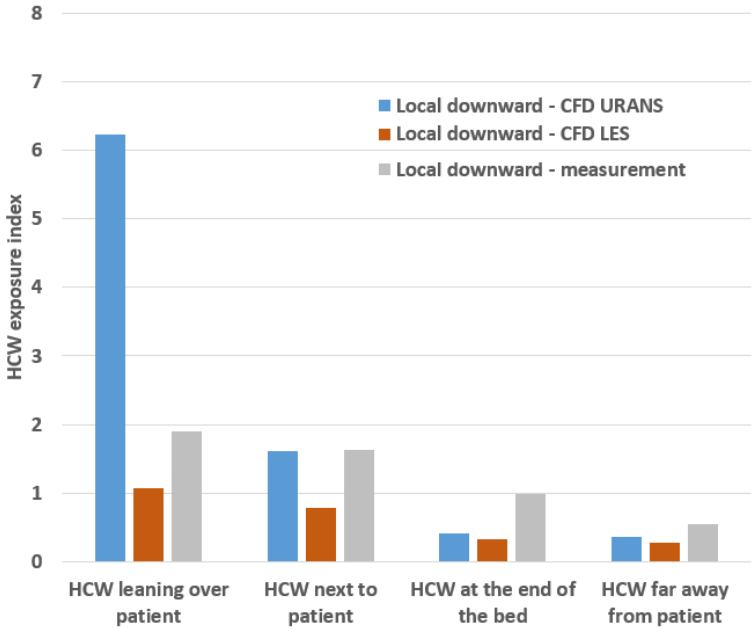

Figure 3.16. The CFD simulation results for HCW exposure with local downward ventilation (ceiling corner exhausts, 12 ACH, URANS) compared to measurements.

Flow pattern

The differences between the URANS and LES simulation results can be seen in **Figures 3.17** and **3.18**. With URANS, the downward supply air flow turns away from the HCW and does not adequately flush the HCW's breathing zone. This differs from the experimental smoke visualisation results (**Figures 2.9** and **2.10**). The reason for this result is that with the URANS method, the turbulent fluctuations are time-averaged and described by a turbulence model. This reduces the fluctuations of the flow pattern and creates a narrower flow [**101**]. In the LES result, the supply air comes directly down towards the patient and effectively flushes the exhaled air. The fluctuations of the flow pattern with LES can be seen in the isosurface structure (**Figure 3.17**).

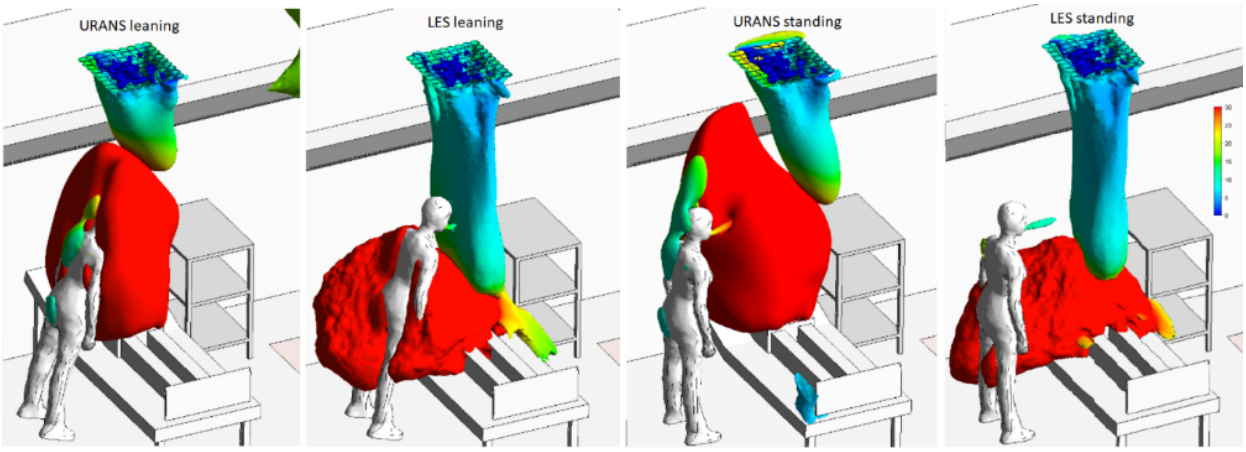

Figure 3.17. The flow pattern close to the HCW and the patient with URANS and LES methods (local downward ventilation, 12 ACH, ceiling corner exhausts) when the HCW was leaning (left) and standing (right). The red isosurface presents a tracer concentration level of 30 ppm near the patient. The airflow pattern is depicted with a velocity isosurface of 0.2 m/s colour coded with the concentration (0 to 30 ppm).

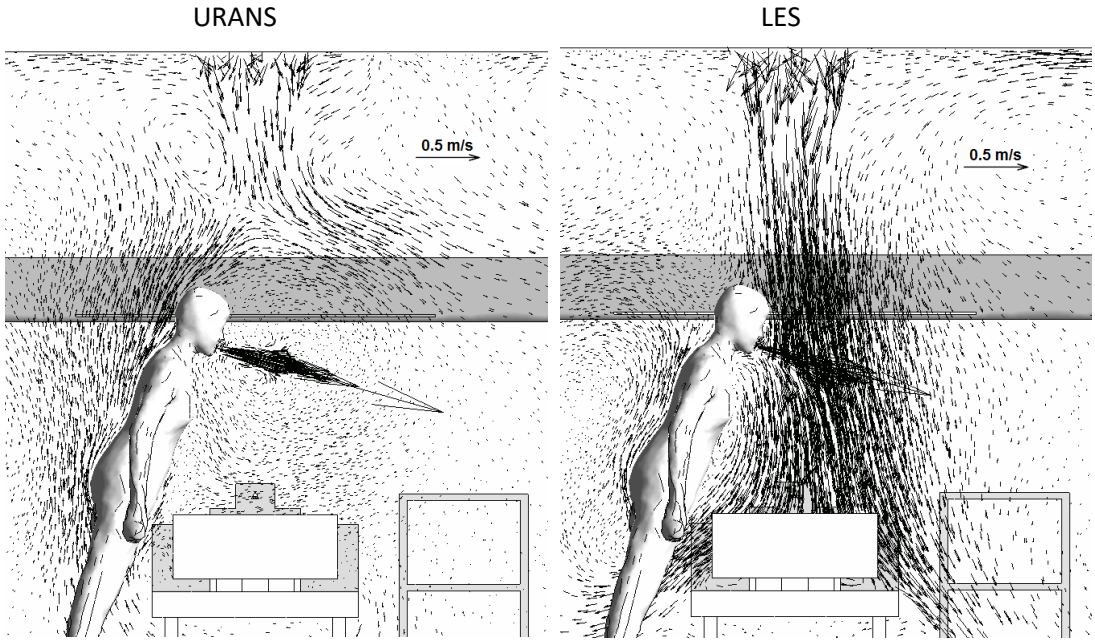

Figure 3.18. The flow pattern close to the HCW and the patient's bed with URANS and LES methods (local downward ventilation, 12 ACH, ceiling corner exhausts).

The spreading of exhaled air with the URANS method can be seen in **Figures 3.19** and **3.20**.

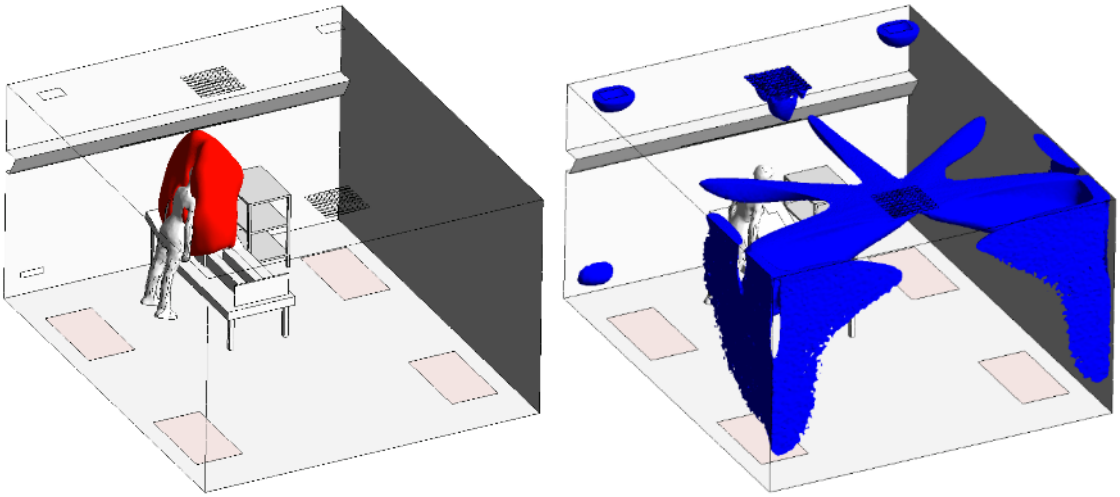

Figure 3.19. Spreading of exhaled air (left) and supply air (right) with local downward ventilation. The red isosurface depicts a concentration of 30 ppm (left), and the blue isosurface depicts a velocity of 0.3 m/s (right) (12 ACH, ceiling corner exhausts, URANS).

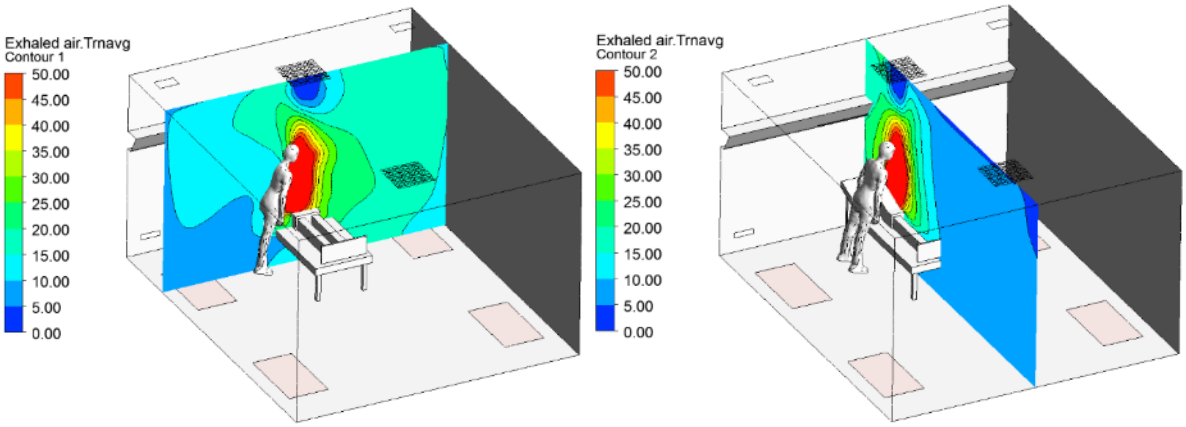

Figure 3.20. Contours of concentration with local downward ventilation (12 ACH, ceiling corner exhausts, URANS).

The velocities above the patient's bed with URANS and LES methods can be seen in **Figure 3.21**.

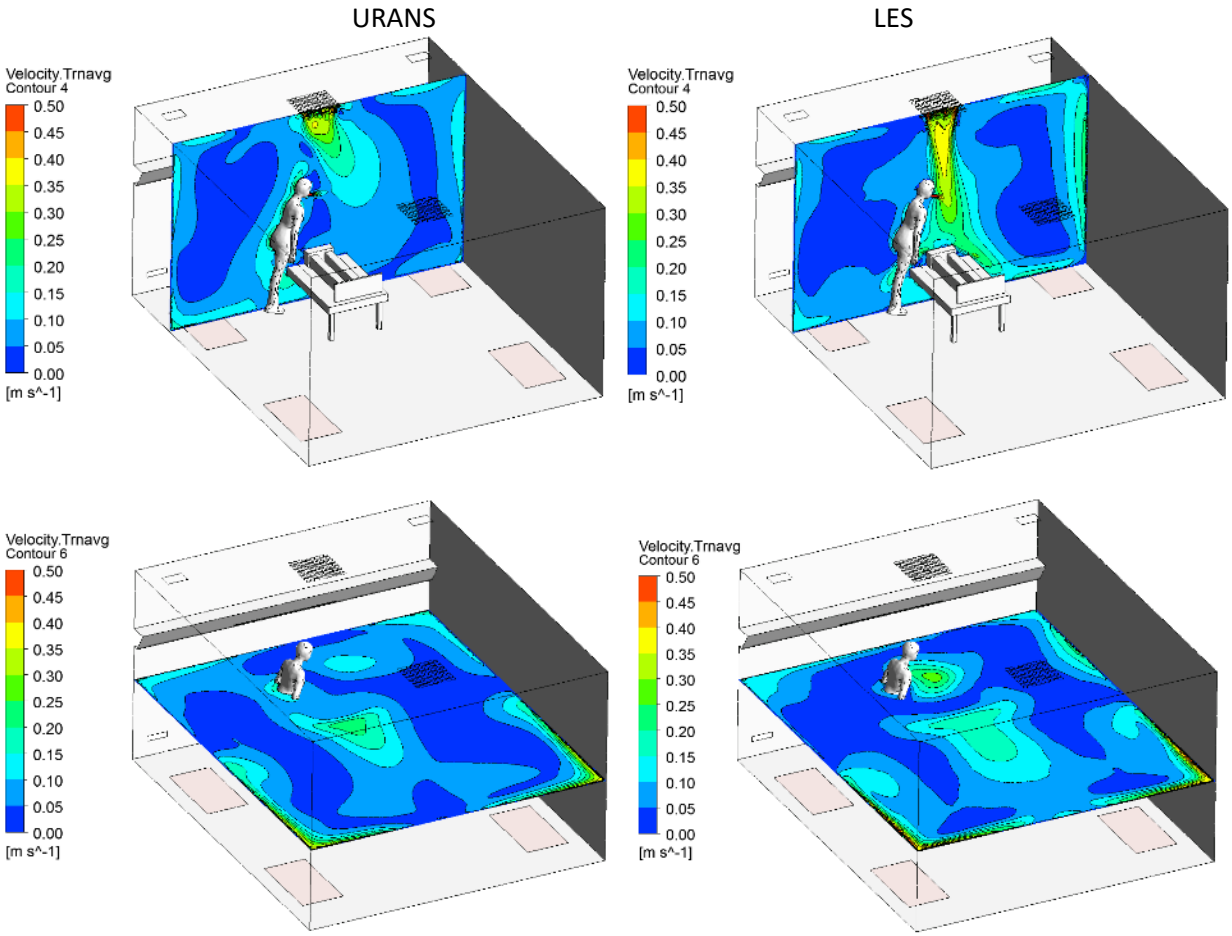

Figure 3.21. Velocity contours in a vertical plane and above the patient's head (1.1 m level) with local downward ventilation using URANS (left) and LES (right) models (12 ACH, ceiling corner exhausts).

3.4.3. Zonal downward ventilation

Exposure

Zonal downward ventilation (ZDV) was studied with CFD simulations only. The modelled HCW exposure results with different exhaust locations are shown in **Figure 3.22**. The modelled exposures were notably lower than with MV. The level of exposure near the patient was the same as the level of exposure far away from the patient. The supply air seemed to effectively flush the exhaled air of the patient from the HCW's breathing zone. When the exhaust was placed in the wall behind the patient's bed, the exhaled air of the patient was effectively captured by the exhaust before spreading to the room. It should be noted that these were purely simulation results and were not backed by experiments.

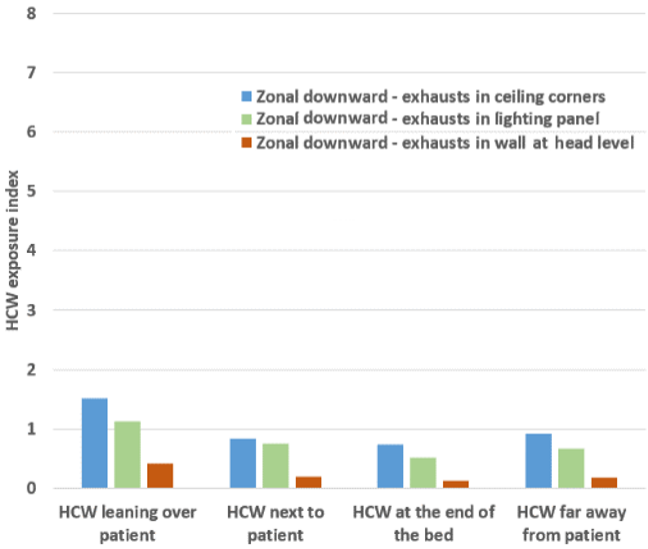

Figure 3.22. CFD simulation results for HCW exposure with zonal downward ventilation (12 ACH, URANS).

Flow pattern

The supply air flow pattern is shown in **Figure 3.23**. The supply air is blown downwards from both sides of the nozzle duct, which forms a downward flow pattern to the whole bed area.

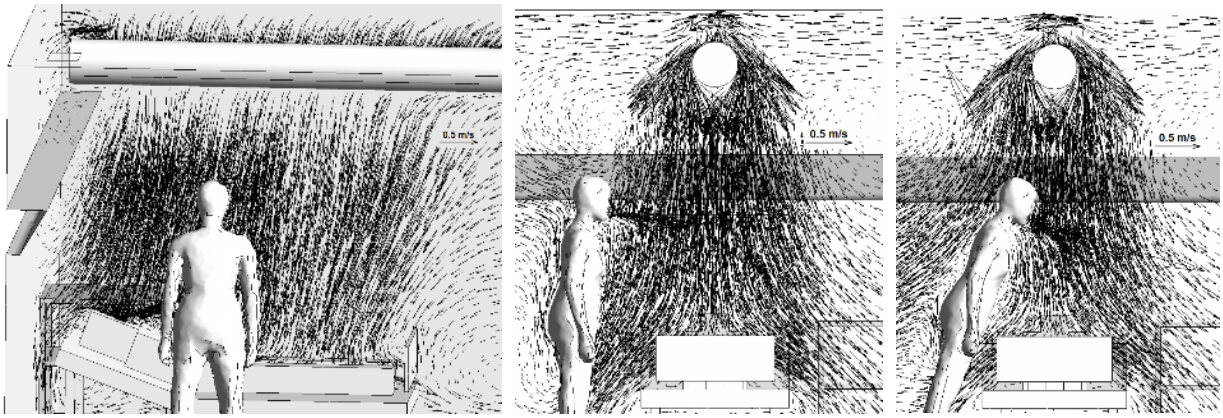

Figure 3.23. The flow pattern close to the HCW and the patient's bed when the HCW was standing (left and middle) and leaning (right) (zonal downward ventilation, 12 ACH, ceiling corner exhausts, URANS).

The spreading of exhaled air can be seen in **Figures 3.24** and **3.25**. The exhaled air is flushed downwards and away from the HCW's breathing zone by the supply air flow. The air velocities above the patient's bed (**Figure 3.26**) are higher than with MV.

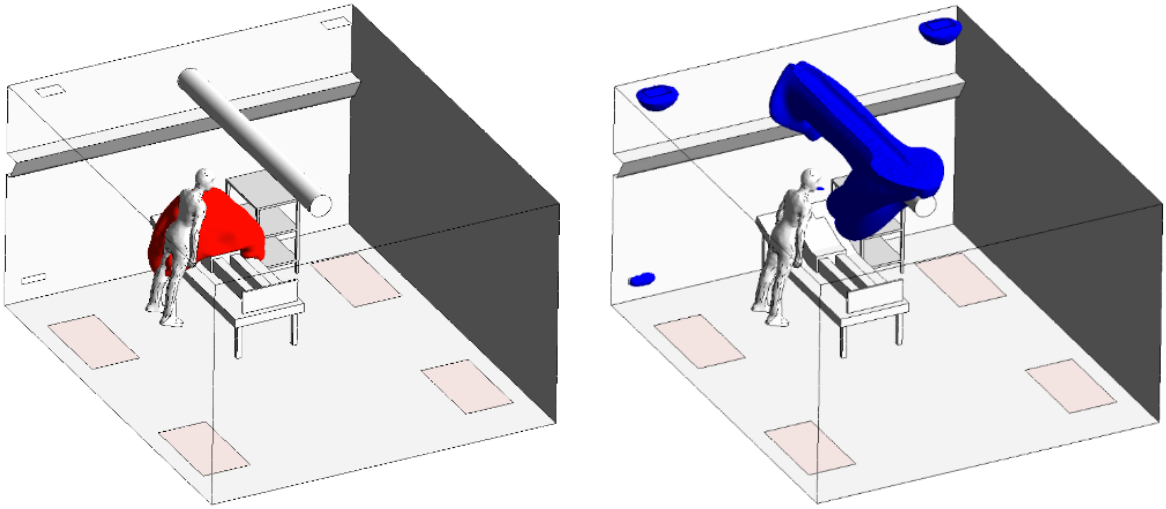

Figure 3.24. Spreading of exhaled air (left) and supply air (right) with zonal downward ventilation. The red isosurface depicts a concentration of 30 ppm (left), and the blue isosurface depicts a velocity of 0.3 m/s (right) (12 ACH, ceiling corner exhausts, URANS).

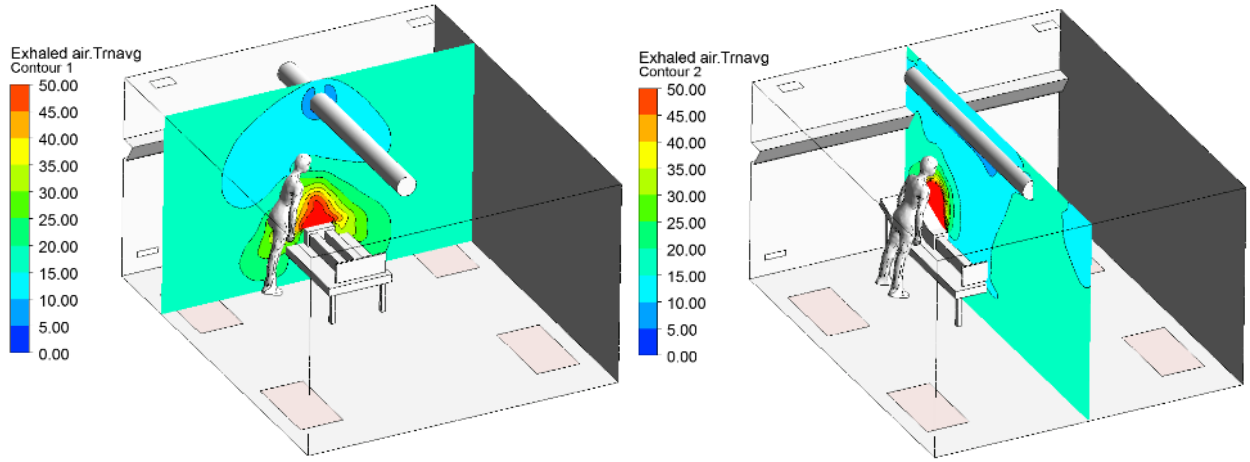

Figure 3.25. Contours of concentration of patient exhaled air with zonal downward ventilation (12 ACH, ceiling corner exhausts, URANS).

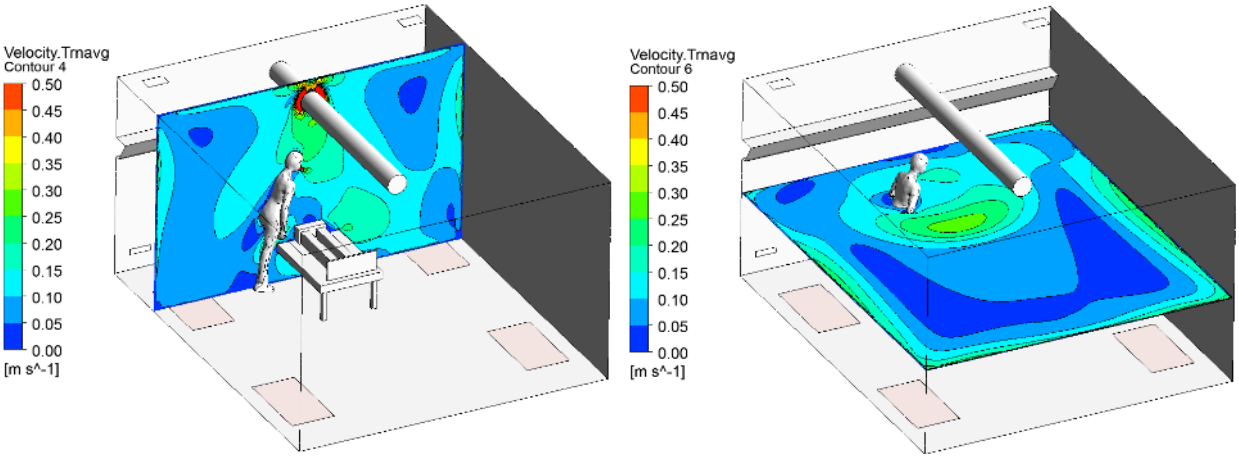

Figure 3.26. Velocity contours above the patient's head (1.1 m level) with zonal downward ventilation (12 ACH, ceiling corner exhausts, URANS).

Effect of exhaust location

The exhaust location had a notable effect on the HCW's exposure (**Figure 3.27**). When the exhaust was placed in the wall at the end of the patient's bed, the exhaled air was effectively removed before spreading to the room, as can be seen in the figure on the far right (**C**). In reality, this effect is probably not as strong as in simulations, due to disturbances and temporal variations in the flow pattern.

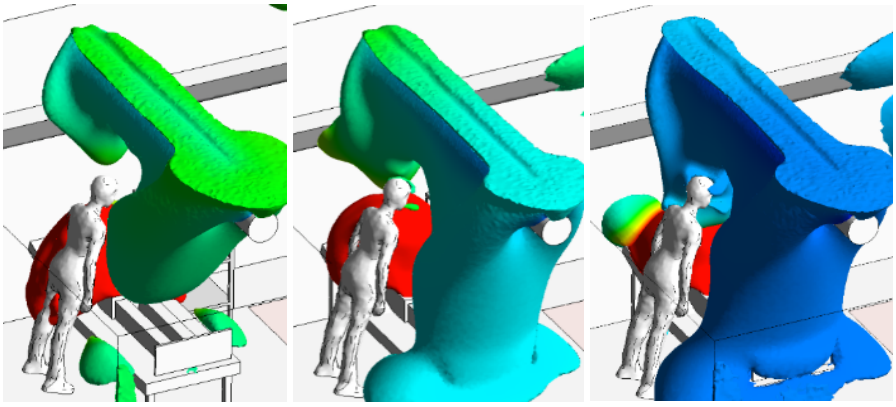

A **B** **C**

Figure 3.27. The flow pattern close to the HCW and the patient with different exhaust locations: in the ceiling corners (**A**), in the lighting panel (**B**) and in the wall at head level (**C**) (zonal downward ventilation, 12 ACH, URANS). The red isosurface depicts a concentration level of 30 ppm. The airflow pattern is depicted with a velocity isosurface of 0.25m/s colour coded with the concentration (0 to 30 ppm).

3.5. Summary of the findings from CFD simulations

- CFD simulation is a useful tool for developing optimal solutions for air distribution in isolation rooms. It helps to understand the flow patterns and spreading of contaminants. However, validation of the models with experiments is important, as it improves the credibility of the simulations.
- CFD simulation with the URANS method predicted the MV case relatively well. The HCW's exposure was close to the measured values, although generally somewhat lower.
- The exhaust location did not have a notable effect on the level of HCW exposure with MV when the HCW was leaning over the patient.
- With MV, the general concentration of exhaled tracer in the room was lowest with the exhaust vent positioned in the lighting panel, just above and behind the patient's head (in this mock-up), where it was able to capture part of the exhaled air of the patient.
- In the case of downward flow (LDV), URANS had notable difficulties in predicting the correct flow pattern. The simulated downward flow appeared to turn away from the patient and did not flush the breathing zone, as shown in the experiments. Also, the simulated HCW exposure was too high in comparison to the experimental measurements when the HCW was leaning over the patient. The LES model produced more realistic results because it was able to simulate the fluctuations of the flow pattern.
- ZDV appears to have useful potential to limit the degree of HCW exposure. The URANS simulation gave promising results with a low degree of HCW exposure. The lowest exposure was observed

when the exhaust was located in the wall near the patient's head, when the supply air flow pattern was able to direct the exhaled contaminants directly towards the exhaust. However, experiments are needed to confirm this predicted behaviour.

- With MV, velocities above the bed were low in the simulations (below 0.1 m/s). With LDV, higher velocities of up to 0.3 m/s occurred in LES simulations. The same velocity levels were seen in ZDV with URANS. As velocities above 0.2 m/s can cause a draught, for LDV and ZDV modes, thermal comfort issues have to be considered.

4. Virus tracer experiments

Although smoke visualisation and tracer gases (like SF_6) are useful tools, for healthcare-related infection control purposes, the use of an organic tracer (or pathogen surrogate) adds a more realistic interpretation to experimental results.

To this end, we used an existing, licensed, cold-adapted, live-attenuated influenza vaccine (LAIV), Fluenz Tetra [**102**]. A vaccine was used as a live virus tracer by another research team as a proxy marker for wild-type influenza virus [**51**]**.**

The vaccine is licensed for use in primary school children and is used at the beginning of the influenza season in the UK every year to immunise children to prevent them from acquiring wild-type influenza infection, which may pose a risk to vulnerable adults [**103**]. It was therefore considered to be a safe and realistic tracer for assessing the exposure risk to HCWs in the experiments outlined below. All the study investigators had been routinely immunised against seasonal influenza with the standard inactivated vaccine recommended for that year.

This live-attenuated influenza vaccine was used as a tracer for both the small-scale and the full-scale experiments assessing the impact of different ventilation set-ups, similar to the tracer gas studies described earlier.

The use of a nebuliser was thought to be responsible for one of the largest SARS-CoV outbreaks in Hong Kong during the 2003 SARS epidemic [**104**]. Since then, although various reports have demonstrated the potential for oxygen masks, nebulisers and other forms of non-invasive ventilation as possible aerosol generators [**26, 105–109**], they have not been accepted universally as aerosol-generating procedures in most guidelines [**110–115**]. Here we show that the side venting from such masks can disseminate live virus and pose a potential risk to nearby HCWs, as the incoming nebuliser or oxygen airflows collide and interact with the patient's exhaled breath, which is carrying a live virus tracer.

4.1. Detection of live-attenuated vaccine virus tracer

The live-attenuated quadrivalent influenza vaccine Fluenz Tetra (MedImmune/AstraZeneca) was obtained from the National Institute for Health and Welfare, Helsinki, Finland, from the surplus reserve following the vaccination campaigns for the 2016–17 and 2017–18 seasons. The doses were stored at 4–8 °C in the original syringes.

According to the manufacturer, each 0.2-ml dose contains $10^{7\pm0.5}$ fluorescent focus units (FFU) of each of four influenza strains included in the vaccine. To prepare the Fluenz Tetra (FT) dilution for the experiments, syringes were emptied into cold Hank's balanced salt solution (HBSS) (Gibco/Thermo Fisher Scientific) while the nozzle was kept under the liquid surface to eliminate mist escape.

4.1.1. Aerosol generation and collection

The FT aerosol was generated using a six-jet collision nebuliser with a glass jar (CH Technologies, USA). The pressure was generated with a standard air compressor (MEC-AIR model MA2021, Mechelin CO, Finland). The pressure was adjusted to 1 bar, resulting in a continuous air flow rate of 10 L/min, corresponding to human exhale volume but without inhale periods. The nebuliser fluid needed to reach the same density for the aerosol as normal exhaled air (1.15 g/m^3). This was important, because the density affects the buoyancy of nebulised air and thus the spreading of the aerosol. Evaporation of the fluid in the nebuliser

lowers its temperature by more than 10 °C. By heating the fluid suitably, an aerosol temperature of 25 °C and a corresponding density of 1.15 g/m^3 were reached.

The recommended maximum nebuliser starting volume of 20-ml FT dilution was used throughout the experiments. Aerosol was collected using an all-glass BioSampler (SKC, Inc., USA) with a total flow rate of 12.5 L/min when connected with a flow pump (KNF N035.1.2AN.18). The BioSampler was supplied with 20 ml of virus medium (VM) containing Dulbecco's Modified Eagle Medium (Gibco/Thermo Fisher Scientific) supplemented with 0.2 per cent BSA, 50 units/ml PenStrep, 2 mM L-glutamine, and tryptose phosphate broth. A drop of Cuplaton (Orion Pharma, Finland), corresponding to 15 mg of simethicone, was added to prevent foaming. After each experiment, 1-ml aliquots of the remaining nebuliser solution, the VM in the BioSampler and untreated FT dilution control were quick-frozen in an alcohol dry-ice bath and stored at -80 °C until analysed.

4.1.2. Test set-ups

All the virus tracer experiments were carried out in the isolation-room model described in section **2.1.1**. Storage, sample handling (after collection) and PCR analysis of the vaccine samples were carried out in the microbiology laboratory of the University of Turku. Three different set-ups were used in the tests: i) direct connection between the nebuliser and the BioSampler, ii) a glass tank between the nebuliser and the BioSampler, and iii) full-scale experiments in the isolation-room model with MV and LDV modes.

The direct connection experiments were carried out to test the feasibility of the aerosol generation and collection. In the direct connection tests, the Collison nebuliser was attached directly to the SKC BioSampler with a 20-cm tube, so that all nebulised aerosols would go through the SKC BioSampler. There was a connection for an additional inlet (HEPA filtered) to compensate for the small flow-rate difference between the nebuliser and the sampler. The system was placed inside a glass tank, which was inside the isolation-room model, to prevent the nebulised aerosol from escaping the test environment. All air that was exhausted from the tank went through the sampler and was HEPA filtered after sampling. Collection of the aerosol was started immediately after the nebulisation was initiated.

The glass tank experiments were carried out to examine the efficacy of the sampling from an air space. In the experiments, the nebuliser was attached to one end of the glass tank (0.6 m x 0.6 m x 1.5 m) and the BioSampler to the other end. There were small hose connectors at both ends of the tank where the nebuliser and BioSampler nozzles were fitted tightly. There was a small connector also for the inward airflow compensating the flow-rate difference between the nebuliser and the BioSampler. The generated aerosols were released from one end into the tank and collected at the other end of the tank (1.5-m distance). The air exhausted from the tank (through the sampler) was HEPA filtered prior to being released back into the isolation-room model. See **Figure 4.1** for further details of the set-up.

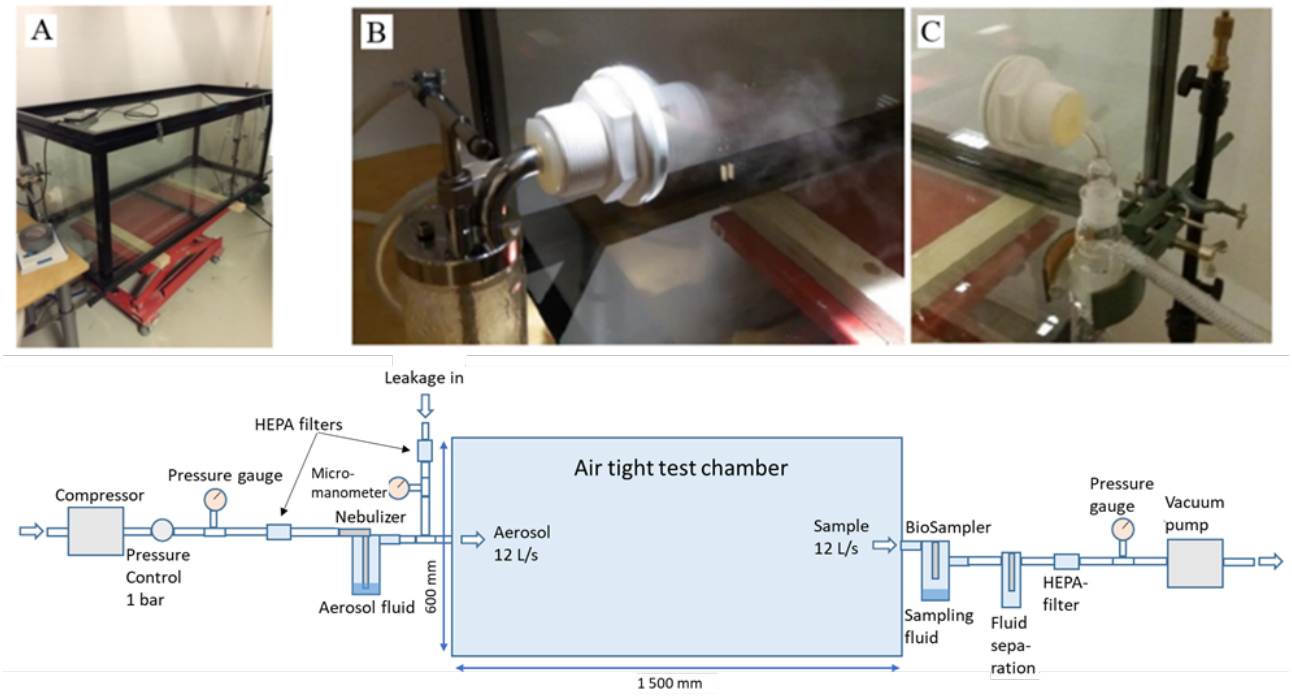

Figure 4.1. Set-up of the tank experiments. The photos show the tank (A), the nebuliser (B) and sampling (C). Below the photos is a schematic diagram of the set-up.

Full-scale experiments were carried out to test the aerosol generation, sampling and the HCW's exposure to the generated aerosols in a realistic isolation-room environment. The focus was on investigating the effect of MV and LDV modes on HCW exposure. The nebuliser was connected to the nosepiece of the heated dummy lying on the bed. The aerosolised FT was therefore released into the room through the nose of the patient. Three SKC BioSamplers were used simultaneously during the experiments. The samplers were placed around the patient's bed, simulating different HCW positions inside the room: i) leaning over the patient (caregiving scenario), ii) standing next to the patient (chatting with the patient) and iii) standing at the foot of the bed (checking the patient's chart). These locations were the same as those used in the tracer gas experiments (see **Figure 2.6** for more details). A more detailed description of the isolation-room model can be found in section **2.1.1**. A 30-minute sampling period was used throughout the experiments. The measurement set-up is illustrated in **Figure 4.2**.

All air exhausted from the isolation-room model was HEPA filtered. Only manikins were exposed to the aerosolised FT during the experiments. Investigators were vaccinated against influenza, and as a safety measure they wore PPE (including FFP3 masks and gloves) when retrieving the sampling equipment after the experiments.

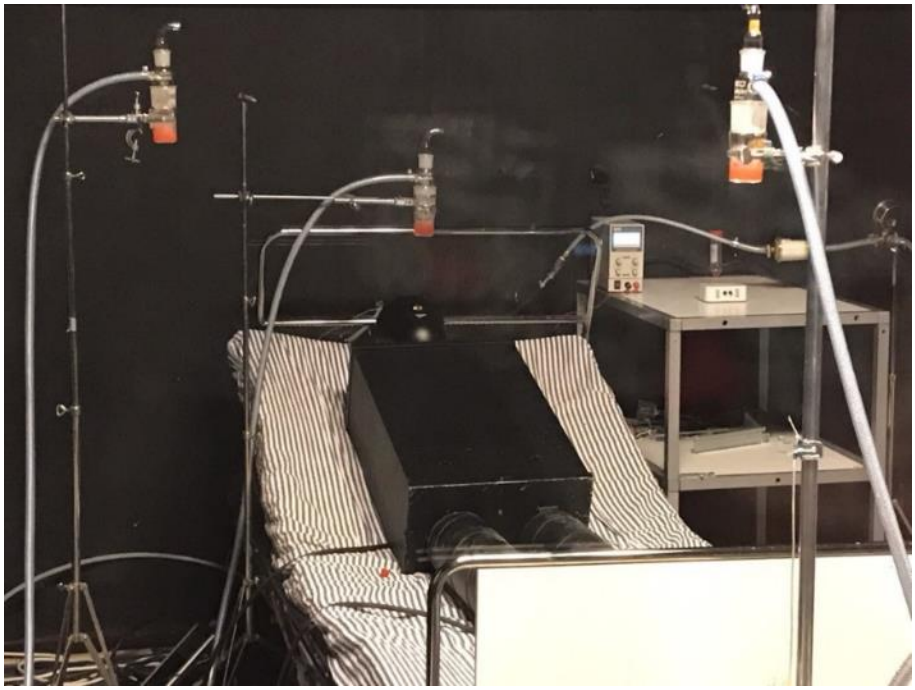

Figure 4.2. Full-scale isolation-room mock-up with the BioSamplers placed around the patient (the dummy lying on the bed).

4.1.3. Nucleic acid extraction and detection

Total nucleic acid fractions were extracted from the thawed samples using a NucliSens easyMAG (bioMérieux) system. The extracts were screened using a quantitative reverse-transcription polymerase chain reaction (qRT-PCR) for influenza A, A/H1pdm09 and B viruses with a one-step modification of the method described earlier [**116**]. Primers and MGB probes (**Table 4.1**) were obtained from Eurogentec, and a SensiFAST Probe No-ROX One-Step Kit (Bioline) was used as the master mix. The reaction volume was 20 µl, including 5 µl of virus ribonucleic acid (RNA) extract. Reactions were amplified using Mic qPCR Cycler (Bio Molecular Systems) at fast cycling mode with the following steps: RT (reverse-transcription) at 50 °C for 10 mins, initial denaturation at 95 °C for 3 mins, and 45 cycles of denaturation at 95 °C for 5 s, annealing at 55 °C for 20 s with fluorometric data collection, and extension at 72 °C for 5 s. A positive control of FT dilution in HBSS corresponding to 10^6 FFU/µl of each virus was included in each run and used as a basis to estimate the relative concentration (FFU/ml) of the viruses in the samples.

4.1.4. Copy number determination by digital PCR

Digital PCR (dPCR) is a relatively new method for gene copy number determination, often referred to as ‘absolute quantitation’ [**117**]. In dPCR, the reaction is partitioned into thousands of independent reactions, with each individual reaction being either positive or negative – that is, either with or without a target molecule. Since only the digital (0/1) end point is considered, the result is independent of variation in reaction efficiency and there is no need for comparison with a standard. The resulting copy number is calculated according to the number of positive-vs-negative reactions using Poisson statistics and at an optimal distribution into 10,000–20,000 partitions; about 20 per cent of them are empty, and each partition contains an average of 1.6 target molecules [**117, 118**]. A dynamic range of accurate determinations goes over three logs.

Final quantitation of the samples was performed for the A/H1pdm09 type by dPCR using QuantStudio 3D (Applied Biosystems/Thermo Fisher Scientific). Samples were first reverse-transcribed to cDNA using random hexamer primers, as described earlier [**116**]. Nanofluidic QuantStudio 3D 20K chips were loaded and amplified with samples, H1pdm oligo reagents and QuantStudio 3D Master Mix v2 according to the manufacturer's recommendations. The sample dilution and amount per chip were adjusted according to the results from qRT-PCR and, when necessary, readjusted after a preliminary dPCR run to obtain optimal partition of the sample. The results of the dPCR experiments were analysed using QuantStudio 3D AnalysisSuite Cloud Software.

Table 4.1. Primers (F and R) and probes (P) used for influenza virus qRT-PCR assays.

Name	Type	Gene	Sequence (5'–3')	Conc. (nM)
AM1F	A	M1	GGCTCTCATGGARTGGCTAA	400
AM1R	A	M1	CAAAGCGTCTACGCTGCAGTCC	400
AM1P	A	M1	Cy5-TTCACGCTCACCGTGC-MGB-DQ	100
H1pdmF	A/pdm09	HA	TACCAGATTTTGGCGATCTATTC	400
H1pdmR	A/pdm09	HA	CCAGGGAGACTASCARTACCA	400
H1pdmP	A/pdm09	HA	FAM-ACWGTCGCCAGTTC-MGB-DQ	100
BM1F	B	M1	ACACAATTGCCTACCTGCTTTC	400
BM1R	B	M1	TCCAAGGCAGAGTCTAGGTCA	400
BM1P	B	M1	HEX-AGAAGATGGAGAAGGCAAAGCAGAACTAGC-DQ	100

4.1.5. Viability

Viral culture was used to assess the viability of any virus collected via the air sampler. The amount of live, viable virus was assessed using Madin–Darby canine kidney cell monolayers in multi-well plates. Briefly, cell cultures were inoculated with serial dilutions of the virus sample, overlaid with microcrystalline cellulose (Avicel). After incubation for 48–72 hrs at 33 °C, cultures were fixed and stained with crystal violet for plaque counting. Alternatively, inoculated cells were cultured without overlay and subjected to immunoperoxidase staining with specific antibodies for examination under an inverted microscope, to identify and quantify the number of influenza virus-infected cells.

4.2. Results with vaccine virus aerosols

In preliminary experiments, we tested the feasibility of nebulisation and BioSampler collection of FT, using qRT-PCR for virus quantitation (data not shown). We observed good transmission of the virus from the nebuliser to the BioSampler when they were directly connected. The preliminary experiments were then carried out in a sealed glass tank (0.6 m x 0.6 m x 1.5 m). These experiments confirmed that it was possible to collect a reasonable quantity of FT nebulised into the air space of the sealed glass tank with an exhaust through the BioSampler. Because of the nature of qRT-PCR assay, the accuracy of the measurements is limited, and less than fourfold differences (that is, ±1 PCR amplification cycle) are usually not significant. In addition, the uncertainty increases at higher amplification cycle numbers, and inter-assay variation is sensitive to assay calibration. Therefore, the final measurements were performed using the dPCR technique.

Figure 4.3 illustrates the copy number variation of the input virus concentration by dPCR within and between sets of experiments. The overall mean ± SD was 4.68 ± 0.26 x10^8 copies/ml, with a coefficient of

variation (CV) of 5.6 per cent. The original live influenza virus A/H1N1 content, based on the manufacturer's information and the dilution, was 5.0 x 10^6 ± 5.0 x 10^5 FFU/ml. Thus, 1 FFU corresponds to 94 copies on average. Input samples of experiments 1 to 3 shown in **Figure 4.3** were analysed by both PCR methods; the overall CV was 28 per cent for qRT-PCR and 2.8 per cent for dPCR.

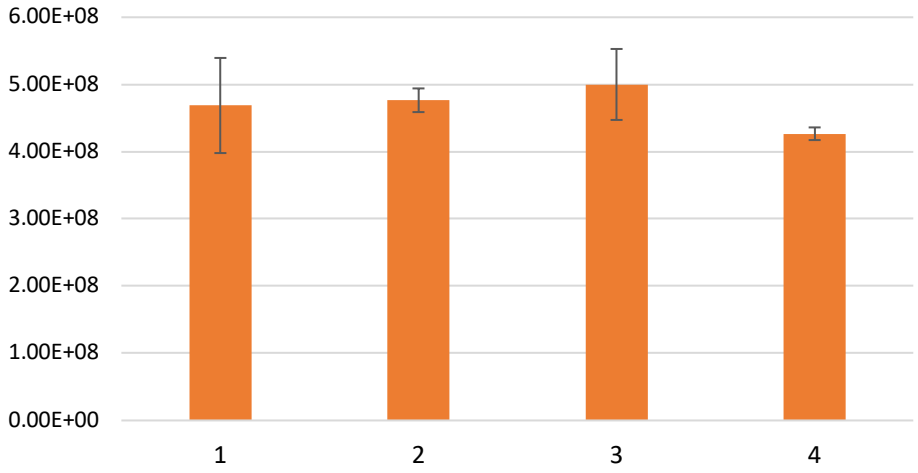

Figure 4.3. Variation of the input virus concentration between repeats (N=3–4) within and between a set of experiments, as measured by dPCR (mean ± SD of FT viral RNA copies/ml).

The maximum quantity of virus that the BioSampler was capable of collecting from the aerosol was assessed by connecting the BioSampler directly to the nebuliser (**Figure 4.4**). The average residual fraction was 53.2 per cent of the input, and 14 per cent was collected by the BioSampler, indicating a loss of 32.5 per cent during the experiment. The theoretical nebulised fraction was calculated by subtracting the copy number of the residual FT in the nebuliser after a 30-minute experiment from that of the input FT. The collected fraction in the BioSampler represented 30.5 per cent of the nebulised fraction. Assuming equal loss (16.3 per cent) in the nebulisation and collection, the generated aerosol contained 30.5 per cent of the input FT, of which 46.8 per cent was collected by the BioSampler. The results calculated as copies/min values are presented in **Figure 4.5**.

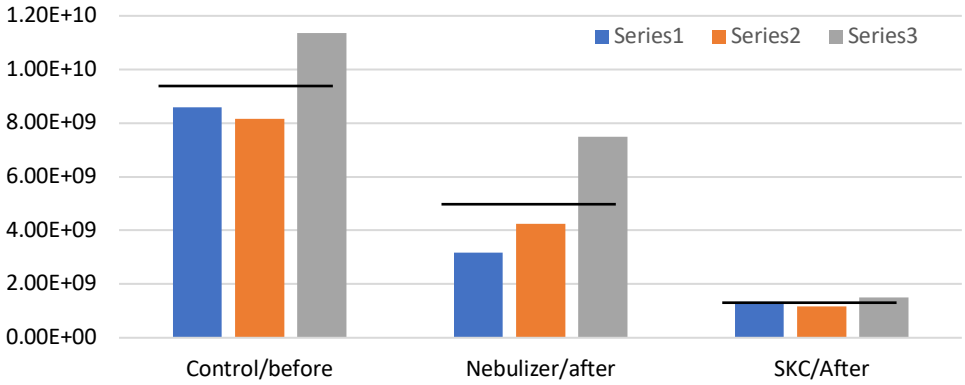

Figure 4.4. Results of three experiments collecting virus with the SKC BioSampler when in direct connection with the nebuliser. The columns represent total virus copy numbers; the line shows the mean of the three repeats. Columns indicate mean ± SD of FT viral RNA copies/min (N=3).

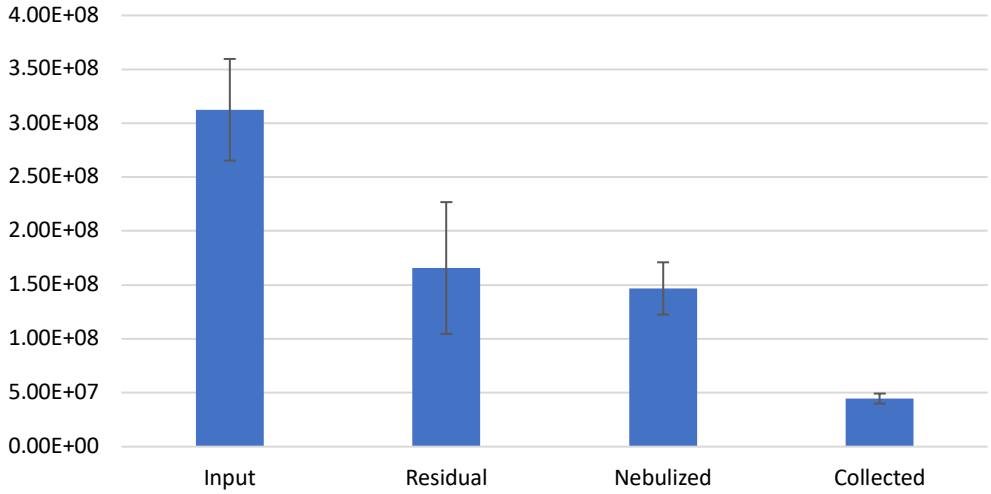

Figure 4.5. Collection of virus with the SKC BioSampler when in direct connection with the nebuliser. Columns indicate mean ± SD of FT viral RNA copies/min (N=3).

The results from a series of tank experiments are presented in **Figure 4.6**. The virus yield collected by the BioSampler from the air space of the tank was 2.3 per cent. The residual fraction was 37.7 per cent of the input, and 60 per cent was not recovered. The maximum possible yield calculated based on the tank airflow and volume in the 30-min experiment would have been 28 per cent of the nebulised fraction. The apparent nebulised fraction (input minus residual) was 62.3 per cent. Subtracting a 16.3-per-cent loss of the input virus in nebulisation, the calculated nebulised fraction was 46.0 per cent. Of that, 12.9 per cent went into the BioSampler, corresponding to 28 per cent of the air flow through. The collection efficacy of the BioSampler was measured in the direct-connection experiment to be 46.8 per cent. Without additional losses in the tank, the expected yield would have been 6.0 per cent.

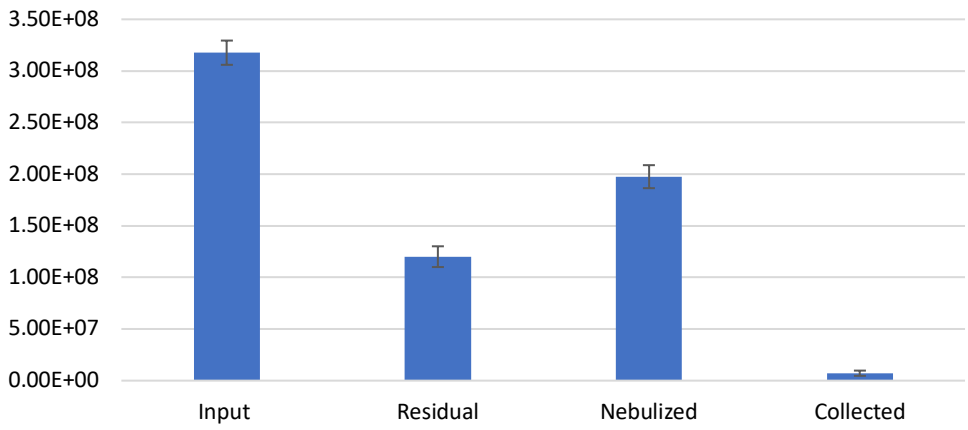

Figure 4.6. Results of tank experiments. Columns indicate mean ± SD of FT viral RNA copies/min (N=4).

Finally, we compared the effect of two different air distribution modes (MV and LDV) on the spread of FT virus in the experimental patient room. The copies/min values are shown in **Figure 4.7**. These results were also converted to exposure index values to enable comparison with the tracer gas results (**Figure 4.8**). The exposure index was calculated using **Equation 2** by dividing the average sampled concentration during the collection period by the corresponding average exhaust concentration. The sampled concentration was corrected with the measured yield of 13 per cent. The average exhaust concentration was calculated from the nebuliser virus input, assuming complete mixing in the room. The nebulised virus input was obtained from the difference between the measured virus counts in the nebuliser fluid before and after the experiment.

The results clearly indicate the effectiveness of downward ventilation in reducing the virus load close to the patient (**Figures 4.7** and **4.8**). With MV, the average increase in virus exposure compared to downward ventilation was 4.3-, 1.4- and 1.1-fold when leaning over the patient (SKC1), standing next to the patient's bed (SKC2) and standing at the foot of the bed (SKC3), respectively.

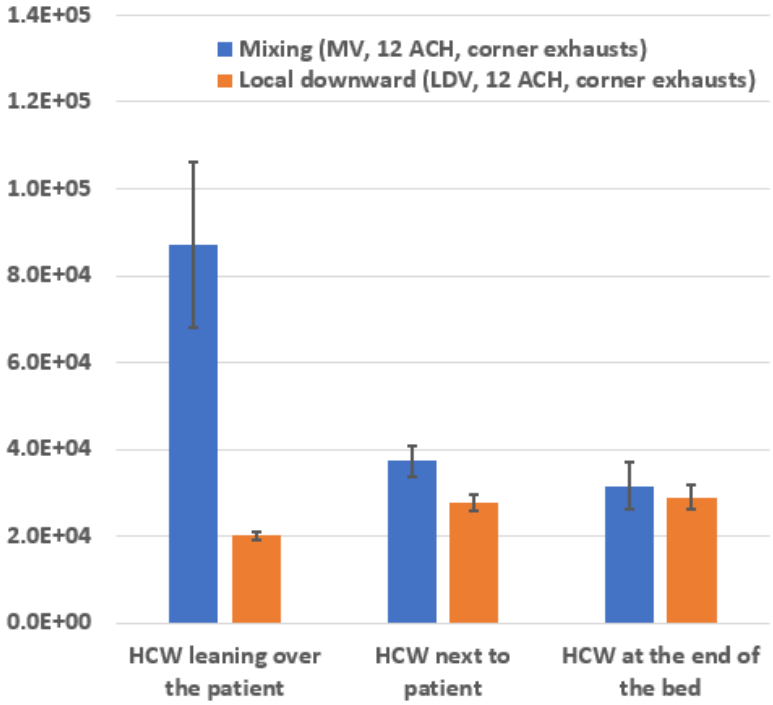

Figure 4.7. Virus tracer measurement results for HCW exposure in different locations inside the isolation room with different supply air distribution modes. Columns represent copies/min of FT viral RNA collected using SKC BioSamplers in different positions under different ventilation modes.

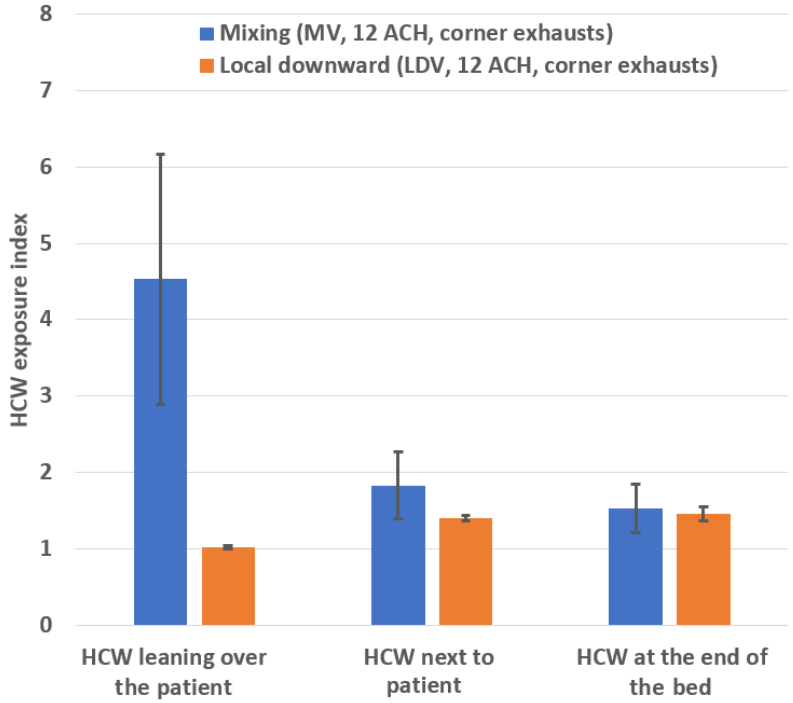

Figure 4.8. The effect of downward ventilation on HCW exposure presented as exposure indices calculated from the values in **Figure 4.7**.

4.3. Viability

There were substantial losses in detectable virus when assessed by viral culture, though less so by PCR methods [**119**]. This was not unexpected [**120**]. In the test chamber, the total experimental yield was estimated to be 6 per cent. In the actual full-scale test room, the experimental losses were much higher, since only a small portion of the aerosolised virus tracer could be collected within 30 minutes. The estimated yield for sampling was 0.1 per cent, assuming total mixing of room air and a ventilation rate of 12 ACH.

In the viability analysis of the samples, however, there were several additional sources of losses. The dilution of the vaccine to the nebuliser fluid seemed to cause an initial loss of 70–80 per cent in viability. The aerosolisation process in the nebuliser circulated the fluid through the nozzles, which created losses in the order of 50 per cent. This could have been caused by the shear stresses in the nozzles and in the jets hitting the container wall.

The total yield of viable virus in the experiments was in the order of 0.04 per cent. The main losses were caused by the culture method and storage of samples. These two, together with the experimental losses, seemed to be responsible for almost all the losses. Therefore, the yields were estimated to be around 90 per cent for the remaining experimental steps (the test chamber and the BioSampler).

The viability of the virus tracer declined during the experiments, and therefore only preliminary results were obtained in the test room. The number of cultured samples remained too small and the variation too large to get reliable estimates. More experiments are needed to get reliable estimates on the durability of viability in room scale.

4.4. Potential risks to HCWs of patients using medical nebulisers

Currently, nebuliser use is not considered to be an aerosol-generating procedure (AGP) in infection control guidelines or peer-reviewed publications [**121, 122**]. However, when such masks are used, either in hospital or in the home, clearly visible ‘smoke’ plumes can emanate from the mask’s side vents (**Figure 4.9 A** and **B**). We investigated the potential for HCW exposure to disseminated airborne virus in a situation in which the patient is wearing a mask connected to a nebuliser dispensing medication in the form of inhalable mist. Such nebuliser masks are commonly used as respiratory support in hospitalised patients with breathing difficulties.



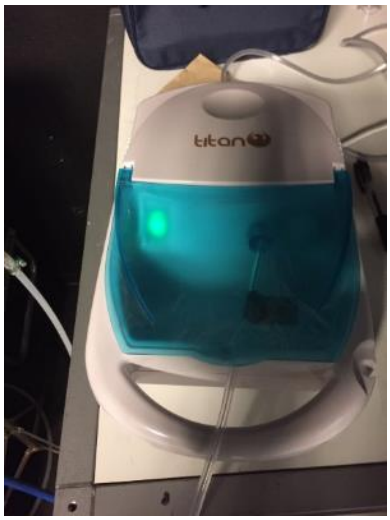

A B C

Figure 4.9. Investigating potential HCW exposure to disseminated airborne virus while a patient is using a nebuliser mask. The images depict the proximity of the HCW (modelled by Co-Investigator PK) to plumes emanating from the side vents of the nebuliser mask (**A**), the experiment conducted with the SKC sampler in the HCW's position (**B**) and the Titan portable home nebuliser (**C**).

4.4.1. Simulated medical nebuliser use

Using the existing full-scale isolation-room set-up with the HCW and patient manikins, we simulated a human patient with an influenza infection wearing a home nebuliser mask (Titan portable home nebuliser, 0.2 ml/min fluid, 6–8 L/min airflow, **Figure 4.9 C**). The patient manikin was a heated dummy lying semi-supine on a hospital bed. The dummy was modified to continuously exhale air (at 10 L/min), which was piped through the nose of the manikin and contained aerosols of FT produced by a Collison nebuliser (10 L/min).

A typical nebuliser mask has side vents on both sides, which allow the escape of a mist consisting of the nebulised medication and the patient's exhaled breath. For these experiments, the medical nebuliser was filled with 10 ml of water, which was completely vaporised during the 10-min experiment. Simultaneous air sampling (with the room ventilation set at 12 ACH), for 10 mins, with 3 SKC BioSamplers at 12 L/min, into VM from three different locations around the bed – 0.40 m (SKC1, head), 1.10 m (SKC2, side or abdomen) and 1.70 m (SKC3, foot) from the manikin's nose (simulating HCW positions during a ward round) (**Figure 4.10**) – was performed in triplicate.

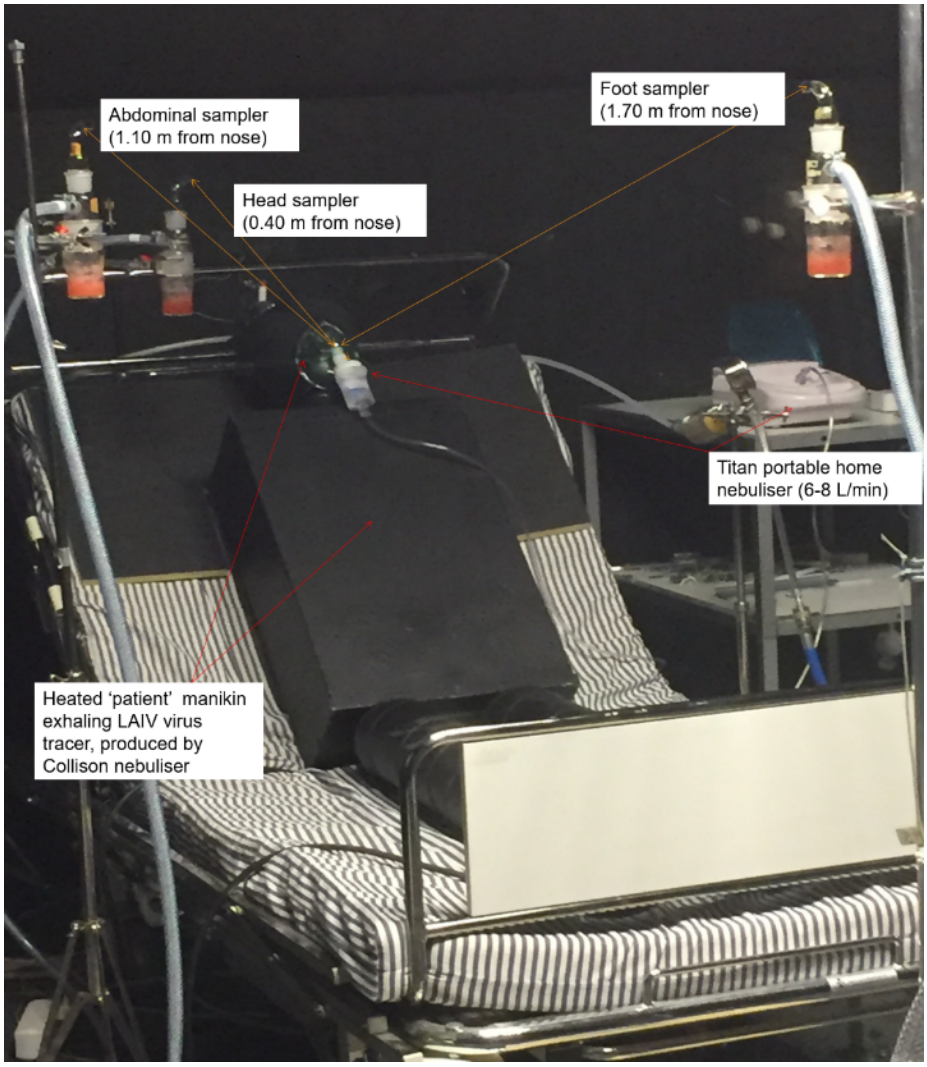

Figure 4.10. The experimental layout, with the heated patient manikin lying semi-supine on the bed and three SKC BioSamplers in different positions.

4.4.2. Air-sampling results

The use of a medical nebuliser was studied with MV only. A mean airborne viral load was obtained using dPCR quantitation of the virus in VM for each SKC.

The experiment was carried out either by starting with FT in 20 ml VM and repeating the 10-min experiment with the remaining input (N=2), or by starting with FT in 7 ml VM and replacing it between experiments (N=3). The mode of input had no effect on any of the measured values, and the results were pooled together (N=5). From a starting virus concentration of $4.96 \pm 0.45 \times 10^8$ copies/ml, the concentrations measured from the SKCs were $13.6 \pm 0.51 \times 10^4$, $3.86 \pm 0.76 \times 10^4$ and $2.61 \pm 0.43 \times 10^4$ copies/ml at the head, side and foot of the bed, respectively (**Figure 4.11**). We were not able to calculate the corresponding exposure index values for these results due to insufficient virus source data in the experiments.

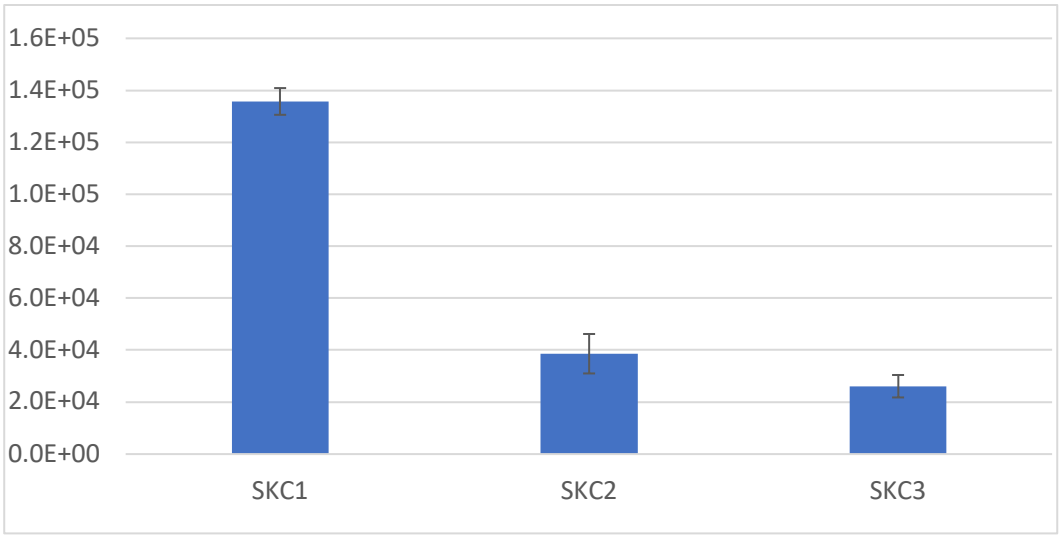

Figure 4.11. HCW exposure to virus aerosols emanating from the side vents of the nebuliser mask worn by the patient manikin in the simulated isolation room under mixing ventilation (12 ACH). The columns represent copies/min of FT viral RNA collected using SKC BioSamplers in different positions: SKC1 (next to the patient's head), SKC2 (at the patient's side) and SKC3 (at the foot of the bed).

The results presented in **Figure 4.11** reveal a similar HCW copies/min exposure risk profile to that shown in **Figure 4.7**, which indicates that the risk of exposure is greatly increased when the HCW is close to the patient's head, whether a medical nebuliser is in use or not.

4.4.3. Interpretation and application

In the full-size room experiments (**Figure 4.10**), the results showed that ~20,000–140,000 influenza vaccine viruses can be detected in aerosols ejected from the side vents when a typical home nebuliser is used at 6–8 L/min for 10 mins, on a patient exhaling from the mouth and nose with a source influenza vaccine virus concentration of ~500 million/ml, with air samples collected for 10 mins at 12.5 L/min (by SKC BioSamplers) with a room ventilation of 12 ACH.

Given these findings, nebulisers – and related simple oxygen-mask use – should be reconsidered and classified more universally as a potential AGP. Indeed, the US CDC has recognised the potential risk posed by nebulisation during the current Covid-19 pandemic [**123–125**], and there is increasing global recognition that the pandemic SARS-CoV-2 virus is likely airborne transmissible [**126–129**].

Therefore, assuming (not unreasonably) that a substantial proportion of all Covid-19 cases were acquired via the airborne route, the results of these experiments indicate that one practical action which can be taken to reduce or prevent cross-transmission from patients using nebulisers (or oxygen masks) is to draw the side curtains around the patient's bed [**130, 131**]. HCWs will still be able to see the patient from the bottom of the bed as they walk by. Inserting a physical barrier (the curtain) between patients for the duration of the nebuliser (or oxygen) therapy helps to reduce or prevent any infection spreading to their nearest neighbours.

4.5. Summary of the findings from virus tracer experiments

- Nebulisation and air sampling of the vaccine virus tracer was successfully tested in direct connection, tank and full-scale isolation-room experiments.
- Culturing the samples showed that the virus tracer stayed viable throughout the process, even in the full-scale isolation-room model. Hence, using this method to assess hospital-acquired infection risk to HCWs from patients infected with aerosol-transmissible pathogens can provide a more realistic picture of the possible infection risk than other engineering methods, such as tracer gas measurements or smoke visualisations.
- The culture method was not standardised throughout the experiments and the reproducibility was suboptimal because the vaccine, obtained as a surplus from the National Institute for Health and Welfare, Finland, was used after the expiry date. Thus, dPCR was used as the main method of virus quantitation, with highly reproducible results. Comparing the dPCR results to the original infectious dose of the vaccine showed that there were about 100 copies of the virus per fluorescent focus unit (FFU).
- Full-scale isolation-room experiments with vaccine virus tracer confirmed similar behaviour to the tracer gas measurements: LDV protected the HCW better than MV, especially close to the patient.
- Constant exhalation and supply of the virus tracer (compared to cyclic exhalation with the tracer gas experiments) may have resulted in a tracer concentration field close to the patient that was different to that produced by the tracer gas experiments.
- In the full-scale room experiments, visualisation of the side-vent jets from the nebuliser masks showed significant plumes escaping and remaining suspended in the vicinity of the patient's head, where HCWs could potentially be exposed.
- Aerosolised viral load samples, during medical nebuliser use, were highest at the head and lower at the side (abdomen) and at the foot of the bed. Although these air samples were not tested for viability by virus culture, data from the small-scale tank studies indicated that infectivity was sustained.

5. Summary of the study findings

- The exhaled air of the patient flowed directly towards the HCW's breathing zone when the patient was in a typical reclining position. The exhaled air of the patient should be flushed away from the HCW's breathing zone to protect the HCW as much as possible.
- The highest HCW exposure to the exhaled air of the patient occurred when the HCW was leaning over the patient giving care (for example, examining the patient or inserting an intravenous drip). In this situation, the inhaled concentration was typically five to six times the average room concentration with MV.
- LDV flow was able to flush the breathing zone of the patient and notably reduced the HCW's exposure. When leaning over the patient, the HCW's level of exposure with LDV was only about a third of that with MV.
- LDV caused higher velocities over the patient's bed than MV. This air movement can cause a draught that may be uncomfortable for the patient. Therefore, the air distribution must be designed carefully in order to minimise this draught to achieve acceptable thermal conditions. There will always be a need to reach a compromise between HCW protection and patient thermal comfort.
- Generally, patient thermal sensation was slightly cooler with LDV mode than with MV, but neither ventilation mode was too far from neutral.
- The potential patient thermal discomfort caused by the higher airflow velocities with LDV may be mitigated if it is only turned on during nursing periods, with MV being used the rest of the time.
- According to the CFD simulations, ZDV was even more effective than LDV at protecting the HCW. However, these results require further rigorous experimental validation.
- The exhaust location also plays a role in HCW protection, although exhausts can capture air only from a short distance away and therefore cannot control the room airflows generally. Nevertheless, placing an exhaust near high-concentration areas can lower the room concentrations notably.
- In this study, the most effective exhaust positions were in the wall behind the patient's bed and in the lighting panel (above and behind the patient), when the supply air was flushing the exhaled air in that direction.
- A higher ventilation rate reduces the HCW's exposure by decreasing the average room concentration and increasing the air mixing and dilution. Our results indicate that increased ventilation rates are effective at lowering the HCW's aerosol exposure near the patient, at least up to 12 ACH, provided that the air distribution is able to mix the air above the patient's bed.
- Masking the patient with an FFP2/N95 mask was found to be an effective method of suppressing the spread of the patient's exhalation jet into the room. However, wearing a mask may be uncomfortable for some patients if maintained for long periods.
- The live cold-attenuated influenza virus vaccine tracer experiments confirmed the findings of the tracer gas measurements: i) the highest exposure occurred when the HCW was leaning over the patient (with MV), and ii) LDV reduced the viral loads compared to MV.
- We demonstrated that a home nebuliser can produce virus-laden aerosols, mostly from the nebuliser mask side vents, which can infect carers and others nearby. Substantial viral loads were detected, which could be sufficient to cause infection if such personnel are present for the duration of the nebulisation session.

6. Conclusions and recommendations

In order to optimise the protection of HCWs from their patients' exhaled breath, which potentially carries airborne pathogens, we recommend that isolation-room designs should take the following factors into account:

- Set the ventilation rate high enough to dilute and flush away exhaled air from the patient that may be carrying pathogens. Ensure that the air above the patient's bed is sufficiently mixed and diluted to achieve this.
- Design the ventilation layout such that patient exhaled breath is directed away from attending HCWs. The optimal placement of the exhaust vent is in the location of the highest concentration of exhaled air – for example, in the wall just above and behind the patient's head while they are lying or reclining in bed.
- Mask the patient where possible to contain exhaled pathogens – until effective ventilation is established and maintained.
- Nebulisers should be treated as AGPs with the appropriate PPE precautions used when setting up and turning off this device

7. Acknowledgements

The authors would like to acknowledge CSC – IT Centre for Science, Finland, for computational resources.

8. References

1. Brosseau LM, Jones R. COMMENTARY: Protecting health workers from airborne MERS-CoV—learning from SARS. 19 May 2014. www.cidrap.umn.edu/news-perspective/2014/05/commentary-protecting-health-workers-airborne-mers-cov-learning-sars. Accessed 18 July 2015.
2. CIDRAP. New coronavirus infects health workers, spreads to Korea. 20 January 2020. www.cidrap.umn.edu/news-perspective/2020/01/new-coronavirus-infects-health-workers-spreads-korea. (Accessed 18 July 2020)
3. Lu H, Stratton CW, Tang YW. Outbreak of Pneumonia of Unknown Etiology in Wuhan China: the Mystery and the Miracle. *J Med Virol*. 16 January 2020. doi: 10.1002/jmv.25678. [Epub ahead of print].
4. ProMed-Mail. Novel coronavirus (16): China (HU), Viet Nam, Singapore ex China, IHR committee WHO. Archive Number: 20200123.6910685. 2020-01-23 23:44:23.
5. Bischoff WE, Swett K, Leng I, Peters TR. Exposure to influenza virus aerosols during routine patient care. *J Infect Dis*. 2013 Apr;207(7):1037–46. doi: 10.1093/infdis/jis773.
6. Tellier R, Li Y, Cowling BJ, Tang JW. Recognition of aerosol transmission of infectious agents: a commentary. *BMC Infect Dis*. 2019 Jan 31;19(1):101. doi: 10.1186/s12879-019-3707-y.
7. Brosseau LM, Jones R. COMMENTARY: Health workers need optimal respiratory protection for Ebola. 17 September 2014. www.cidrap.umn.edu/news-perspective/2014/09/commentary-health-workers-need-optimal-respiratory-protection-ebola. Accessed 18 July 2015.
8. Jones R, Brosseau LM. COMMENTARY: Ebola virus transmission via contact and aerosol — a new paradigm. 18 November 2014. www.cidrap.umn.edu/news-perspective/2014/11/commentary-ebola-virus-transmission-contact-and-aerosol-new-paradigm. Accessed 18 July 2015.
9. Osterholm MT, Moore KA, Kelley NS, Brosseau LM, Wong G, Murphy FA, *et al*. Transmission of Ebola viruses: what we know and what we do not know. mBio. 2015 Feb 19;6(2):e00137. doi: 10.1128/mBio.00137-15.
10. Tang JW, Li Y, Eames I, Chan PK, Ridgway GL. Factors involved in the aerosol transmission of infection and control of ventilation in healthcare premises. *J Hosp Infect*. 2006 Oct;64(2):100–14. doi: 10.1016/j.jhin.2006.05.022.
11. Tang JW. The effect of environmental parameters on the survival of airborne infectious agents. *J R Soc Interface*. 2009 Dec 6;6 Suppl 6(Suppl 6):S737–46. doi: 10.1098/rsif.2009.0227.focus.
12. Eames I, Tang JW, Li Y, Wilson P. Airborne transmission of disease in hospitals. *J R Soc Interface*. 2009 Dec 6;6 Suppl 6(Suppl 6):S697–702. doi: 10.1098/rsif.2009.0407.focus.
13. Tang JW, Wilson P, Shetty N, Noakes CJ. Aerosol-Transmitted Infections—a New Consideration for Public Health and Infection Control Teams. *Curr Treat Options Infect Dis*. 2015;7(3):176–201. doi: 10.1007/s40506-015-0057-1.
14. Tang JW, Settles GS. Images in clinical medicine. Coughing and aerosols. *N Engl J Med*. 2008 Oct 9;359(15):e19. doi: 10.1056/NEJMicm072576.

15. Tang JW, Liebner TJ, Craven BA, Settles GS. A schlieren optical study of the human cough with and without wearing masks for aerosol infection control. *J R Soc Interface*. 2009 Dec 6;6 Suppl 6(Suppl 6):S727–36. doi: 10.1098/rsif.2009.0295.focus.

16. Xie X, Li Y, Sun H, Liu L. Exhaled droplets due to talking and coughing. *J R Soc Interface*. 2009 Dec 6;6 Suppl 6(Suppl 6):S703–14. doi: 10.1098/rsif.2009.0388.focus.

17. Tang JW, Nicolle AD, Pantelic J, Jiang M, Sekhr C, Cheong DK, *et al*. Qualitative real-time schlieren and shadowgraph imaging of human exhaled airflows: an aid to aerosol infection control. *PLoS One*. 2011;6(6):e21392. doi: 10.1371/journal.pone.0021392.

18. Tang JW, Nicolle AD, Klettner CA, Pantelic J, Wang L, Suhaimi AB, *et al*. Airflow dynamics of human jets: sneezing and breathing - potential sources of infectious aerosols. *PLoS One*. 2013;8(4):e59970. doi: 10.1371/journal.pone.0059970.

19. Asadi S, Wexler AS, Cappa CD, Barreda S, Bouvier NM, Ristenpart WD. Aerosol emission and superemission during human speech increase with voice loudness. *Sci Rep*. 2019 Feb 20;9(1):2348. doi: 10.1038/s41598-019-38808-z.

20. Bourouiba L. Turbulent Gas Clouds and Respiratory Pathogen Emissions: Potential Implications for Reducing Transmission of COVID-19. *JAMA*. 2020 Mar 26. doi: 10.1001/jama.2020.4756.

21. Hamner L, Dubbel P, Capron I, Ross A, Jordan A, Lee J, *et al*. High SARS-CoV-2 Attack Rate Following Exposure at a Choir Practice – Skagit County, Washington, March 2020. *MMWR Morb Mortal Wkly Rep*. 2020 May 15;69(19):606–10. doi: 10.15585/mmwr.mm6919e6.

22. Gupta JK, Lin CH, Chen Q. Characterizing exhaled airflow from breathing and talking. *Indoor Air*. 2010 Feb;20(1):31–9. doi: 10.1111/j.1600-0668.2009.00623.x.

23. Lindsley WG, Blachere FM, Thewlis RE, Vishnu A, Davis KA, Cao G, *et al*. Measurements of airborne influenza virus in aerosol particles from human coughs. *PLoS One*. 2010 Nov 30;5(11):e15100. doi: 10.1371/journal.pone.0015100.

24. Tang JW, Nicolle AD, Klettner CA, Pantelic J, Wang L, Suhaimi AB, *et al*. Airflow dynamics of human jets: sneezing and breathing – potential sources of infectious aerosols. *PLoS One*. 2013;8(4):e59970. doi: 10.1371/journal.pone.0059970.

25. Nicas M, Nazaroff WW, Hubbard A. Toward understanding the risk of secondary airborne infection: emission of respirable pathogens. *J Occup Environ Hyg*. 2005 Mar;2(3):143–54.

26. Ip M, Tang JW, Hui DS, Wong AL, Chan MT, Joynt GM, *et al*. Airflow and droplet spreading around oxygen masks: a simulation model for infection control research. *Am J Infect Control*. 2007 Dec;35(10):684–9.

27. Tang JW, Settles G. Images in clinical medicine. Coughing and masks. *N Engl J Med*. 2009 Dec 24;361(26):e62. doi: 10.1056/NEJMicm0904279.

28. Olmedo I, Nielsen PV, Ruiz de Adana M, Jensen RL, Grzelecki P. Distribution of exhaled contaminants and personal exposure in a room using three different air distribution strategies. *Indoor Air*. 2012 Feb;22(1):64–76. doi: 10.1111/j.1600-0668.2011.00736.x.

29. ANSI/ASHRAE/ASHE Standard 170-2018: Ventilation of Health Care Facilities. The American Society of Heating, Refrigerating and Air-Conditioning Engineers (ASHRAE), Atlanta, Georgia, USA, 2018.

30. CDC Guidelines for Preventing the Transmission of Mycobacterium tuberculosis in Health-care Settings, vol. 54, MMWR, Washington, DC, 2005.

31. Health Technical Memorandum (HTM) 03-01: Specialised ventilation for healthcare premises. Part A: Design and validation. Department of Health, UK, 2007.

32. DIN 1946-4 Ventilation and air conditioning – Part 4: Ventilation in buildings and rooms of health care. Deutsches Institut für Normung, Germany, 2008.

33. Pantelic J, Tham KW. Adequacy of air change rate as the sole indicator of an air distribution system's effectiveness to mitigate airborne infectious disease transmission caused by a cough release in the room with overhead mixing ventilation: A case study. *HVAC&R Research*. 2013;19; 947–61. doi.org/10.1080/10789669.2013.842447.

34. Cao G, Nielsen PV, Jensen RL, Heiselberg P, Liu L, Heikkinen J. Protected zone ventilation and reduced personal exposure to airborne cross-infection. *Indoor Air*. 2015 Jun;25(3):307–19. doi: 10.1111/ina.12142.

35. Yang C, Yang X, Zhao B. The ventilation needed to control thermal plume and particle dispersion from manikins in a unidirectional ventilated protective isolation room. *Build Simul*. 2015;8;551–65. doi 10.1007/s12273-014-0227-6.

36. Tang JW. Investigating the airborne transmission pathway – Different approaches with the same objectives. *Indoor Air*. 2015;doi:10.1111/ina.12175.

37. Tang JW, Gao CX, Cowling BJ, Koh GC, Chu D, Heilbronn C, *et al*. Absence of detectable influenza RNA transmitted via aerosol during various human respiratory activities--experiments from Singapore and Hong Kong. *PLoS One*. 2014 Sep 10;9(9):e107338. doi: 10.1371/journal.pone.0107338.

38. Milton DK, Fabian MP, Cowling BJ, Grantham ML, McDevitt JJ. Influenza virus aerosols in human exhaled breath: particle size, culturability, and effect of surgical masks. *PLoS Pathog*. 2013 Mar;9(3):e1003205. doi: 10.1371/journal.ppat.1003205.

39. Tang JW, Eames I, Li Y, Taha YA, Wilson P, Bellingan G, *et al*. Door-opening motion can potentially lead to a transient breakdown in negative-pressure isolation conditions: the importance of vorticity and buoyancy airflows. *J Hosp Infect*. 2005 Dec;61(4):283–6.

40. Tang JW, Nicolle A, Pantelic J, Klettner CA, Su R, Kalliomaki P, et al. Different types of door-opening motions as contributing factors to containment failures in hospital isolation rooms. *PLoS One*. 2013 Jun 24;8(6):e66663. doi: 10.1371/journal.pone.0066663.

41. Saarinen PE, Kalliomäki P, Tang JW, Koskela H. Large Eddy Simulation of Air Escape through a Hospital Isolation Room Single Hinged Doorway – Validation by Using Tracer Gases and Simulated Smoke Videos. *PLoS One*. 2015 Jul 7;10(7):e0130667. doi: 10.1371/journal.pone.0130667.

42. Kalliomäki P, Saarinen P, Tang JW, Koskela H. Airflow patterns through single hinged and sliding doors in hospital isolation rooms. *Build Environ* 2016;107:154–68.

43. Melikov A. Breathing thermal manikins for indoor environment assessment: important characteristics and requirements. *Eur J Appl Physiol*. 2004 Sep;92(6):710–13.

44. Melikov A, Kaczmarczyk J. Measurement and prediction of indoor air quality using a breathing thermal manikin. *Indoor Air*. 2007 Feb;17(1):50–9.

45. Qian H, Li Y, Nielsen PV, Hyldgaard CE, Wong TW, Chwang AT. Dispersion of exhaled droplet nuclei in a two-bed hospital ward with three different ventilation systems. *Indoor Air*. 2006 Apr;16(2):111–28.

46. Pantelic J, Sze-To GN, Tham KW, Chao CY, Khoo YC. Personalized ventilation as a control measure for airborne transmissible disease spread. *J R Soc Interface*. 2009 Dec 6;6 Suppl 6:S715–26. doi: 10.1098/rsif.2009.0311.focus.

47. Licina D, Melikov A, Pantelic J, Sekhar C, Tham KW. Human convection flow in spaces with and without ventilation: personal exposure to floor-released particles and cough-released droplets. *Indoor Air*. 2014 Dec 17. doi: 10.1111/ina.12177.

48. Licina D, Melikov A, Sekhar C, Tham KW. Human convective boundary layer and its interaction with room ventilation flow. *Indoor Air*. 2015 Feb;25(1):21-35. doi: 10.1111/ina.12120.

49. Pantelic J, Tham KW, Licina D. Effectiveness of a personalized ventilation system in reducing personal exposure against directly released simulated cough droplets. *Indoor Air*. 2015 Jan 23. doi: 10.1111/ina.12187.

50. Blachere FM, Lindsley WG, Slaven JE, Green BJ, Anderson SE, Chen BT, *et al*. Bioaerosol sampling for the detection of aerosolized influenza virus*. Influenza and Other Respir Viruses*. 2007 May;1(3):113–20. doi: 10.1111/j.1750-2659.2007.00020.x.

51. Bischoff WE, Reid T, Russell GB, Peters TR. Transocular entry of seasonal influenza-attenuated virus aerosols and the efficacy of n95 respirators, surgical masks, and eye protection in humans. *J Infect Dis*. 2011 Jul 15;204(2):193–9. doi: 10.1093/infdis/jir238.

52. Beggs CB, Kerr KG, Noakes CJ, Hathway EA, Sleigh PA. The ventilation of multiple-bed hospital wards: review and analysis. *Am J Infect Control*. 2008 May;36(4):250–9.

53. King MF, Noakes CJ, Sleigh PA. Modeling environmental contamination in hospital single- and four-bed rooms. *Indoor Air*. 2015 Jan 23. doi: 10.1111/ina.12186.

54. Richmond-Bryant J, Eisner AD, Brixey LA, ja Wiener R. Short-term dispersion of indoor aerosols: can it be assumed the room is well-mixed? *Building and Environment*. 2006;41:156–63.

55. Richmond-Bryant J, Eisner AD, Brixey LA, ja Wiener R. Transport of small airborne particles within a room. *Indoor Air*. 2006;16:48–55.

56. Goodfellow H, Tähti E (eds.). Industrial Ventilation Design Guidebook. 2001. Academic Press, San Diego, CA, USA. ISBN 0-12-289676-9.

57. Nielsen P. Control of airborne infectious diseases in ventilated spaces. *J R Soc Interface*. 2009; 6:S747–S755.

58. Chau OKY, Liu C-H, Leung MKH. CFD analysis of the performance of a local exhaust ventilation system in a hospital ward. *Indoor and Built Environment*. 2006;15:3:257–71.

59. Sadrizadeh S, Holmberg S. 2015. Cross-Infection in a hospital wardroom with individual return openings. In proceedings of Healthy Buildings Europe, 18–20 May 2015, Eindhoven, The Netherlands.

60. Nielsen P, Jiang H, Polak M. 2007. Bed with integrated personalized ventilation for minimizing cross infection. In proceedings of Roomvent 2007 conference; 10th International Conference on Air Distributions in Rooms. 13–15 June 2007, Helsinki, Finland.

61. Melikov A, Bolashikov Z, Georgiev E. 2011. Novel ventilation strategy for reducing the risk of airborne cross infection in hospital rooms. In proceedings of Indoor Air conference; 12th International Conference on Indoor Air Quality and Climate. 5–10 June 2011, Austin, Texas, USA.

62. Bivolarova M, Melikov A, Mizutani C, Kajiwara K, Bolashikov Z. Bed-integrated local exhaust ventilation system combined with local air cleaning for improved IAQ in hospital patient rooms. *Build Environ*. 2016;100:10–18.

63. Hagström K, Sandberg E, Koskela H, Hautalampi T. Classification for the room air conditioning strategies. *Build Environ*. 2000;35:699–707.

64. Zhou Q, Qian H, Ren H, Li Y, Nielsen P. The lock-up phenomenon of exhaled flow in a stable thermally-stratified indoor environment. *Build Environ*. 2017;116:246–56.

65. Berlanga F, Ruiz de Adana M, Olmedo I, Villafruela J, San Jose J, Castro F. Experimental evaluation of thermal comfort, ventilation performance indices and exposure to airborne contaminant in an

Airborne Infection Isolation Room equipped with a displacement air distribution system. *Energy and Buildings*. 2018;158:209–21.

66. Yang B, Melikov A, Kabanshi A, Zhang C, Bauman F, Cao G, *et al*. A review of advanced air distribution methods – theory, practice, limitations and solutions. *Energy and Buildings*. 2019; 202, 27 p.
67. Qian H, Li Y. Removal of exhaled particles by ventilation and deposition in a multibed airborne infection isolation room. *Indoor Air*. 2010;20:284–97.
68. Qian H, Li Y, Nielsen P, Hyldgaard C. Dispersion of exhalation pollutants in a two-bed hospital ward with a downward ventilation system. *Build Environ*. 2008;43:344–54.
69. Huang J-M, Tsao S-M. The influence of air motion on bacterial removal in negative pressure isolation rooms. *HVAC&R Research*. 2005;11(4):563–85.
70. Cheong K, Phua S. Development of ventilation design strategy for effective removal of pollutant in the isolation room of a hospital. *Build Environ*. 2006;41:1161–170.
71. ASHRAE. HVAC Design Manual for Hospitals and Clinics. The American Society of Heating, Refrigerating and Air-Conditioning Engineers (ASHRAE), Atlanta, Georgia, USA, 2013.
72. Health Building Note 04-01, Supplement 1 – Isolation Facilities for Infectious Patients in Acute Settings, Department of Health, UK, 2013.
73. Kalliomäki P, Saarinen P, Tang JW, Koskela H. Airflow patterns through single hinged and sliding doors in hospital isolation rooms. *Int J Vent*. 2015;14(2):111–26.
74. Höppe P.Temperatures of Expired Air under Varying Climatic Conditions. *Int J Biometeor*. 1981;25:2:127–132.
75. McMurray RG, Soares J, Caspersen CJ, McCurdy T. Examining variations of resting metabolic rate of adults: a public health perspective. *Medicine & Science in Sports & Exercise*. 2014;46(7):S1352–8.
76. SAE Information Report, J2234: Equivalent temperature. Society of Automotive Engineers, Warrendale, PA, USA, 1993.
77. Nilsson H, Holmer I, Bohm M, Noren O. Definition and theoretical background of the equivalent temperature. In: ATA Conf, Florence, 1999, abstract no.A4082.
78. ASHRAE standard 55-2004 Thermal environmental conditions for human occupancy. ASHRAE, Atlanta, GA, USA, 2013.
79. EN ISO standard 7730:2005 Ergonomics of the thermal environment – Analytical determination and interpretation of thermal comfort using calculation of the PMV and PPD indices and local thermal comfort criteria. CEN, Brussels, Belgium, 2005.
80. Noakes CJ, Fletcher LA, Sleigh PA, Booth WB, Beato-Arribas B, ja Tomlinson N. Comparison of tracer techniques for evaluating the behaviour of bioaerosols in hospital isolation rooms. Proceedings of Healthy Buildings. 2009; 9th international conference and exhibition, Syracuse, NY, USA. Paper #504.
81. Bivolarova M, Ondráček J, Melikov A, Ždímal V. A comparison between tracer gas and aerosol particles distribution indoors: The impact of ventilation rate, interaction of airflows, and presence of objects. *Indoor Air*. 2017. Nov;27(6):1201-1212. doi: 10.1111/ina.12388.
82. Kierat W, Bivolarova M, Zavrl E, Popiolek Z, Melikov A. Accurate assessment of exposure using tracer gas measurements. *Build Environ*. 2018;131:163–73.
83. Bennett DH, McKone TE, Evans JS, Nazaroff WW, Margni MD, Jolliet O, Smith KR. Peer reviewed: defining intake fraction. *Environ Sci Technol*. 2002;36:206A–11A.

84. Ai Z, Hashimoto K, Melikov A. Influence of pulmonary ventilation rate and breathing cycle period on the risk of cross-infection. *Indoor Air*. 2019. 29(6):993-1004. doi: 10.1111/ina.12589.

85. Olmedo I, Nielsen P, Ruiz de Adana M, Jensen R. The risk of airborne cross-infection in a room with vertical low-velocity ventilation. *Indoor Air*. 2013;23:62–73.

86. Villafruela J, Castro F, San Jose J, Saint-Martin J. Comparison of air change efficiency, contaminant removal effectiveness and infection risk as IAQ indices in isolation rooms. *Energy and Buildings*. 2013;57:210–19.

87. EN ISO standard 15251:2007 Indoor environmental input parameters for design and assessment of energy performance of buildings addressing indoor air quality, thermal environment, lighting and acoustics. CEN, Brussels, Belgium, 2007.

88. Berlanga F, Olmedo I, Ruiz de Adana M, Villafruela M, San Jose J, Castro F. Experimental assessment of different mixing air ventilation systems on ventilation performance and exposure to exhaled contaminants in hospital rooms. *Energy and Buildings*. 2018; 177:207–19.

89. Cho J. Investigation on the contaminant distribution with improved ventilation system in hospital isolation rooms: Effect of supply and exhaust air diffuser configurations. *Appl Therm Eng*. 2019;148:208–18.

90. Qian Y, Willeke K, Grinshpun SA, Donnelly J, Coffey CC. Performance of N95 respirators: Filtration efficiency for airborne microbial and inert particles. *Am Ind Hyg Assoc* J;59:128–32.

91. Chu DK, Akl EA, Duda S, Solo K, Yaacoub S, Schünemann HJ, et al. Physical distancing, face masks, and eye protection to prevent person-to-person transmission of SARS-CoV-2 and COVID-19: a systematic review and meta-analysis. *Lancet.* 2020; 395(10242):1973-87.

92. Li Y, Tokura H, Guo YP, Wong ASW, Wong T, Chung J, *et al*. Effects of wearing N95 and surgical facemasks on heart rate, thermal stress and subjective sensations. *Int Arch of Occup Environ Health*. 2005;78: 501–9.

93. Sadrizadeh S. Design of hospital operating room ventilation using computational fluid dynamics. 2016. Doctoral thesis, KTH Royal Institute of Technology, Stockholm, Sweden. ISBN: 978-91-7595-810-1.

94. Noakes C, Sleigh P, Escombe A, Beggs C. Use of CFD analysis in modifying a TB ward in Lima, Peru. *Indoor Built Environ*. 2006;15(1):41–7.

95. Liu J, Wang H, Wen W. Numerical simulation on a horizontal airflow for airborne particles control in hospital operating room. *Build Environ*. 2009;44(11):2284–9.

96. Romano F, Marocco L, Gusten J, Joppolo C (2015). Numerical and experimental analysis of airborne particles control in an operating theatre. *Build Environ*, 89(2015), 369–79.

97. Zhai Z, Zhang Z, Zhang W, Chen Q. Evaluation of various turbulence models in predicting airflow and turbulence in enclosed environments by CFD: Part 1 – Summary of prevalent turbulence models. *HVAC&R Research*. 2007;13(6):853–70.

98. Nicoud F, Ducros F. Subgrid-scale stress modelling based on the square of the velocity gradient tensor. *Flow, Turbulence and Combustion*. 1999;62:183–200.

99. Kanerva P, Koskela H, Kalliomäki P, Saarinen P, Mustakallio P. Simulation of the airflow pattern from multi-nozzle diffuser. In Proceedings of Room Ventilation 2018, 2–5 June 2018, Espoo, Finland.

100. Koskela H. Momentum source model for CFD-simulation of nozzle duct air diffuser. *Energy and Buildings*. 2004;36:1011–20.

101. Brockmann T, Koskela H, Mustakallio P, Siikonen T. A Comparison of LES and RANS in a simulation of colliding plane jets, Roomvent 2011, 12th International Conference on Air Distribution in Rooms, Trondheim, Norway, 19–22 June 2011.

102. EMA (European Medicines Agency). Assessment report. Fluenz Tetra. Common name: influenza vaccine (live attenuated, nasal). Procedure No. EMEA/H/C/002617/0000. 19 September 2013. www.ema.europa.eu/en/documents/assessment-report/fluenz-tetra-epar-public-assessment-report_en.pdf?fbclid=IwAR3gv8rmapoB80OZi6h1lD7WrHJIT5UYYtRi2bW7cX1MzI0jil2wGSzZxPw. (Accessed 18 July 2020).

103. PHE (Public Health England) UK. The National Childhood Flu Immunisation Programme 2019/20 Information for healthcare practitioners. July 2019. https://assets.publishing.service.gov.uk/government/uploads/system/uploads/attachment_data/file/815744/Childhood_flu_programme_information_for_healthcare_practitioners_2019_2020.pdf (Accessed 18 July 2020).

104. Wong TW, Lee CK, Tam W, Lau JT, Yu TS, Lui SF, *et al*. Cluster of SARS among medical students exposed to single patient, Hong Kong. *Emerg Infect Dis*. 2004 Feb;10(2):269–76.

105. Hui DS, Ip M, Tang JW, Wong AL, Chan MT, Hall SD, *et al*. Airflows around oxygen masks: A potential source of infection? *Chest*. 2006 Sep;130(3):822–6.

106. Hui DS, Hall SD, Chan MT, Chow BK, Ng SS, Gin T, *et al*. Exhaled air dispersion during oxygen delivery via a simple oxygen mask. *Chest*. 2007 Aug;132(2):540–6.

107. Hui DS, Chow BK, Chu LCY, Ng SS, Hall SD, Gin T, *et al*. Exhaled air and aerosolized droplet dispersion during application of a jet nebulizer. *Chest*. 2009 Mar;135(3):648–54. doi: 10.1378/chest.08-1998.

108. Hui DS, Chow BK, Ng SS, Chu LCY, Hall SD, Gin T*, et al*. Exhaled air dispersion distances during noninvasive ventilation via different Respironics face masks. *Chest*. 2009 Oct;136(4):998–1005. doi: 10.1378/chest.09-0434.

109. Simonds AK, Hanak A, Chatwin M, Morrell M, Hall A, Parker KH, *et al*. Evaluation of droplet dispersion during non-invasive ventilation, oxygen therapy, nebuliser treatment and chest physiotherapy in clinical practice: implications for management of pandemic influenza and other airborne infections. *Health Technol Assess*. 2010 Oct;14(46):131–72. doi: 10.3310/hta14460-02.

110. Tran K, Cimon K, Severn M, Pessoa-Silva CL, Conly J. Aerosol generating procedures and risk of transmission of acute respiratory infections to healthcare workers: a systematic review. *PLoS One*. 2012;7(4):e35797. doi: 10.1371/journal.pone.0035797.

111. Thompson KA, Pappachan JV, Bennett AM, Mittal H, Macken S, Dove BK, *et al*. EASE Study Consortium. Influenza aerosols in UK hospitals during the H1N1 (2009) pandemic – the risk of aerosol generation during medical procedures. *PLoS One*. 2013;8(2):e56278. doi: 10.1371/journal.pone.0056278.

112. World Health Organization (WHO). Infection prevention and control of epidemic- and pandemic-prone acute respiratory diseases in health care. June 2007. WHO Interim Guidelines. https://apps.who.int/iris/bitstream/handle/10665/69707/WHO_CDS_EPR_2007.6_eng.pdf;jsessionid=B457EE7954E060048F1E46B0AFA4319A?sequence=1. (Accessed 18 July 2020).

113. World Health Organization (WHO). Epidemic- and pandemic-prone acute respiratory diseases: Infection prevention and control in health care. April 2008. AIDE-MEMOIRE. www.who.int/csr/resources/publications/EPR_AM3_E3.pdf?ua=1. (Accessed 18 July 2020).

114. Public Health England (PHE). Infection control precautions to minimise transmission of acute respiratory tract infections in healthcare settings. October 2016.

https://assets.publishing.service.gov.uk/government/uploads/system/uploads/attachment_data/file/585584/RTI_infection_control_guidance.pdf. (Accessed 18 July 2020).

115. Centers for Disease Control and Prevention (CDC). Infection Prevention and Control Recommendations for Hospitalized Patients Under Investigation (PUIs) for Ebola Virus Disease (EVD) in U.S. Hospitals. 30 August 2018. www.cdc.gov/vhf/ebola/clinicians/evd/infection-control.html. (Accessed 18 July 2020).
116. Jokela P, Vuorinen T, Waris M, Manninen R. Performance of the Alere i influenza A&B assay and mariPOC test for the rapid detection of influenza A and B viruses. *J Clin Virol*. 2015; 70:72–6. doi: 10.1016/j.jcv.2015.07.294.
117. Majumdar N, Banerjee S, Pallas M, Wessel T, Hegerich P. Poisson Plus Quantification for Digital PCR Systems. *Sci Rep*. 2017;7:9617. doi:10.1038/s41598-017-09183-4.
118. Quan P-L, Sauzade M, Brouzes E. dPCR: A technology review. Sensors (Basel). 2018;18:1271. doi: 10.3390/s18041271.
119. Tang JW, Waris M, Kalliomäki P, Koskela H. Use of a live vaccine virus as a tracer for infection control related air-sampling and ventilation studies, Proceedings of Room Ventilation 2018, 2–5 June 2018, Espoo, Finland.
120. Brown JR, Tang JW, Pankhurst L, Klein N, Gant V, Lai KM, *et al*. Influenza virus survival in aerosols and estimates of viable virus loss resulting from aerosolization and air-sampling. *J Hosp Infect*. 2015;91(3):278–81.
121. World Health Organization (WHO). Infection prevention and control during health care when novel coronavirus (nCoV) infection is suspected. Updated 19 March 2020. www.who.int/publications-detail/infection-prevention-and-control-during-health-care-when-novel-coronavirus-(ncov)-infection-is-suspected-20200125. Accessed 6 May 2020.
122. Public Health England (PHE). COVID-19: infection prevention and control guidance. Updated 27 April 2020. https://assets.publishing.service.gov.uk/government/uploads/system/uploads/attachment_data/file/881489/COVID-19_Infection_prevention_and_control_guidance_complete.pdf. Accessed 6 May 2020.
123. Tang JW, Kalliomaki P, Varila TM, Waris M, Koskela H. Nebulisers as a potential source of airborne virus. *J Infect* 2020. www.journalofinfection.com/article/S0163-4453(20)30302-9/fulltext.
124. NIOSH (National Institute for Occupational Safety and Health). Health and Safety Practices Survey of Healthcare Workers. Aerosolized Medications. 30 March 2017. www.cdc.gov/niosh/topics/healthcarehsps/aerosolizedmeds.html. (Accessed 18 July 2020)
125. Heinzerling A, Stuckey MJ, Scheuer T, Xu K, Perkins KM, Resseger H, Magill S, Verani JR, Jain S, Acosta M, Epson E. Transmission of COVID-19 to Health Care Personnel During Exposures to a Hospitalized Patient – Solano County, California, February 2020. *MMWR Morb Mortal Wkly Rep*. 2020 Apr 17;69(15):472–6. doi: 10.15585/mmwr.mm6915e5.
126. Morawska L, Cao J. Airborne transmission of SARS-CoV-2: The world should face the reality. *Environ Int*. 2020 Jun;139:105730. doi: 10.1016/j.envint.2020.105730.
127. Morawska L, Tang JW, Bahnfleth W, Bluyssen PM, Boerstra A, Buonanno G, *et al*. How can airborne transmission of COVID-19 indoors be minimised? *Environ Int*. 2020 Sep;142:105832. doi: 10.1016/j.envint.2020.105832.
128. Kimberly A, Prather KA, Chia C, Wang CC, Schooley RT. Reducing Transmission of SARS-CoV-2. *Science*. 27 May 2020. doi: 10.1126/science.abc6197. https://science.sciencemag.org/content/early/2020/06/02/science.abc6197.1.

129. Somsen GA, van Rijn C, Kooij S, Bem RA, Bonn D. Small droplet aerosols in poorly ventilated spaces and SARS-CoV-2 transmission. *Lancet Resp Med*. 27 May 2020. https://doi.org/10.1016/S2213-2600(20)30245-9.

130. Ching WH, Leung MKH, Leung DYC, Li Y, Yuen PL. Reducing risk of airborne transmitted infection in hospitals by use of hospital curtains. *Indoor Built Environ* 2008;17(3):252–9.

131. Centers for Disease Control and Prevention (CDC). Interim Infection Prevention and Control Recommendations for Patients with Suspected or Confirmed Coronavirus Disease 2019 (COVID-19) in Healthcare Settings. Updated 15 July 2020. 7. Implement Engineering Controls. https://www.cdc.gov/coronavirus/2019-ncov/hcp/infection-control-recommendations.html. (Accessed 16 July 2020).

IOSH is the Chartered body for health and safety professionals. With over 50,000 members in more than 130 countries, we're the world's largest professional health and safety organisation.

We set standards and support, develop and connect our members with resources, guidance, events and training. We're the voice of the profession and campaign on issues that affect millions of working people.

IOSH was founded in 1945 and is a registered charity with international NGO status.

IOSH
The Grange
Highfield Drive
Wigston
Leicestershire
LE18 1NN
UK

+44 (0)116 350 0700
www.iosh.com

twitter.com/IOSH_tweets
facebook.com/IOSHofficial
tinyurl.com/IOSH-linkedin
youtube.com/IOSHchannel
instagram.com/ioshofficial

Institution of Occupational Safety and Health
Founded 1945
Incorporated by Royal Charter 2003
Registered charity in England and Wales No. 1096790
Registered charity in Scotland No. SC043254

PS01201.1/060820/PDF